PAUL SCHERRER INSTITUT
PSI

Annual Report 2007

Electrochemistry Laboratory

http://ecl.web.psi.ch

COVER PHOTO:

Pulsed laser deposited $Li_xMn_2O_{4-\delta}$ thin film model electrode on a *p*-doped Si substrate. After cycling in the 1M $LiPF_6$ EC/DMC electrolyte, etching structures on the subjacent Si substrate appear.

CONTENTS

During the past year 2007 we were successful to acquire several new projects with industrial and governmental partners. Particularly important for us is the fact that we could increase the number of projects with partners from Swiss industry. We hope to develop long lasting relations to the benefit of the Swiss working place, bringing electrochemical conversion and storage devices "Made in Switzerland" to the market.

Our comprehensive approach, namely to carry out research and development of electrochemical energy conversion and storage systems at the materials, cell, and systems level for fuel cells, batteries, and supercapacitors is well esteemed by our industrial as well as by our academic partners. It also provides a challenging interdisciplinary environment to our PhD-students, co-workers, and guests.

Within the present Annual Report 2007 of the Electrochemistry Laboratory, all our four research groups, namely Fuel Cells, Fuel Cell Systems, Batteries, and Interfaces and Capacitors communicate the progress made during the past year in numerous contributions. Again, topics range from materials development for the different electrochemical systems to the development of novel characterization methods adapted to the respective electrochemical system, i.e. fuel cell, battery, or capacitor. As in past years, success of our continuous efforts is well documented in our list of peer reviewed publications, invited contributions to conferences, and talks and poster presentations at various conferences and workshops worldwide

Our 23rd One-Day-Symposium took place on May 3, 2007, addressing the subject of "Electrocatalysis", with contributions from Holger Kuhn (MTU CFC Solutions GmbH, Munich, DE), Brian E. Hayden (University of Southampton, GB), Timo Jacob (Fritz-Haber-Institut der MPG, Berlin, DE), Elena R. Savinova (University of Novosibirsk, RU & University of Strasbourg, FR), Thomas J. Schmidt (PEMEAS GmbH, Frankfurt/M, DE), Gunther Wittstock (University of Oldenburg, DE), covering topics of electrochemical catalytic reactions for energy conversion in various types of fuel cells and in bioelectrocatalysis.

The 24th Symposium will take place on May 7, 2008, addressing the topic of "Electrochemical Materials Processing".

With its wide range of topics, this report gives proof that we successfully continued our effort to contribute to the field of Electrochemistry and in particular to Electrochemical Energy R&D. In this context, transfer of our know-how to industrial partners as well as the education of students and young scientists will continue to be prime targets for 2008. As in past years, our work is carried out in the context of R&D for a sustainable energy development, within Paul Scherrer Institut and the Domain of the Swiss Federal Institutes of Technology

Günther G. Scherer

SCIENTIFIC CONTRIBUTIONS 2007

FUEL CELLS

MEMBRANES

DURABILITY OF STYRENE RADIATION GRAFTED ETFE-BASED MEMBRANES

H. Ben youcef, S. Alkan Gürsel, L. Gubler,
A. Wokaun, G.G. Scherer
+41 56 310 4188
hicham.ben-youcef@psi.ch

The development of the poly(ethylene-alt-tetrafluoro-ethylene) (ETFE) based membrane was already reported and results on the optimization of the synthesis parameters and the effect of crosslinking on fuel cell performance were presented [1-4]. Thereby, the membrane prepared with a concentration of 5% divinylbenzene (DVB) as the cross-linker (styrene : DVB = 95 : 5 (v/v)) was found to exhibit optimum performance. In this study, the first long term testing with this optimized membrane over a period of 2100 h is reported.

Experimental

Membranes based on ETFE films (25 μm) were prepared, as described previously [2]. The membrane selected for durability testing (graft level ~25.2 m-%) was characterized for its fuel cell relevant properties (conductivity 62 mS/cm, IEC ~1.62 meq/g, water uptake ~21 m%), and subsequently assembled into a 30 cm^2 single fuel cell. The membrane was hotpressed with electrodes (E-TEK/ Pt: 0.5 mg/cm^2) to form a membrane electrode assembly (MEA). The in situ characterization of the MEA was carried out by means of pulse-resistance, polarization measurements, electro-chemical impedance spectroscopy (EIS), and H$_2$ crossover.

Results

The MEA durability test was carried out at a constant current density of 500 mA/cm^2 (Figure 1).
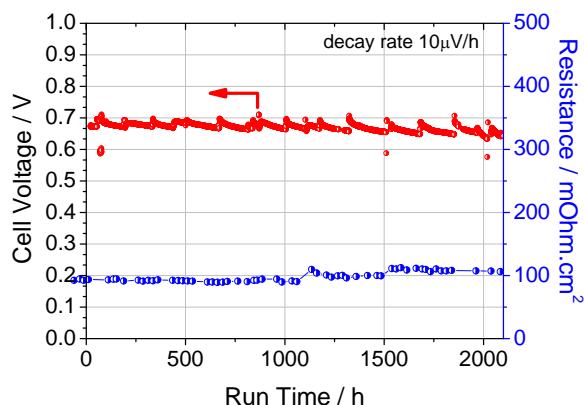
Figure 1. *Single cell durability test using a radiation grafted membrane based on ETFE (5% DVB) @500mA/cm^2, cell temperature 80°C; H$_2$/O$_2$ at a stoichiometry of 1.5/1.5.*

The evaluated drop in voltage after 1100 h was around 11 mV, whereas this value was of about 21 mV at the end of the test (2100 h). Moreover, the observed decrease in cell voltage is in good agreement with the increase in the ohmic resistance. No change was noticed for the pulse measured ohmic resistance up to 1100 h, while an increase of 6 % was observed up to 1508 h, and then a further in-crease of 7 % was measured up to 2100 h. Indeed, the membrane resistance increases from initially 94.5 mΩ.cm^2 to ~100 mΩ.cm^2 after 1100h, and then reaches a value of ~106 mΩ.cm^2 at the end of test. Both stepwise changes in resistance were observed after restarting the cell, which may indicate the adverse effect of start-stop cycles and their association with degradation phenomena.
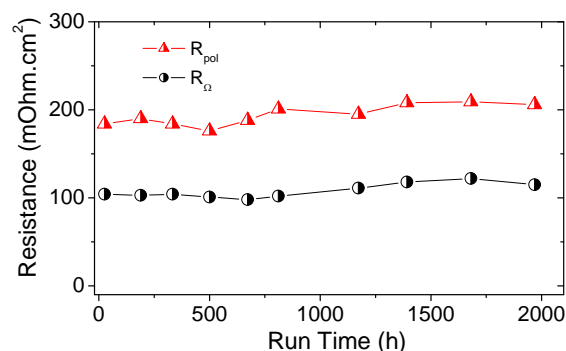
Figure 2. *Extracted ohmic (R_{Ω}) and polarization resistance (R_{pol}) from the EIS-spectra @500mA/cm^2.*

Impedance measurements were performed intermittently over the testing period (Figure 2). The polarization resistance shows slight variations with time. The ohmic resistance does not show any change up to 800 h, whereas a slight increase of ~4% after 1200h was observed. We should note here that the absolute values determined by EIS and the current-pulse are different. However, there is a good qualitative agreement between the results obtained with both techniques.
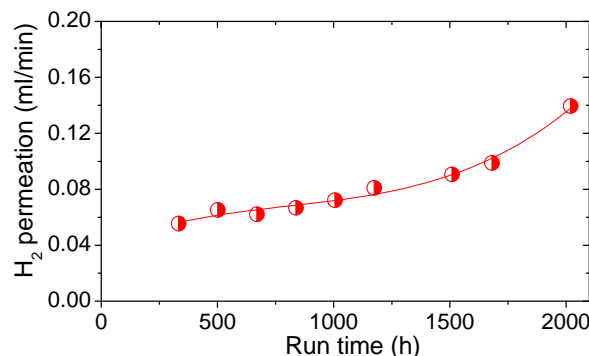
Figure 3. *Hydrogen crossover measured in H2/N2 mode.*

The hydrogen crossover was evaluated after polarization measurements to follow possible changes in the morphology of the membrane and its mechanical integrity (Figure 3). The hydrogen permeation shows a steady increase with increasing testing time. This indicates clearly that to some extent changes in the membrane morphology occur over the operating time. We note here that the investigation was mainly focused on the membrane bulk properties, not emphasizing the interfacial properties.

Post mortem analysis will be performed to evaluate the extent and localization of the membrane degradation in the H$_2$/O$_2$ inlet and in regions associated with channel and land areas of the flow field.

References

[1] L. Gubler, N. Prost, S. Alkan Gürsel, G.G. Scherer, Solid State Ionics **176**, 2849-2860 (2005).

[2] S. Alkan Gürsel, H. Ben youcef, A. Wokaun, G.G. Scherer, Nucl. Instrum. Methods Phys. Res., Sect. B **265**, 198-203 (2007).

[3] L. Gubler, H. Ben youcef, S. Alkan Gürsel, A. Wokaun, G.G. Scherer, Electrochem. Soc. Trans. **11**(1), 27-34 (2007).

[4] H. Ben youcef, S. Alkan-Gürsel, A. Wokaun, G.G. Scherer, J. Membr. Sci., **311**, 208-215 (2008).

MECHANICAL PROPERTIES OF STYRENE GRAFTED ETFE-BASED FILMS AND MEMBRANES

H. Ben youcef, S. Alkan Gürsel, L. Gubler,
A. Wokaun, G. G. Scherer
+41 56 310 4188
hicham.ben-youcef@psi.ch

For the preparation of radiation grafted fuel cell membranes, poly(ethylene-*alt*-tetrafluoroethylene) (ETFE) base film was shown to possess superior mechanical properties and good resistance to irradiation in comparison to those of poly(tetrafluoroethylene-*co*-hexafluoropropylene) (FEP) [1]. In this study, we evaluate the influence of the crosslinker concentration on the mechanical properties of the grafted films and membranes. It was also of interest to determine the effect of each membrane preparation process step on the mechanical properties of the optimized ETFE-based membrane.

Experimental

ETFE (25 μm, Dupont) based grafted films and membranes were prepared in the presence of styrene and the crosslinker divinylbenzene (DVB) with a fixed graft level (GL) of 25% (m-%) and with varying the DVB concentration as described previously [2]. Selected grafted films and membranes (converted to salt form (K^+) and dried for 24h @ 60°C) with different DVB concentration in the initial grafting solution (0%, 3%, 5%, 8%, 10%, and 15%) were tested. Samples with rectangular shapes and with dimensions of (1cm x 10cm) were investigated in both directions (machining direction (MD) and transverse direction (TD)). The measurements were carried out using Universal Testing Machine (Zwick Roell Z005) at cross head speed of 100 mm/min.

Results

Elongation at break of the grafted films and membranes decreases significantly while the tensile strength shows an increase as DVB concentration increases (Figure 1 and 2).
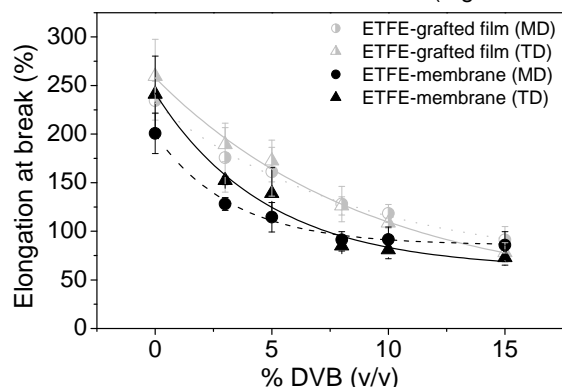
Figure 1. *Elongation at break of the ETFE based grafted films and membranes in both directions (MD and TD) as function of the DVB concentration.*

Although both MD and TD results exhibit a similar tendency (in terms of tensile strength and elongation at break versus the increase of crosslinker concentration) slight differences are observable.

The observed trends result from the significant changes occurring in the structure of the films by crosslinking. In fact, it is to be expected that the crosslinking has a negative effect on the elongation at break of the grafted films and membranes. Indeed, the DVB is well known as a stiff crosslinker, which is expected to increase the brittleness of the grafted films and the resulting membranes. Moreover, the introduction of DVB brings about a 3D network structure and increases the entanglement of chains.
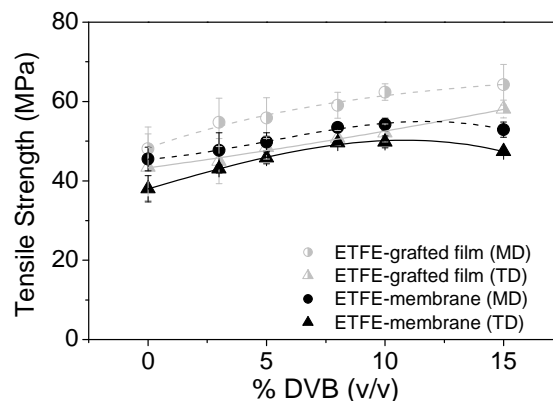
Figure 2. *Tensile strength of ETFE-based grafted films and membranes in both directions (MD and TD) as function of the DVB concentration.*

It is important to evaluate the changes and damages caused by the preparation process on the mechanical properties of the film. For that aim, a comparison was made between the ETFE-based membrane (5% DVB and GL~25%) and a Nafion 112 standard under identical conditions (Figure 3).

The general observation is that the major loss of the elongation at break occurs after the grafting process. Indeed, we observed a decrease of about 50% in the elongation at break value due to the grafting and then loss occurs after the sulfonation process. However, no significant change on the tensile strength was observed after grafting and only a slight loss occurs after sulfonation.
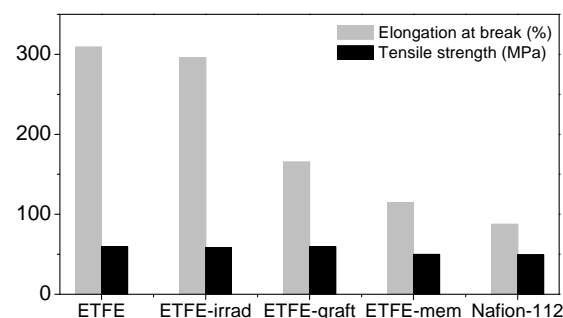
Figure 3. *Comparison of the mechanical properties in MD of the ETFE base material with Nafion-112 based membrane during the overall process (irradiation, grafting and sulfonation).*

Crosslinking is a key parameter for the control of the *ex situ* properties of ETFE-based membranes. Furthermore, the ETFE-based membrane with 5% DVB shows comparable mechanical properties to a Nafion 112 membrane and exhibits the highest elongation. Further investigation will be devoted to the study of the influence of temperature and humidity on the mechanical properties of these membranes.

References

[1] H.P. Brack, F.N. Büchi, J. Huslage, M. Rota, G.G. Scherer, ACS Symp. **744**, 174-188 (2000).

[2] L. Gubler, H. Ben youcef, S. Alkan Gürsel, A. Wokaun, G.G. Scherer, Electrochem. Soc. Trans. **11**(1), 27-34 (2007).

TEMPERATURE DEPENDENCE OF THE AMS/MAN GRAFTING ON FEP BASE FILM

F. Wallasch, L. Gubler, G.G. Scherer, A. Wokaun
+41 56 310 2132
frank.wallasch@psi.ch

The need for PEFC membranes with enhanced chemical and mechanical properties to obtain the required long-term stability is ongoing. The preparation of membranes by the pre-irradiation grafting procedure and subsequent sulfonation is a viable process [1]. The substitution of polystyrene as grafted component by an α-methylstyrene (AMS) / methacrylonitrile (MAN) copolymer extends the lifetime [2,3] in the fuel cell by enhancing the resistance of the grafted polymer against radical attack.

Experimental

The grafting reactions were carried out with 25 kGy pre-irradiated FEP films (DuPont 100A, thickness 25 μm). The grafting solution consists of 30 % (v/v) monomers, at a molar ratio $R_{m,sol.}$ of 1.5, 20 % (v/v) water and 50 % (v/v) isopropanol. The mixture was flushed for 60 min with N_2 at room temperature for de-oxygenation. The reactions at temperatures between 35 and 80 °C were stopped after the designated time heating by passing air through the solution. The remaining monomers and homopolymer formed via chain transfer were dissolved by storing the grafted films in acetone for 4 h. After drying of the film at 60 °C under reduced pressure, the degree of grafting *DoG* was calculated from the mass difference before and after grafting. The molar ration $R_{m,graft.}$ of AMS:MAN in the graft component was calculated from the areas of the infrared absorption bands of a twisting benzene ring vibration at 1600 cm^{-1} and the CN-stretching vibration 2230 cm^{-1}, respectively.

Results

A total of ten reaction profiles in the temperature range from 35 to 80 °C were recorded, whereby a series of eight samples was prepared for each temperature. In Figure 1 only six reaction profiles are shown for reasons of clarity.
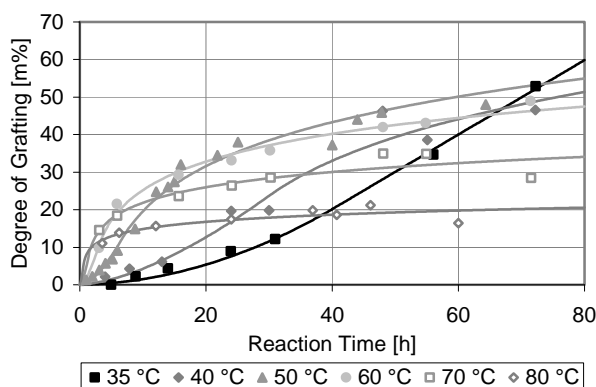
Figure 1. Evolution of the degree of grafting at different grafting temperatures (lines as an assistance).

Different grafting behaviour was observed at the various temperatures. While at low temperatures (< 45 °C) the initial increase of the *DoG* and therefore the polymerization was very slow, a fast initial grafting without any delay took place at high temperatures (> 70 °C). For reaction times > 30 h at temperatures < 45 °C, the *DoG* was still increasing, which may be caused in a slow decomposition of the peroxides, formed during the irradiation under air. A decrease of the *DoG* set in after

approximately 50 h for temperatures > 70 °C, which my be due to the cleavage of AMS-AMS bonds, as a consequence of the low ceiling temperature of AMS (61 °C). "Typical" reaction profiles were recorded at temperatures between 50 and 65 °C, where at the beginning the profiles show a short delay, related to the cleavage of the peroxides, the diffusion of the monomers into the film, or the removal of the stabilizers present in the used monomers. This step is followed by a stage with a constant polymerization rate (linear behaviour between *DoG* and time) and for long reaction times the polymerization levelled off at a constant *DoG*, with no further polymerization occurring.

The simplified kinetic model [4,5] used earlier cannot be applied for the fitting of the "untypical" reaction profiles and a more precise model has to be developed. The simplified model does not consider the delay at the beginning of the grafting process and therefore does not allow the calculation of kinetic rate constants for the quantitative comparison of the polymerization at different temperatures.

In Figure 2 the *DoG* after 48 h of grafting is plotted against the temperature. The $R_{m,graft.}$ and the total *DoG* (diamonds) were used to calculate the degrees of grafting for AMS (square) and MAN (triangle), respectively.
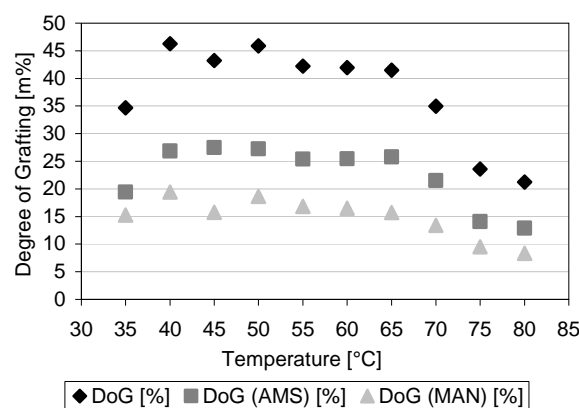
Figure 2. Dependency of the degrees of grafting, total, for AMS only, and MAN only, from the temperature after 48 h.

Between a temperature of 40 and 65 °C, no significant changes were observed, neither in the total *DoG* nor in the ratio between the *DoG*s of AMS and MAN. Not shown are the results after 24 h of grafting, but the observed trends were the same with no variation between 45 and 65 °C.

For the preparation of membranes with a certain *DoG* and $R_{m,graft.}$, the variation of the temperature between 45 and 65 °C has no influence. However, it is likely that films prepared at different temperature exhibit considerable differences in structure and morphology, such as different average graft chain length. Investigations into such phenomena are subject to ongoing work.

References

[1] L. Gubler, S. A. Gürsel, G. G. Scherer, Fuel Cells **5**, 317-335 (2005).

[2] L. Gubler, M. Slaski, A. Wokaun, G. G. Scherer, Electrochem. Commun. **8**, 1215-1219 (2006).

[3] M. Slaski, Dissertation ETH Zürich, Nr. 16995 (2007).

[4] F. Wallasch, PSI Electrochemistry Laboratory - Annual Report 2006, ISSN 1661-5379, 16 (2007).

[5] T. Rager, Helv. Chim. Acta **86**, 1966-1981 (2003).

LONG-TERM FUEL CELL TEST RESULTS OF AN UNCROSSLINKED, FEP BASED, AMS-*CO*-MAN GRAFTED MEMBRANE

F. Wallasch, L. Gubler, G.G. Scherer, A. Wokaun
+41 56 310 2132
frank.wallasch@psi.ch

The commercial success of fuel cells depends on the costs and the longevity of the catalyst as well as of the membrane electrolyte. A variety of *ex situ* characterization methods to probe membrane properties, such as ion exchange capacity *IEC*, proton conductivity σ, swelling, and hydration, is available and widely used. Some accelerated *ex situ* test methods to determine the durability of membranes are under discussion, for instance the treatment with H_2O_2 for the chemical degradation. However, the correlation of these test results to real fuel cell experiments is still a challenge. For the final proof of longevity fuel cell experiments in real time have to be conducted.

Experimental

The tested membrane was prepared by pre-irradiation grafting of an FEP film (DuPont 100A, thickness 25 μm) and subsequent sulfonation [1]. The pristine FEP base film was pre-irradiated with a dose of 25 kGy (Leoni-Studer AG, CH-Däniken) and grafted in a solution consisting of 30 % (v/v) AMS/MAN at a molar ratio R_m of 1.5, 20 % (v/v) water, and 50 % (v/v) 2-propanol. The grafting co-polymerization was carried out at 50 °C for 16 h and stopped by passing air through the solution. The remaining monomers were dissolved with acetone and the film dried over night at 60 °C under reduced pressure. The degree of grafting *DoG* was calculated to 32.0 % from the mass difference before and after grafting. The molar ratio R_m of AMS to MAN in the graft copolymer of 0.73 was determined from the areas of the infrared absorption bands at 1600 cm^{-1} (AMS) and at 2230 cm^{-1} (MAN). To obtain the essential proton conductivity, sulfonic acid groups were introduced by sulfonation of the AMS benzene ring. Therefore the film was stirred at room temperature for 6 h in a solution of 4.4 % (v/v) chlorosulfonic acid in dichloromethane. The membrane was rinsed twice with water to remove remaining acid and then heated for 8 h to 80 °C in water. The water treatment at 80 °C was repeated until pH 6 was reached. The results of the *ex-situ* characterization of the prepared membrane were summarized in Table 1.

IEC [mEq/g]	Conductivity [mS/cm]	Thickness [μm]	Swelling [%]	Hydration [H$_2$O/SO$_3$H]
1.45 ± 0.07	103 ± 9	41.6 ± 0.6	52 ± 4	19 ± 2

Table 1. *Ex situ membrane properties*

Results

The membrane (active area of 29.2 cm^2) was assembled in a fuel cell, using E-TEK 140 W electrodes with a Pt-loading of 0.5 mg/cm^2 on both sides. The fuel cell test was performed at constant current density (500 mA/cm^2) and temperature 80 °C, using fully humidified H$_2$/O$_2$ (80/80 °C) with a stoichiometry λ of 1.5/1.5. The cell voltage was continuously recorded, as shown in Figure 1 (top). The membrane resistance was mesured daily and the hydrogen permeation weekly, both are reported in Figure 1 (middle and lower illustration).
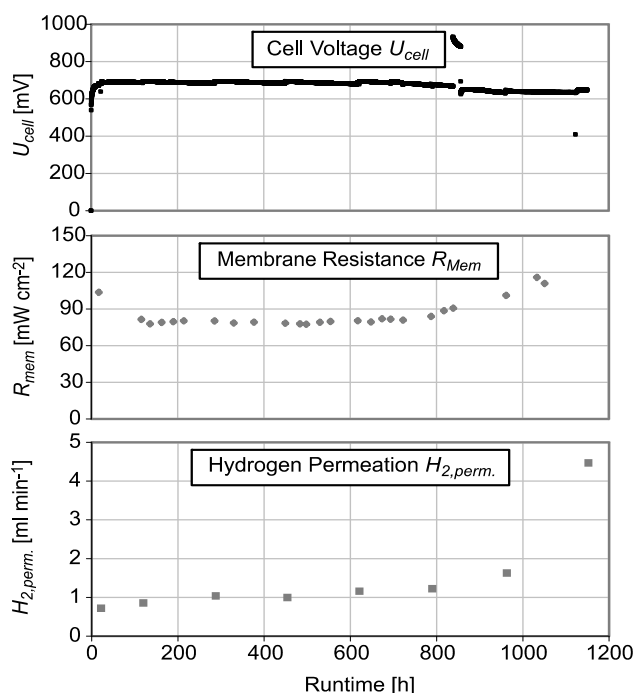
Figure 1. *Measured cell voltage, membrane resistance, and hydrogen permeation as a function of time*

The cell voltage as a function of current density (polarization plot) and the corresponding membrane resistance are shown in Figure 2 for different run times.
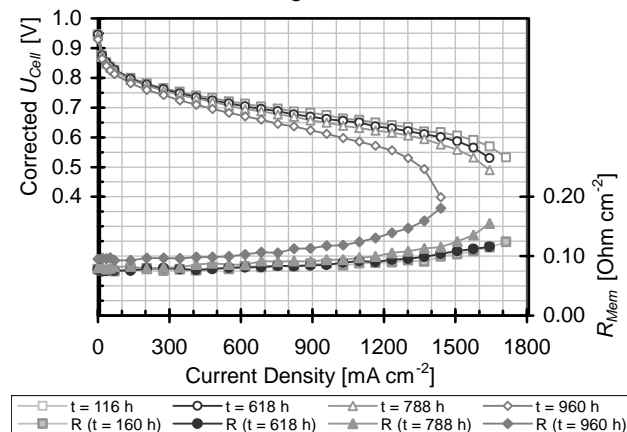
Figure 2. *Polarization plot and membrane resistance*

The membrane performance was stable up to approximately 850 h. After that the cell was operated at OCV, caused by a problem with the hydrogen supply of the test rig. The impact of this event can be seen in the drop of the cell voltage, the increasing membrane resistance, the rising hydrogen permeation, and the slope of the polarization curve.

Under comparable conditions, FEP based membranes grafted with poly(styrene-sulfonic acid) showed lifetimes less than 100 hours [2]. The clear improvement of the AMS/MAN graft component is due to the replacement of the α-hydrogen by a methyl group in the vinyl group. The effect of MAN on the stability of the membrane under fuel cell conditions is under investigation.

Reference

[1] M. Slaski, Dissertation ETH Zürich, Nr. 16995 (2007).

[2] L. Gubler, M. Slaski, A. Wokaun, G.G. Scherer, Electrochem. Commun. **8**, 1215-1219 (2006).

RAPID AGING STUDIES OF THE PSI FUEL CELL MEMBRANE

L. Gubler, M. Schisslbauer[1], G.G. Scherer
+41 56 310 2673
lorenz.gubler@psi.ch

The durability of the electrolyte membrane in the polymer electrolyte fuel cell (PEFC) is a critical lifetime factor. Loss of proton conductivity, and thus cell performance, is associated with the loss of fixed ionic sites in the membrane through **chemical degradation** of the polymer. This is thought to proceed via aggressive radical species (HO$^\bullet$ / HOO$^\bullet$) formed *in situ*. The **loss of mechanical integrity** of the membrane through crack or pinhole formation leads to catastrophic failure of the membrane electrode assembly (MEA).

Conventional lifetime testing of cell components over thousands of hours is resource-intensive and inefficient. High throughput characterization of membranes and MEAs calls for rapid aging methodologies, whereby the cell is operated under more aggressive conditions to accelerate degradation. In this study, MEAs based on PSI membranes and a Nafion 112 (DuPont) standard are characterized using a rapid aging protocol involving both chemically and mechanically induced degradation.

Experimental

The membranes evaluated were two PSI membranes based on styrene grafted and sulfonated FEP (25 μm starting film thickness). Crosslinked membranes were prepared using 10 vol-% divinylbenzene (DVB) in the grafting solution as co-monomer to styrene. Crosslinked membranes have a somewhat lower conductivity, but an improved dimensional stability (Table 1).

membrane	dimensional change wet → dry [%]	proton conductivity [mS/cm]
g-FEP	29.0	72 ± 6
g-FEP **XL**	15.1	41 ± 1
Nafion 112	25.9	82 ± 6

Table 1. *Ex situ properties of tested membranes. g-FEP is the styrene grafted and sulfonated PSI membrane based on a 25 μm FEP film, g-FEP* **XL** *is the crosslinked version. Dimensional change is the area reduction when the water-swollen membrane is dried. Proton conductivity was measured in swollen state at room temperature.*

The membranes were sandwiched between two gas diffusion electrodes and assembled into single cells. Aging tests were carried out at 80 °C and 3 bar$_a$, using H$_2$ and O$_2$ as reactant gases. In order to accelerate chemical aging, cells were held at open circuit voltage (OCV), where the maximum rate of chemical degradation is observed [1]. Mechanical stress in the membrane is induced by cyclic change of the reactant gas relative humidity between 0 (2 min) and 100 % (2 min). The periodic change in membrane hydration causes build-up of internal stresses in the polymer, since the membrane is spatially confined in the fuel cell, leading to membrane deterioration due to fatigue [2]. This simultaneous exposure of the MEA to aggressive chemical and mechanical conditions is a powerful accelerated aging test to assess membrane durability.
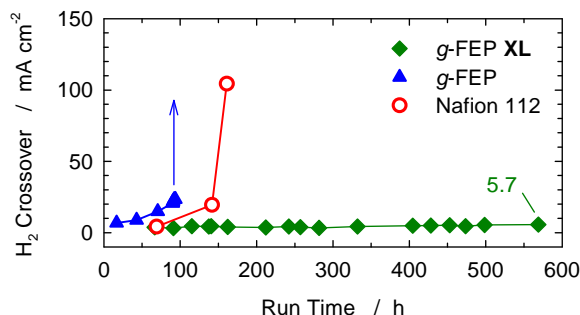
Figure 1. *H$_2$ crossover, a measure for mechanical membrane integrity, is measured electrochemically in H$_2$ / N$_2$ mode.*
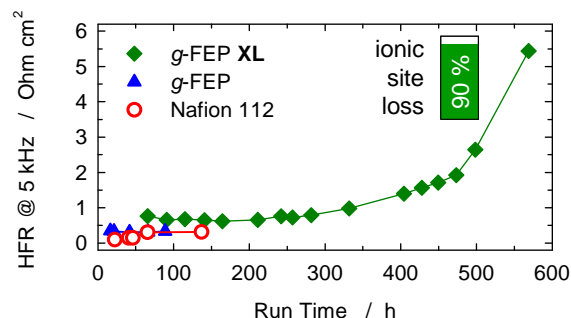
Figure 2. *Chemical integrity of the membrane is measured via high frequency resistance (HFR).*

Results

The mechanical integrity of the tested membranes is monitored via electrochemical H$_2$ crossover measurement (Figure 1). Both the uncrosslinked PSI membrane (*g*-FEP) and Nafion 112 start to develop faults after around 100 and 150 h, respectively, leading to failure of the MEA. The integrity of the crosslinked PSI membrane (*g*-FEP **XL**), on the other hand, does not seem to be affected, probably because of the higher dimensional stability (Table 1) leading to less build-up of internal stress in the membrane.

The ohmic cell resistance is a measure for the chemical integrity of the polymer (Figure 2). Although the crosslinked PSI membrane remained leak tight for almost 600 h (2'650 wet-dry cycles), the strong increase in the resistance suggests notable loss of proton conductivity. Indeed, 90 % ionic site loss was found in *post mortem* analysis. Under constant humidification and a current density of 0.5 A/cm^2, the *g*-FEP **XL** membrane has a durability of over 4'000 h [3].

It has to be emphasized that the knowledge of aging kinetics (chemical / mechanical) is essential in identifying meaningful rapid aging test protocols. Which mechanisms are accelerated and to which degree ? To what extent are the accelerated conditions representative of the conditions in regular cell testing ? These questions need to be addressed in future studies for a quantitative understanding of the underlying fundamental degradation mechanisms.

References

[1] W. Liu, M. Crum, ECS Transactions **3**, 531-540 (2007).

[2] M.F. Mathias, R. Makharia, H.A. Gasteiger, J.H. Conley, T.J. Fuller, C.J. Gittleman, S.S. Kocha, D.P. Miller, C.K. Mittelstaedt, T. Xie, S.G. Yan, P.T. Yu, Electrochem. Soc. Interface **3**, 24-35 (2005).

[3] L. Gubler, H. Kuhn, T.J. Schmidt, G.G. Scherer, H.P. Brack, K. Simbeck, Fuel Cells **4**, 196-207 (2007).

[1] Fachhochschule Amberg-Weiden, Germany

INSIGHT INTO FUEL CELL MEMBRANE DEGRADATION BY PULSE RADIOLYSIS EXPERIMENTS

S.M. Dockheer, A. Domazou[1], L. Gubler,
G.G. Scherer, A. Wokaun, W.H. Koppenol[1]
+41 56 310 4003
sindy.dockheer@psi.ch

The development of proton exchange membranes with enhanced lifetime is a critical issue in the progress of polymer electrolyte membrane fuel cells. Accordingly, understanding the mechanisms of degradation is crucial to improve suitable membrane materials. A complex interplay of mechanical, thermal, electrochemical, and chemical conditions favors membrane degradation in a fuel cell. This work addresses the issue of chemical membrane degradation, where hydroxyl and/or hydroperoxyl radicals are assumed to play a key role. The chemical mechanism is studied in *ex situ* experiments because of the complexity of degradation in a fuel cell. Initial experiments have been carried out that probe the reactivity of the hydroxyl radical towards model molecules that represent membranes based on poly(styrene sulfonic acid).

Experimental

The technique of irradiating dinitrogen monoxide saturated (24.4 mM) aqueous sample solutions with high energy electron pulses from a 2.0 MeV Febetron 705 accelerator allows the specific generation of hydroxyl radicals with quantitative yield, and UV/VIS spectrophotometry was used to follow the kinetics of radicals [1]. Doses between 5 and 60 Gy/pulse were applied. We investigated oligomer and polymer solutions at concentrations from 15 – 500 µM and variable pH at room temperature. Poly(sodium styrene sulfonate) with average molecular weight 1360 (polymerization degree 6) and with average molecular weight 70´000 were examined first. The relative absorption of transient intermediates as a function of time was recorded in the wavelength range from 260 - 360 nm. Curve fitting was carried out with exponential model fitting under pseudo-first-order reaction conditions or second-order model fitting.

Results and Discussion

The hydroxyl radical reacts with aromatics, preferentially in an addition reaction to form a hydroxycyclohexadienyl radical. It has been reported that the addition is several times faster than α-hydrogen abstraction producing a carbon-centered radical [2]. Figure 1 shows the time resolved spectra of transients being formed after irradiation of a 30 µM oligomer solution. The hydroxycyclohexadienyl radical is characterized by a broad absorption and accounts for the increase of optical absorption at higher wavelengths. Notably, the evaluation under pseudo-first-order reaction conditions, given that the [oligomer] is at least 5 times the [hydroxyl radical], demonstrated that the addition reaction with the oligomer is diffusion controlled with a rate constant of $(1.3 \pm 3)\cdot 10^{10}$ $M^{-1}s^{-1}$. The best-fit curves for the decline of absorption at these higher wavelengths yielded a second-order rate constant in the order of 10^5 $M^{-1}s^{-1}$ for both the oligomer and the polymer. We attribute the increase of absorbance with a peak at 280 nm to the formation of a recombination product.
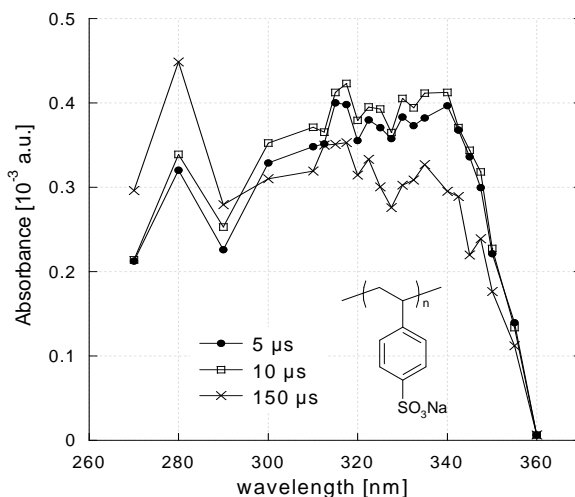
Figure 1. *Time resolved absorption spectra of transients, normalized to 1 Gy, obtained from pulse irradiating 30 µM poly(sodium styrene sulfonate) with polymerization degree n=6, N$_2$O-saturated solution at pH 6.*

Carbon-centered radicals, whether formed by an addition reaction or a hydrogen abstraction, react efficiently with dioxygen to produce peroxyl radicals with rate constants around 10^9 $M^{-1}s^{-1}$. Peroxyl radicals undergo a variety of well known decomposition reactions, some of which are depicted in Figure 2 [3].
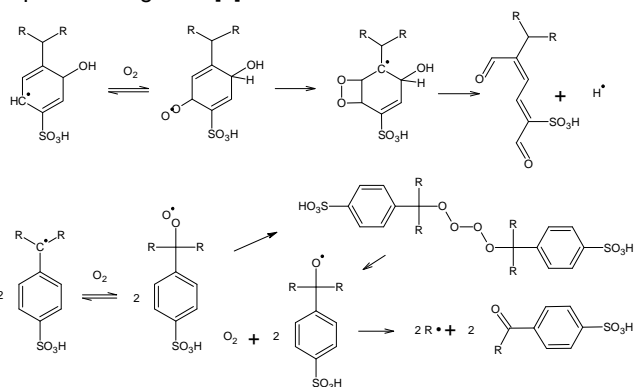
Figure 2. *A selection of subsequent reaction steps of peroxyl radicals, a) resulting in ring opening, and b) leading to chain scission.*

Conclusions

Especially electron rich compounds such as aromatics are susceptible to attack by the strongly oxidising hydroxyl radical. Due to its high reactivity, this radical species generates an organic radical. Subsequent reaction steps involve formation of peroxyl radicals, which lead to direct chain scission in the case of membranes based on poly(styrene sulfonic acid).

References

[1] T. Nauser, R.E. Bühler, J. Chem. Soc. Faraday Trans. **90**, 3651 (1994).

[2] D. Behar, J. Rabani, J. Phys. Chem. **92,** 5288 (1988).

[3] C. von Sonntag, H. Schuchmann, Angew. Chem. **103**, 1255 (1991).

---

[1] ETH Zürich

MICROSTRUCTURED PROTON CONDUCTING MEMBRANES BY SYNCHROTRON RADIATION INDUCED GRAFTING

P. Farquet, C. Padeste, M. Börner[1],
H. Ben Youcef, S. Alkan-Gürsel, G.G. Scherer,
H.H. Solak, V. Saile[1], A. Wokaun
+41 56 310 2580
patrick.farquet@psi.ch

Radiation-grafted proton-conducting polymers are promising candidates to replace the highly expensive Nafion®-separator membranes used in fuel cells [1]. Under operation conditions, mechanical stress caused by temperature, pressure, and water gradients can induce membrane tear leading to failure of the fuel cell. Selective irradiation of mechanically robust fluoropolymer films through shadow masks followed by grafting of styrene and sulfonation is a promising method to obtain micro-structured proton-conducting membranes with increased mechanical strength. In such films shaded areas remain un-grafted and conserve the favourable mechanical properties of the pristine film [2, 3].

Experimental

ETFE films of 25μm and 100μm thickness were exposed at ANKA (Angströmquelle Karlsruhe) at the LIGA3 beamline through high aspect ratio nickel shadow masks with 10-15 keV photons. The irradiated ETFE films were grafted using a solution of pure styrene (20%v) in an isopropanol/water mixture with addition of divinyl benzene as a crosslinker (5% (v/v)) in the monomer feed. Grafting reactions were performed under inert atmosphere at 60 °C for grafting with times varying between 105 min and 165 min for the 25 μm films and overnight for 100 μm films. The grafted films were sulfonated by immersing samples in a 2%$_{vol}$ chlorosulfonic acid / dichloromethane solution for 5 hours, then hydrolyzed overnight in a 4g/l NaOH solution, and finally transformed in the protonated form by a 4h immersion in a 2M H_2SO_4. For the scanning electron microscopy (SEM) analysis, samples were dyed with cesium chloride in order to obtain a higher contrast between grafted and un-grafted parts.

Results

In this structured membranes, a perfect discrimination between exposed and shaded areas was observed (Figure 1).
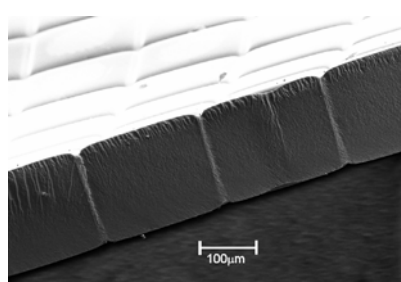
Figure 1. *Cross-section of a structured proton-conducting membrane produced by exposing an ETFE film through a 85 μm thick Ni-grid with 15 μm features (90% opened area), followed by grafting of styrene and suflonation.*

[1] Institute for Microstructure Technology (IMT), Forschungszentrum Karlsruhe, Germany

The grid structure is conserved after grafting all along the film thickness, demonstrating that grafting only occurred in the exposed areas of the film.

Single fuel cell performance for different membranes is shown in Figure 2. The cells were operated at a constant current voltage (0.5A/cm^2) until total failure due to excessive gas crossover occurred. The cell operated with an un-structured membrane showed a performance identical to the Nafion 112 one (Fig. 2). A fuel cell containing a structured membrane shows a twice higher ohmic resistance but with only a 10% loss of performance compared to the un-structured one. This difference in cell resistance between the two grafted membrane is assigned, first as a difference in internal resistance due that structured ETFE features are not contributing for the proton transport and second, to a higher contact resistance because the 3 dimensional grid shape affects its adhesion with the electrode.
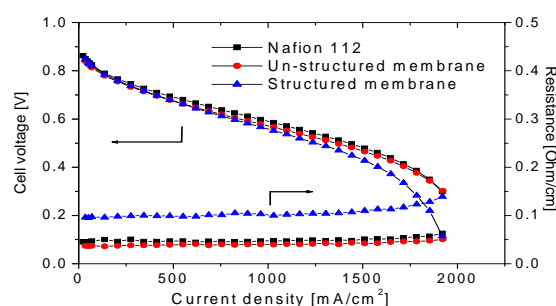
Figure 2. *Single cell performance after 150 hours of a reference Nafion 112 membrane ■ and of a structured ▲ and an un-structured membrane •: 25 μm ETFE exposed at ANKA and grafted with styrene/DVB achieving 35% of degree of grafting. Electrodes: E-TEK 0.6 mgPt cm^{-2}, cell temperature: 80 °C, reactants: H_2/O_2 at a stoichiometry of 1.5/1.5, gas pressure 1 bar, gases fully humidified.*

For both tested membranes a slight increase of the ohmic resistance of the membrane was observed over the time of operation. A tremendous loss in cell performance, coinciding with a sudden MEA failure, occurred at 580 hours for the structured membrane and 320 hours for the un-structured one. Post-mortem analysis revealed high degree of degradation (>70%) at the cathode side of the membrane. However, the structured membrane showed a much smaller cathodic degradation area, it appears that degradation was confined in finite areas separated by the ungrafted ETFE features.

High photon energy beams with high fluence produced by synchrotron facilities allow fast exposures at LIGA beamlines through Ni shadow masks. The synthesized microstructured membranes showed clear distinction between grafted and non-grafted parts. The tested structured proton conducting membrane showed a longer lifetime and only localized chemical degradation due to structuring than the respective un-structured one. However, structuring resulted in a slightly lower performance. Those results have to be confirmed by further experiments.

References

[1] L. Gubler, S.A. Gürsel, G.G. Scherer, Fuel Cells **5**, 317-335 (2005).

[2] H.P. Brack, C. Padeste, M. Slaski, S.A. Gürsel, H.H. Solak, J. Am. Chem. Soc. **126**, 1004-1005 (2004).

[3] S.A. Gürsel, C. Padeste, H.H. Solak, G.G.. Scherer, Nucl. Instr. Meth. Phys. Res. B **236**, 449-455 (2005).

CO_2 SEPARATION MEMBRANE PERFORMANCE MONITORING WITHIN THE NANOGLOWA PROJECT

H.C. Zellweger, A. Wokaun, G.G. Scherer, I.A. Schneider
+41 56 310 2165
hans.zellweger@psi.ch

The goal of the European Union project NanoGLOWA, which is short for *nano membranes against global warming*, is the reduction of CO_2 emissions as required by the Kyoto protocol. The combustion of fossil energy sources causes 13% of the European CO_2 emissions. By the Kyoto protocol it is required to reduce the emissions by 8% till 2010, which can be achieved by the separation of 50% of these emissions [1]. To meet these requirements, the goal of the project is the development of nanostructured membranes for CO_2 capture from power plants with process costs below 20 Euro/ton CO_2. The installed membranes should be monitored with a build-in, smart, diagnostic technique based on AC impedance response. Suitable, reliable, and economical membranes are currently non-existing. The on the market available state-of-the-art technology is still very expensive. Current techniques like liquid sorption, cryogenic distillation, and solid sorption of CO_2-capture vary between 30 and 60 Euro/ton CO_2 [2]. Also, the energy consumption of 25% of the produced electrical power should be reduced to 8%. From the economical point of view, the development of nanostructured porous material membranes has large scale production prospects. The project goal is not just to develop and to test the materials in the laboratory but also in the field. For this reason, it's foreseen to test at least 3 suitable membrane types and to develop application modules, which are appropriate to be implemented in 4 different fossil-fired power plants. The organization of training activities and workshops (membrane development, production, emission reduction, and future power plant design for low CO_2 emission) is as well taken into account as the establishment of new industries, with an increase of global competitiveness of the European membrane industry. Fruitful spin-offs from the project can be expected in the fields of nanomaterials and membranes (catalysis, polymer chemistry, waste treatment, cost reduction for hydrogen production). The project includes 26 partners from 14 countries [3].

The Project

The first step is the membrane development with the goal to lower the cost price for the membranes and to increase the performance. The following membrane types are investigated: Diffusion transport membranes, fixed-site carrier-type membranes, ionomer high voltage membranes, carbon molecular sieve membranes, and ceramic membranes. The second step is the smart module development for large flow with low degradation. At the same time the process will be developed, which solves the module integration into a power plant. Finally, the prototypes will be tested in four fossil-fired power plants. Beside the above mentioned process steps, a diagnostics tool will be developed to *in situ* monitor the performance of the membranes.

The Diagnostic Workpackage

The goal of the diagnostic work package (Figure 1) is the development of an inspection method based on AC Impedance Spectroscopy (IS) to continuously monitor long term stability, ageing, and fouling of the membranes during industrial applications. Further, a laboratory scale monitoring method is investigated for characterization of membranes *in situ* with AC impedance measurements. The correlation between the impedance response and the behavior of molecular amino groups, grafting layer, and water changes as well as pore size reduction and their influence of the performance will be carried out. This includes the development of a dielectric sensor based on a ceramic substrate, which guarantees the robustness and reliability in the prevailing flue gas environment. With the ability to detect changes in the bulk behavior of the membrane as well as possible fouling (gypsum, fly ash contamination), it can be distinguished between harmful and un-harmful ageing. The measurement system will be validated under laboratory and industrial operation conditions and characterized in order to optimize process conditions.

Figure 1. *Further news are presented on the webpage www.nanoglowa.com*

The leader of the Workpackage is the PSI, which is also responsible for the construction of a laboratory set up to simulate the flue gas conditions by different mixtures of gases. Then AC impedance measurements will be conducted on membranes under these controlled flue gas conditions. Further, electric field distribution within the sensor will be modeled with focus of the impact of fouling effects (scaling, layer deposition, corrosion, etc.), which will lead to the definition of test parameters and "environmental" conditions of the sensor. For the Sensor development the project partner Laser Zentrum Hannover (LZH) has investigated a procedure to engrave the electrode structure by laser ablation. The final equipment development and the integration into the power plants will be managed by the project partner from Greece, the Integrated Aerospace Corporation (INASCO). This step will be accompanied by the Dutch coordinator KEMA, which is in charge of the testing and integration. Further, updates and information are available on the webpage www.nanoglowa.com.

References

[1] R. Quadrelli, S. Peterson, The energy-climate challenge: Recent trends in CO_2 emissions from fuel combustion, Energy Policy **35**, 5938-5952 (2007).

[2] U.S. Department of Energy, Carbon Sequestration Research and Development, December 1999.

[3] Sixth Framework Programme, Nano Membranes against Global Warming – "Description of Work", September 2006.

FUEL CELLS

DIAGNOSTICS

IMPEDANCE RESPONSE OF THE PROTON EXCHANGE MEMBRANE IN POLYMER ELECTROLYTE FUEL CELLS

I.A. Schneider, M.H. Bayer, A.Wokaun,
G.G. Scherer
+41 56 310 2795
ingo.schneider@psi.ch

Perfluorinated proton exchange membranes are used in Polymer Electrolyte Fuel Cells (PEFCs) as the proton conducting electrolyte. The ionic conductivity of the membrane is governed by the local water content and can be determined via ac impedance: At high modulation frequencies, the ac voltage drop across the interfacial electrode impedance of cathode and anode becomes negligibly small and consequently, the high frequency resistance is used as a measure for the membrane resistance.

However, towards lower modulation frequencies, the ac voltage drop across the interfacial electrode impedance cannot be neglected and, consequently, the hydration state of the membrane can change due to varying water drag at the anode, and changing water concentration at the cathode. As an important consequence, the low frequency impedance response of the proton exchange membrane cannot be assumed to show the behavior of a pure resistor under conditions where the ionic conductivity of the membrane is a function of cell current, especially in case that thick membranes are used or when the cell is operated under low-humidity conditions.

Principle of Measurement

In analogy to the high frequency resistance R, which is commonly used as a measure for the membrane resistance, we define a more general complex impedance $Z_R(\omega)$, which is used here as a measure for the membrane impedance. The definition of $Z_R(\omega)$ takes into account (Eq 1) that the voltage response of the membrane and therefore, the time dependent voltage drop $\eta_R(t)=R(t)i(t)$ over R can show complex values at lower modulation frequencies, as a consequence of a changing hydration state of the solid polymer electrolyte with ac current $i_p(t)$.

$$Z_R(\omega) = \frac{\eta_R(\omega)}{i_p(\omega)} = \frac{F\{R(t)i(t)\}}{F\{i_p(t)\}} \qquad [1]$$

Experimental

Both, current step and ac impedance measurements were performed in galvanostatic mode in a linear 63cm^2 PEFC [1]. The experimental conditions are shown in Figure 1a. In both types of experiment, a sinusoidal high frequency current (f_{hf}=1kHz) was superimposed to the cell current for the simultaneous determination of the high frequency resistance R. The complex impedance $Z_R(\omega)=\eta_R(\omega)/i_p(\omega)$ was calculated after discrete Fourier transform of $\eta_R(t)$ and $i_p(t)$. The complex impedance of the cell $Z(\omega)=\eta(\omega)/i_p(\omega)$ was calculated after discrete Fourier transform of the time dependent voltage response of the cell $\eta(t)$ and $i_p(t)$.

Results

This work was highly motivated by results obtained earlier in our laboratory using simultaneous local EIS and neutron radiography in PEFCs [2]. These measurements have shown that drying in parts of the cell did not only result in higher values for the local high frequency resistance, but

was always associated with the formation of a large low frequency inductive loop (f≲1Hz) in the local impedance spectra of the dry region. However, the low frequency inductive loop was virtually absent in the local spectra of the flooded region of the cell and therefore, the appearance at low humidity operation could be associated with the process of hydration of the polymer electrolyte by product water. The impedance spectra obtained in this work (Figure 1a) show the same trend.
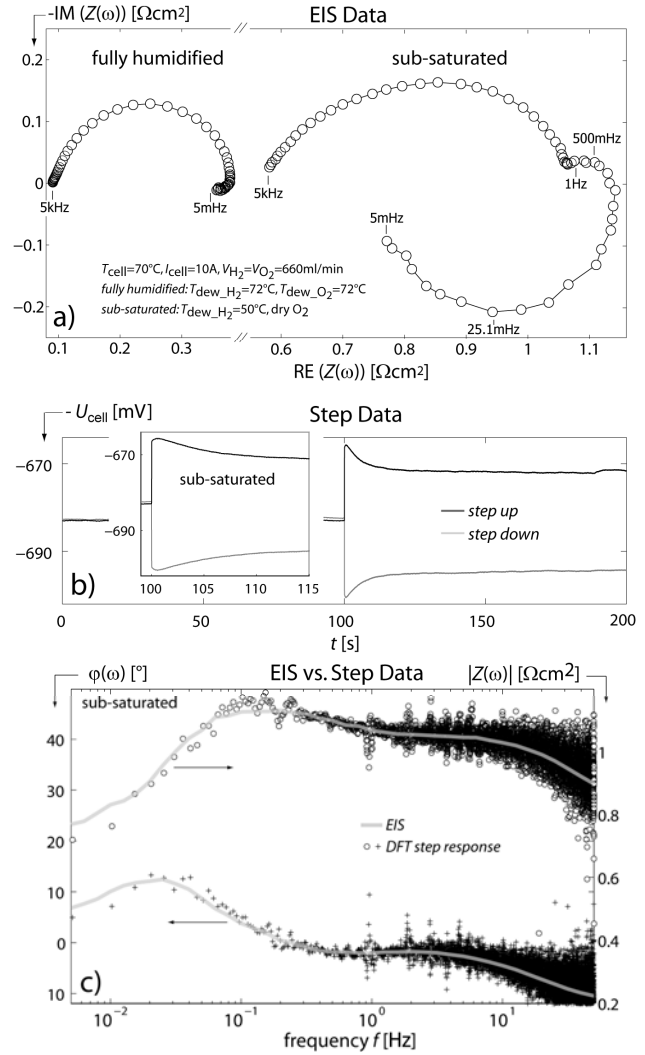
Figure 1. (a) EIS data (5mHz≤f≤5kHz, 10pts/sec), (b) transient response cell voltage, (c) Fourier transformed step data vs EIS.

The result of step experiments (Figure 1b, 1c) obtained under the same conditions reveals that the slow process associated with the formation of the inductive loop at low humidity (Figure 1a) lowers the overall polarization losses towards higher current density and therefore, could be related to the hydration of the ionomer by product water. In this context note that, the cell voltage responds virtually instantaneously under fully humidified conditions (not shown here).

The contribution of losses from changing iR drop to the overall transient response of the cell voltage (Figure 1b) can be identified by evaluating the transient response of the high frequency resistance (Figure 2a). As presented in Figure 2b the iR polarization losses decrease significantly after the step. This effect is a consequence of slow hydration of the ionomer by product water after the current step and can account by far for the slow decay of the cell voltage at low humidity as shown in Figure 1b. As an

important result, the formation of the low frequency inductive loop in the impedance spectrum at low humidity (Figure 1a) is associated with the hydration of the ionomer by the product water formed at the cathode.
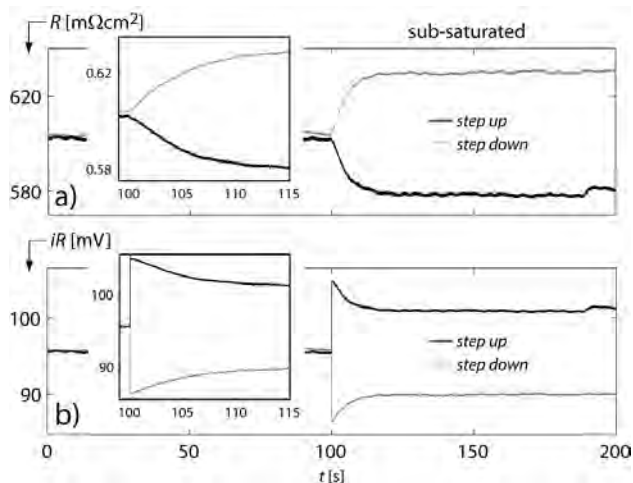
Figure 2. (a) Transient response of R and, (b) calculated iR drop (200pts/sec) for sub-saturated operation of the cell.

The complex impedance response of $Z_R(\omega)$, which is characteristic for the impedance response of the proton exchange membrane can be calculated with knowledge of $\eta_R(t)$ and $i_p(t)$ by using Equation 1. The time dependent voltage drop $\eta_R(t)=R(t)i(t)$ over R was obtained by the measurement of the high frequency resistance $R(t)=R_{ss}+R_p(t)$ and the cell current $i(t)=i_{ss}+i_p(t)$ during the frequency sweep of an EIS measurement (Figure 3).
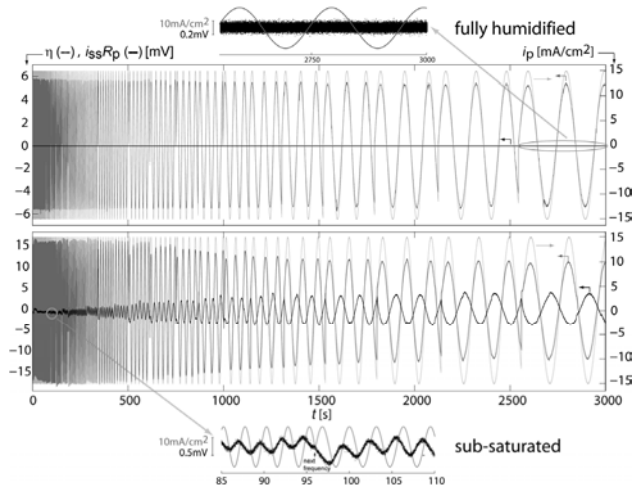
Figure 3. AC perturbation current i_p, ac cell voltage η and ac voltage $i_{ss}R_p$ caused by variation of R ($1Hz \leq f \leq 5mHz$).

Under fully humidified conditions no oscillation could be detected, even at low modulation frequencies (Figure 3). In contrast, at low humidity, the high frequency resistance starts to oscillate already at modulation frequencies of around $f=1Hz$ (Figure 3). The impedance spectra for $Z_R(\omega)$, are shown in Figure 4a ($f=1Hz-5mHz$). Evidently, under fully humidified conditions, the low frequency impedance response of $Z_R(\omega)$ shows a single point on the real axis. The membrane exhibits the characteristic of a pure ohmic resistor even at low frequencies. In contrast, at low humidity, the impedance spectrum of $Z_R(\omega)$ exhibits an inductive loop at low modulation frequencies (Figure 4a). The inductive behavior can be explained by taking into account the slow hydration/dehydration of the ionomer (Figure 2b). Under quasi steady state conditions ($f \rightarrow 0Hz$)

the hydration state of the membrane is virtually identical to the equilibrium value at a given cell current i.e., $R_p(t)$ and $i_p(t)$ are out of phase ($\varphi \approx 180°$) as shown in Figure 3. Yet, towards higher modulation frequencies, the hydration of the ionomer starts to lag the ac current (Figure 3). The increasing phase shift between the ac current $i_p(t)$ and the resistance oscillation $R_p(t)$ towards higher frequencies and therefore the inductive behaviour (Figure 4a) are a result of this effect.

As illustrated in Figure 4c, correction of $Z(\omega)$ by $Z_R(\omega)$ reduces the size of the low frequency inductive loop significantly. This shows, that the inductive response of $Z(\omega)$ is dominated by the impedance of the solid polymer electrolyte $Z_R(\omega)$. Interestingly, after correction, the characteristic frequency of the small residual inductive loop of $Z(\omega)-Z_R(\omega)$ is unchanged. This result indicates that other processes that depend upon the dynamics of membrane hydration with ac current contribute to the low frequency impedance response of the cell $Z(\omega)$. In particular anode kinetics must be taken into account here [3,4], where water is required for the hydration of protons (Eq 2).

$$Pt\text{-}H_{ad} + xH_2O \rightarrow Pt + H(H_2O)_x^+ + e^- \qquad [2]$$
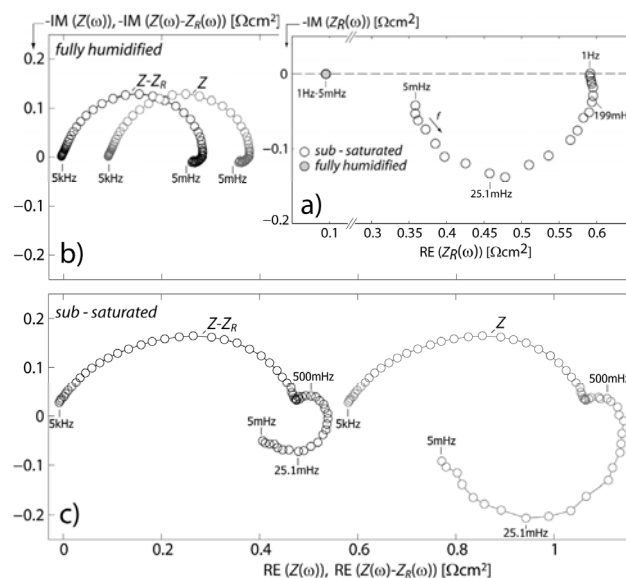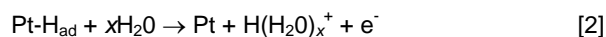
Figure 4. (a) Spectra for $Z_R(\omega)$ (measure for membrane impedance) and, (b,c) original and $Z_R(\omega)$-corrected spectra.

Conclusions

The results show that the formation of the inductive loop at low humidity is associated with the slow uptake and release of water by the bulk of the solid polymer electrolyte. In this context, the appearance of a low frequency inductive loop in the impedance spectrum of a low humidity PEFC is indicative of a limitation of cell performance by the hydration of the ionomer, due to product water formed at the cathode.

References

[1] I.A. Schneider et al., J. Electrochem. Soc. **154**, B770 (2007).

[2] I.A. Schneider et al., Electrochem. Comm. **7**, 1393 (2005).

[3] B. Andreaus et al., Solid State Ionics **168**, 311 (2004).

[4] K. Wiezell et al., J. Electrochem. Soc. **153**, A749 (2006).

MODELING THE IMPEDANCE RESPONSE OF THE PROTON EXCHANGE MEMBRANE IN PEFCS

M.H. Bayer, A. Wokaun, G.G. Scherer,
I.A. Schneider
+41 56 310 5304
michael.bayer@psi.ch

Recent progress made in our laboratory has shown that the formation of a low frequency inductive loop (f<1Hz) in the impedance spectrum of a low humidity PEFC is associated with the effect of water concentration oscillations [1]. At low frequencies the water concentration is no longer constant with ac current. As a consequence, the hydration state, i.e., the ionic resistance of the membrane changes with water concentration and this leads to oscillations in membrane resistance and to a complex impedance response of the membrane.
A model is presented, which is able to describe the experimentally obtained complex impedance behavior of the membrane and the cell impedance qualitatively.

Model and parameters

The model is one dimensional and consists of 8 points in space. The model explicitly calculates the transient response of the water concentration, the cell voltage and the membrane resistance to a load step. The cell impedance $Z(\omega)=\eta(\omega)/i(\omega)$ is obtained from the time dependent cell voltage $\eta(t)$ and the time dependent cell current $i(t)$ after Fourier transform of the time domain data (Eq 1)

$$\eta(\omega) = \int \eta(t)\exp(-i\omega t)dt \qquad [1]$$

The membrane impedance is calculated in the same manner by using the voltage response of the membrane $\eta_R(t)=i(t)*R(t)$ instead of $\eta(t)$.

Model assumptions are:

- The gas concentration in the channels is equal to the concentration at the gas outlets.
- The pressure is constant during the load step. Reactant concentrations are calculated from the water concentration at anode and cathode.
- Channel and electrode gas concentrations are in equilibrium at all times.

In the present work the transient response of η and η_R to a symmetrical current step of 15 mA/cm^2 (duration 240s) was calculated for the operating conditions as stated in [1]. After Fourier transform of the time domain data the minimum frequency is 4.2 mHz. Membrane and diffusion parameters were taken from literature [2-4].

Results

The calculated spectra for the membrane impedance $Z_R(\omega)$, the cell impedance $Z(\omega)$ and the '$Z_R(\omega)$ corrected' spectra $Z(\omega)-Z_R(\omega)$ are shown in Figure 1 for fully humidified and sub-saturated conditions. Though the model makes use of several simplifications, the consistency of modeled and experimental data is impressive. As presented in Figure 1, the membrane impedance Z_R shows a virtually perfect inductive behavior at low humidity at the given operating conditions (thin 50 µm membrane) [1].
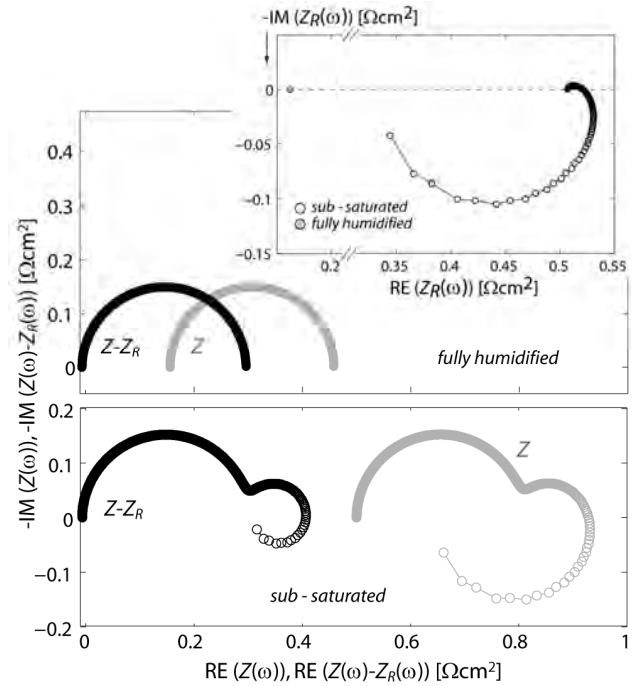
Figure 1. Integral cell impedance Z, membrane impedance Z_R and 'Z_R –corrected' impedance $Z-Z_R$ (4.2 mHz<f<833Hz) for fully humidified and sub-saturated cell operation [1].

The calculated impedance spectra of the cell $Z(\omega)$ were corrected for the membrane impedance $Z_R(\omega)$. As presented in Fig 1, there is still a low frequency capacitive and inductive loop left in the corrected spectrum of $Z(\omega)-Z_R(\omega)$ at low humidity. This is attributed here to a water concentration dependent Nernst potential at the anode (figure 1). For the anode the following reaction scheme is used [5]:

$$H_2 + xH_2O \leftrightarrow 2H_{aq}^+ + 2e^- \qquad [2]$$
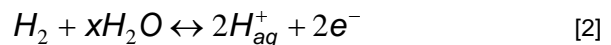
In the model calculation (Figure 1) a stoichiometric factor of x=2.5 was assumed.
Calculations have shown, that thicker membranes can develop also a capacitive behavior at intermediate frequencies (1Hz<f<100mHz), where electro osmotic drag becomes dominant. In addition, water concentration dependent (Nernst) effects, become more relevant for thicker membranes, as a result of the increasing water concentration difference between anode and cathode and the increasing time constant for back diffusion of water from the cathode.

For a quantitative description of the experimental data the model has to be expanded. In particular, a convective flow in the gas channels has to be considered here. However, the low complexity of the present model allows easily to 'switch on/off' single processes. This allows rapid insights into the impact of different processes on fuel cell impedance response.

References

[1] I.A. Schneider, M.H. Bayer et al. (previous article)

[2] T.E. Springer et al., J. Electrochem. Soc **138**, 2334 (1991).

[3] A.A. Kulikovsky, J. Electrochem. Soc. **150**, A1431 (2003).

[4] Y. Wang, C-Y. Wang, Electrochim. Acta **50**, 1307 (2005).

[5] B. Andreaus et al., Solid State Ionics **168**, 311 (2004).

TRANSIENT RESPONSE OF THE LOCAL HIGH FREQUENCY RESISTANCE IN PEFCS

I.A. Schneider, M.H. Bayer, A. Wokaun,
G.G. Scherer
+41 56 310 2795
ingo.schneider@psi.ch

Perfluorinated proton exchange membranes are used in Polymer Electrolyte Fuel Cells (PEFCs) as the proton conducting electrolyte. High water content throughout the membrane is important to achieve good overall proton conductivity. In this context, thin membranes (≤51 m) provide enhanced back diffusion of water from the cathode to the anode, which tends to become dehydrated as water molecules are transferred with the protons formed at the anode towards the cathode. It was shown that anode dehydration occurs at higher current densities and causes an overall increasing membrane resistance when thick membranes (>120μm) are used [1,2]. Yet, this effect was not observed for thin Nafion 112 membranes under steady state conditions [1].

The situation is different under transient conditions. Several models were published in the literature, which scrutinize the transient behaviour of water transport in the membrane [3,4]. Numerical simulations have shown that an abrupt load change might lead to temporary dehydration of the anode even in case of thin membranes when the cell is operated under low-humidity conditions. Yet, this effect is expected to occur on a time scale of some hundreds of milliseconds and no experimental evidence was reported so far. In this work, we have characterized the local transient response of the high frequency resistance to load changes in a low humidity PEFC with a high time resolution of around 1ms.

Results

The local transient behaviour of the membrane resistance obtained under low humidity conditions is demonstrated here for the first time (Fig. 1) in a nine-fold segmented cell with linear flow field [5].
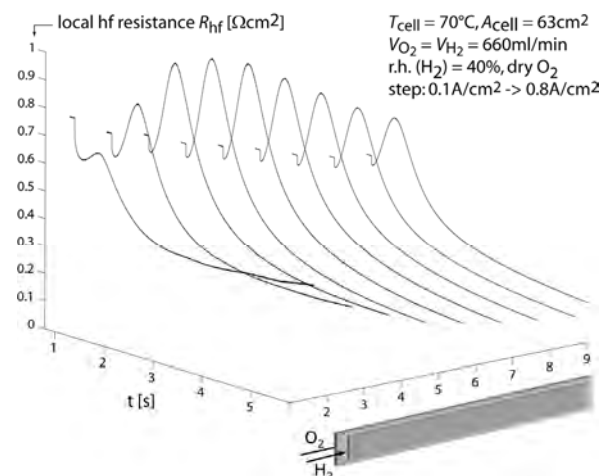
Figure 1. Local transient response of the hf resistance after a current step (MEA: Nafion 111, TKK 70%Pt/C).

The local transient response is governed by two processes: i) depletion of the water content at the anode due to higher electro-osmotic drag from the anode to the cathode after the step, and ii) higher water production rate at the cathode and diffusion of water back into the bulk of the electrolyte.

The results show that even for a thin membrane (thickness 25 μm) the high frequency resistance increases locally within a few hundreds of milliseconds after the step as a consequence of anode drying. Yet, as product water starts to rehydrate the anode the resistance passes a maximum and then decreases within a time frame of around 10 s as a consequence of the improving hydration of the membrane at an overall higher current density.

The transient behaviour of water transport in the membrane, i.e. the interplay between electro-osmotic drag and water back diffusion is further illustrated in figure 2a-c for thin membranes of different thickness.
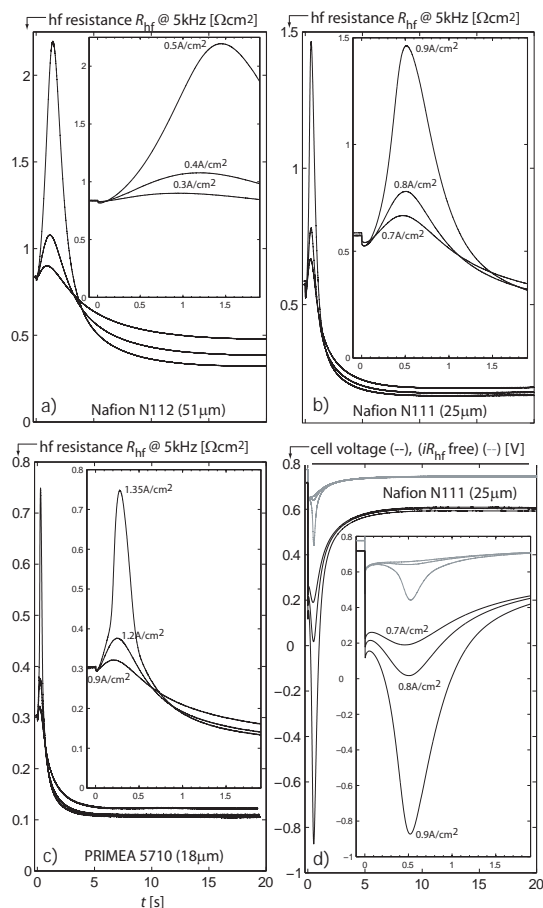
Figure 1. Integral transient response of the hf resistance (a-c) and cell voltage (d) (conditions as stated in Fig 1).

As can be seen in Figure 2a-c the rehydration of the anode occurs faster when the thickness of the membrane material is decreased. Note that in case of the 18μm GORE MEA, the high frequency resistance increases only for large current steps, which emphasizes the overall superior transient behaviour of the thin 18μm membrane under low humidity conditions.

Yet, the voltage loss caused by the increasing resistance after the step contributes significantly to the cell voltage and can cause temporary voltage reversal (Fig 2d) before a new steady state is reached. In fact, instant pinhole formation was observed during the experiments which might be attributed to temporary high local power loss during the transient.

References

[1] F.N. Büchi et al., J. Electrochem. Soc. **148**, A183 (2001).

[2] B. Andreaus et al., Solid State Ionics **168**, 311 (2004).

[3] Y. Wang et al., Electrochim. Acta. **51**, 3924 (2006).

[4] F. Chen et al., J. Electroanal. Chem. **566**, 85 (2004).

[5] I.A. Schneider et al., to be published.

NEUTRON RADIOGRAPHY ON MICRO POLYMER ELECTROLYTE FUEL CELLS

B. Seyfang, P. Boillat, G.G. Scherer, A. Wokaun
+41 56 310 2092
bernhard.seyfang@psi.ch

Micro fuel cells are expected to be a possible replacement for Li Ion batteries as energy source for handheld devices, such as laptops or cell phones. The main reasons are a higher specific energy as well as fast recharge [1]. At PSI, a concept for a Micro PEFC was developed and first cell tests delivered a power density of 425 mW/cm^2 [2]. During operation, irregular water removal form the cell is observed as well as a steep decrease of the cell voltage at a limiting current density of ~1 A/cm^2.

Neutron radiography to detect liquid water in operating PEFCs has been carried out in our laboratory for several years [3]. By application of novel scanning methods, the resolution of the radiograms could be improved substantially such that it is possible to observe water even across the membrane-electrode-assembly (MEA) [4].

Experimental

The micro fuel cell consists of two micro-structured glassy carbon plates, which are separated by a catalyst-coated membrane (Nafion 112; Tanaka catalyst, Pt/C 40%, anode: 0.15 mg$_{Pt}$/cm^2, cathode 0.25 mg$_{Pt}$/cm^2). The seven channel flow fields were shaped in meander form. To distinguish between the particular channels in in-plane mode, a horizontal meander was chosen. A special housing was designed for neutron radiography experiments. Here, material of choice is aluminium, due to its low interaction with neutrons.
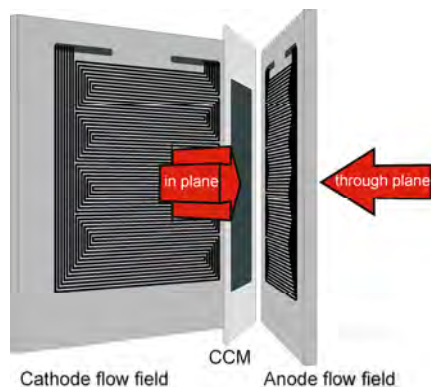
Figure 1. Two flow fields with a horizontal seven channel structure and a CCM in between. The arrows show the direction of the neutron beam.

Neutron radiography experiments were carried out at the ICON beamline of the spallation neutron source SINQ at PSI. By tilting the neutron detector, a resolution of up to 2.5 μm/pixel could be achieved across the MEA plane [4].

The fuel cell was operated at a temperature of 50°C during all experiments; the gases had a relative humidity of 80 %; stoichiometries were 1.7 for H$_2$ and 2.1 for O$_2$.

Results

The irregular water removal from the cell, which is described above, is accompanied by fluctuation in both, the cell voltage and the pressure drop along the flow fields. This behaviour can be studied by through-plane neutron radiography. The two micrographs in Figure 2 were recorded at a current density of 750 mA/cm^2. On the left hand side, one can easily see two channels that are filled with water. Twelve minutes later, when we recorded the radiogram on the right hand side, only one channel is filled with water. Quantification of the signal reveals that the channels, which are 110 μm deep, are completely filled with water.
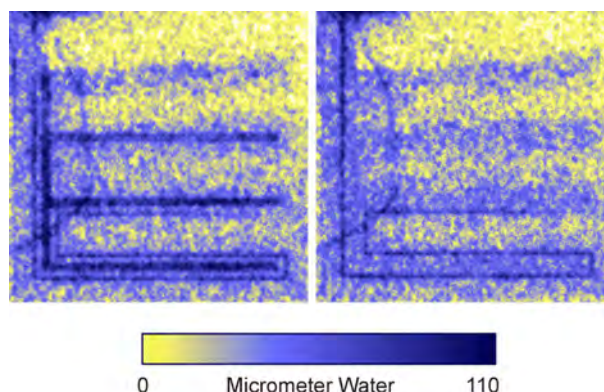
Figure 2. Radiograms (through plane) recorded at 750 mA/cm^2 and a time difference of 12 minutes (left to right). The inner channel is completely filled with water (left), while it has been removed at once (right).

We assume that mass transport is hindered at these spots and the reaction continues in non flooded areas of the cell, until water accumulates there too, leading to a draining of the completely filled channels, due to the increased pressure drop.
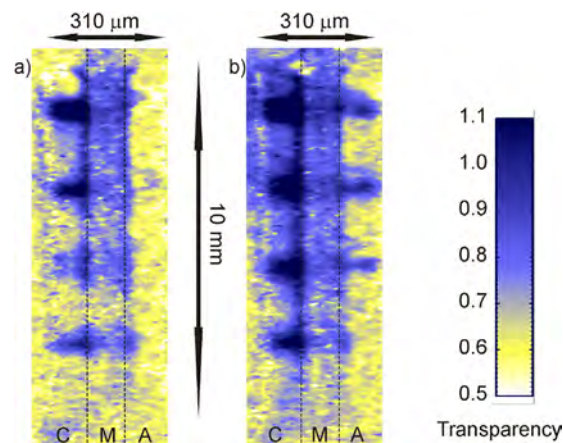
Figure 3. Radiograms (in plane) recorded at 250 (a) and 750 mA/cm^2 (b). On the cathode side, a water layer is visible at the boundary of cathode flow field (C) and membrane (M).

The steep decrease of the cell voltage at a limiting current density of ca. 1 A/cm^2 can be explained by another effect. In-plane neutron radiography gives evidence that a water layer is formed at high current densities directly on the catalyst layer (Fig.3). As a consequence, the access of gas to the active sites is hindered.

References

[1] C.K. Dyer,.J. Power Sources **106**, 31-34 (2002).

[2] B. C.Seyfang, M. Kuhnke, T. Lippert, G.G. Scherer,. A. Wokaun, Electrochem. Comm. **9**, 1958-1962 (2007).

[3] D. Kramer, J. Zhang, R. Shimoi, E. Lehmann, A. Wokaun, K. Shinohara, G.G.Scherer, Electrochim. Acta **50**, 2603-2614 (2005).

[4] P. Boillat, D. Kramer, B.C. Seyfang, G. Frei, E. Lehmann, G.G. Scherer, A. Wokaun, Y. Ichikawa, Y. Tasaki, K. Shinohara, Electrochem. Commun. **10**, 546-550 (2008).

RELATIONSHIP BETWEEN GAS FLOW HUMIDITIES, WATER DISTRIBUTION, AND PERFORMANCE IN A PEFC AT A LOCAL SCALE

P. Boillat, G.G. Scherer, G. Frei, E. Lehmann, A. Wokaun
+41 56 310 2743
pierre.boillat@psi.ch

Water management is a critical topic in Polymer Electrolyte Fuel Cells (PEFCs): Water is required for the proton conductivity of the electrolyte, but can impede the access of gaseous reactants to the respective interfaces. Therefore, knowledge of the relationship between local operating conditions (e.g. gas flow humidities), water distribution and cell performance is of high interest for the improvement of this technology. Taking advantage of the recent improvements in spatial resolution realized at the ICON neutron radiography beamline of the SINQ spallation source at PSI [1,2], this relationship was studied to give a new in-sight in the transport processes occurring in an operating PEFC.

Experimental

A new fuel cell was designed, which allows in plane imaging with the flow channels parallel to the neutron beam, as shown in Figure 1. Thus, it is possible to distinguish in the in plane images the areas under the ribs and under the channels of the flow fields. The flow fields were made of 4 parallel flow channels machined into graphite plates (Sigracet BMA 5, SGL Carbon Group, Germany), with rib and channel width of both 1mm and channel depth of 0.5mm. The active area was 0.5cm x 1cm. The membrane electrolyte assembly (MEA) was symmetrical and consisted of a catalyst coated membrane (Nafion 112 with 0.5mgPt/cm2 on each side, Paxitech, France) plus carbon cloth gas diffusion layers (GDL) including a microporous layer (Elat LT1400W, Pemeas E-Tek, USA). The cell was sealed using PTFE gaskets.
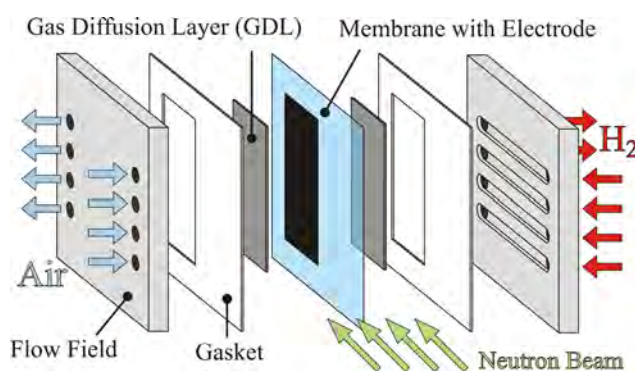
Figure 1. *Design of the fuel cell for in plane imaging (active area is 0.5 cm2). For the sake of simplicity the cell housing is not shown here.*

This cell can be seen as a differential cell, meaning it is not intended to be operated as technical device but is used as a model cell to approximate local conditions in a technical sized fuel cell. Therefore, the gas flows are fixed to generate flow velocities in the same range as those of a technical fuel cell, not to correspond to realistic stoichiometries.

In order to study the effect of liquid water quantity and distribution on the cell performance, the cell was kept working at a current density of 1 A/cm2, while varying separately the humidification of the anode and cathode gas flows. A total of 35 combinations of relative humidities ranging from 60% to 110% on the anode side and from 0% to 110% on the cathode side were tested (110% "relative humidity" means that also some liquid water is brought into the cell). The cell was operated on H2 and air at a constant temperature and pressure of respectively 70°C and 2 bars absolute.

Results and Discussion

The radiograms corresponding to three selected conditions are show in Figure 2. At middle humidity levels (Figure 2b), a strong separation of the water content can be observed in the cathode side GDL, virtually all liquid water being concentrated under the ribs. At higher humidities (Figure 2c), the distribution is more homogeneous and the trend is even inverted: the water content is slightly higher under the channels than under the ribs.
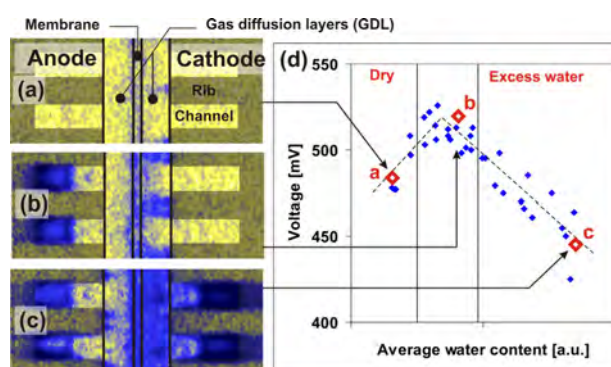
Figure 2. *(a-c) In plane Neutron Radiograms of a PEFC showing the water distribution at 1A/cm2 for different inlet relative humidities at the anode/cathode: (a) 60% / 0% (b) 110% / 40% (c) 90% / 110%; (d) relationship between average water content and cell performance.*

The relationship between the average water content in the MEA and the cell voltage is shown in Figure 2d by plotting these values for the 35 different conditions tested. As expected, both, excessively dry (Figure 2a) and excessively wet (Figure 2c) conditions have a negative impact on cell performance.

Conclusion

In plane neutron radiography was used successfully for unravelling the correlations existing between operating conditions, water distribution, and cell performance. For the materials combination used here, a strong effect of the rib/channel structure on the water distribution in the gas diffusion layers was observed and the correlation between water content and performance was established.

References

[1] E.H. Lehmann, G. Frei, G. Kühne, P. Boillat, Nucl. Instrum. Meth. A 576, 389 (2007).

[2] P. Boillat, D. Kramer, B.C. Seyfang, G. Frei, E. Lehmann, G.G. Scherer, A. Wokaun, Y. Ichikawa, Y. Tasaki, K. Shinohara, Electrochem. Comm., in print (2008).

FUEL CELL MEMBRANE DEGRADATION IN CHANNELS AND LANDS UNDER DIFFERENT OPERATING CONDITIONS

L. Gubler, M. Schisslbauer[1], G.G. Scherer
+41 56 310 2673
lorenz.gubler@psi.ch

Current limitations in polymer electrolyte fuel cell (PEFC) technology are insufficient durability and reliability of the materials and their high cost. PSI is developing fuel cell membranes based on the radiation grafting technique, which are potentially cost-effective and allow tailoring of the composition in a wide range. We have shown that the degradation of the membrane, caused by the loss of the fixed ionic sites, is not homogeneous over the electrochemically active area [1]. In particular, there appear to be distinct differences in the extent of degradation between membrane regions facing channel and land areas of the flow field (Figure 1). In the study reported here, the effect of operating conditions and membrane type were more thoroughly investigated.
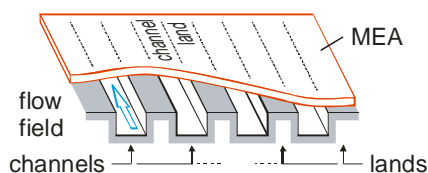
Figure 1. *Schematic of the single cell configuration. The membrane electrode assembly (MEA) is sandwiched between two flow field plates (only bottom plate shown) for distribution of reactant gases through channels and current collection via lands.*

Experimental

A series of styrene grafted and sulfonated PSI membranes based on 25 μm FEP films were artificially aged in single cell tests and, subsequently, analyzed using infrared spectroscopy for the extent of degradation in regions associated with channel and land areas of the flow field [1].

To maximize effects of different operating conditions in channel and land areas, a cell with 2 mm wide channels and lands, respectively, was used (16 cm^2 active area).

Tests were carried out with uncrosslinked membranes (*g*-FEP) and crosslinked ones (*g*-FEP **XL**) as model systems. The operating conditions were 80 °C cell temperature, H$_2$ / air reactant, 3 bar$_a$ pressure and 50 % relative humidity. One set of experiments was carried out at open circuit voltage (OCV). For high current density aging, the *g*-FEP **XL** membrane was operated at a constant voltage of 0.2 V (resulting current density ~0.5 A/cm^2), for the (uncrosslinked) *g*-FEP membrane, fully humidified H$_2$ / O$_2$ was used to enable operation at 2.25 A/cm^2.

Results

Through comparison of the infrared band intensity of sulfonic acid groups in the membrane before and after the aging test, the extent of degradation can be determined. Local analysis in channel and land areas was possible through the use of a slit mask. As an example, the local degradation in the *g*-FEP membrane operated at high current density is shown in Figure 2. The degradation in regions associated with lands appears to be substantially higher compared to channel areas.
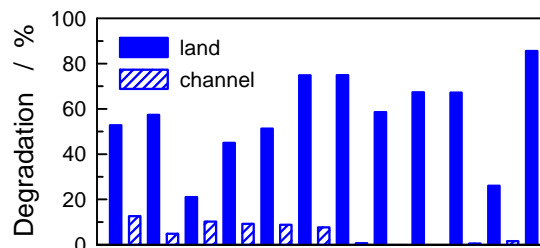
Figure 2. *Local degradation analysis of an uncrosslinked PSI membrane operated at a current density of 2.25 A/cm^2 for 142 h.*

membrane	OCV		high current	
	land	channel	land	channel
g-FEP **XL**	593 h / 8 %	18 %	285 h / (0 %)	(0 %)
g-FEP	531 h / 69 %	76 %	142 h* / 57 %	5 %

*test stopped due to membrane failure (pinhole formation)

Table 1. *Overview of local membrane degradation for crosslinked (XL) and uncrosslinked PSI membranes operated at open circuit voltage (OCV), i.e. no current, and at high current, respectively. The denoted times in hours indicate the duration of the test.*

The overview of the *post mortem* analysis is presented in Table 1. Following insights can be gained from the results:

- Degradation is lower in crosslinked membranes. Crosslinking is an effective means to improve membrane durability [2].
- On average, the degradation rate is higher at OCV. OCV hold tests are therefore often used as accelerated tests to assess chemical membrane stability.
- Under OCV conditions, higher degradation is observed in the channel areas compared to the land areas. This could be a consequence of higher local reactant concentration in the channel areas.
- No degradation following high current operation was observed for the crosslinked membrane. However, the uncrosslinked membrane showed substantial degradation in the land areas, whereas degradation was almost negligible in channel areas. This contrasts with the result obtained at OCV. The reason for this partitioning is unclear at this point. It may be related to the local differences in operating conditions (current density, temperature, potential, reactant, and water concentration).

Understanding fuel cell membrane degradation on a local scale is essential in gaining insight into fundamental aging mechanisms and their correlation with local operating conditions influenced by flow field geometry.

References

[1] L. Gubler, R. Müller, G.G. Scherer, PSI Electrochemistry Annual Report 2006, 20, ISSN-1661-5379 (2007).

[2] T.J. Schmidt, K. Simbeck, G.G. Scherer, J. Electrochem. Soc. **152**, A93-A97 (2005).

---

[1] Fachhochschule Amberg-Weiden, Germany

UNDERSTANDING THE DIFFUSIVITY OF GAS DIFFUSION LAYERS BY MEANS OF A UNIT CELL MODEL

R. Flückiger, D. Kramer, G.G. Scherer, A. Wokaun, F.N. Büchi

+41 56 310 4189

reto.flueckiger@psi.ch

Gas diffusion layers (GDLs) in Polymer Electrolyte Fuel Cells are collecting current from the catalyst layers and simultaneously allow access of gases to the reaction zones. Especially at high current densities the gas diffusion is strongly hindered under the ribs of the flowfield.

The influence of PTFE and Micro Porous Layer treatment on the anisotropic, effective diffusivity of different carbon paper GDLs has been experimentally investigated for the first time [1]. For this investigation a novel electrochemical diffusimetry method was applied and further developed [2]. The measured relationship between effective relative diffusivity and porosity was correlated with a unit cell model in order to abstract the results and support further optimization. The unit cell consists of two regularly spaced ellipsis representing fiber sections and in-plane (*ip*) and through-plane (*tp*) oriented flaps. For more complex materials a secondary porosity ε_s was introduced. The width was adapted to meet the porosities of the measurements at different compressions. The effective diffusivity of the unit cell was calculated with conformal maps [3]. Finally there were three fit parameters. These parameters could be attributed to GDL structural properties. H_B was associated with binder agglomerated in the corner of crossing fibers. H_A was correlated to PTFE that is clogging the *ip* diffusion while the secondary porosity was interpreted as an intrinsic property of the binder.

Results and Discussion

The resulting unit cell geometries and the corresponding diffusivities are compared with the measured data in Figure 1. The fit parameters are indicated in the figure. The predicted curves match the measured data above a relative thickness of about 50%. At stronger compressions the unit cell quickly approaches a percolation threshold where the diffusion halts. In reality the percolation threshold porosity is lower than predicted by the unit cell model due to structural deformations.

In order to fit the basic Toray GDL material without PTFE (TGP-H-060) the *ip* flap length H_B was sufficient. With increasing PTFE content both *ip* and *tp* flap lengths are growing reducing diffusivity in both directions. Consequently an optimum PTFE content is expected. For SIGRACET® GDL25 with a high binder content, the secondary porosity was required. The small anisotropy of this material is given by the large amount of isotropic binder and similar *ip* and *tp* flap lengths.

Conclusion

The unit cell model provides a simple and useful tool for abstraction and correlation of measured diffusivities with GDL structures. It contributes to the understanding and further optimization of GDLs.
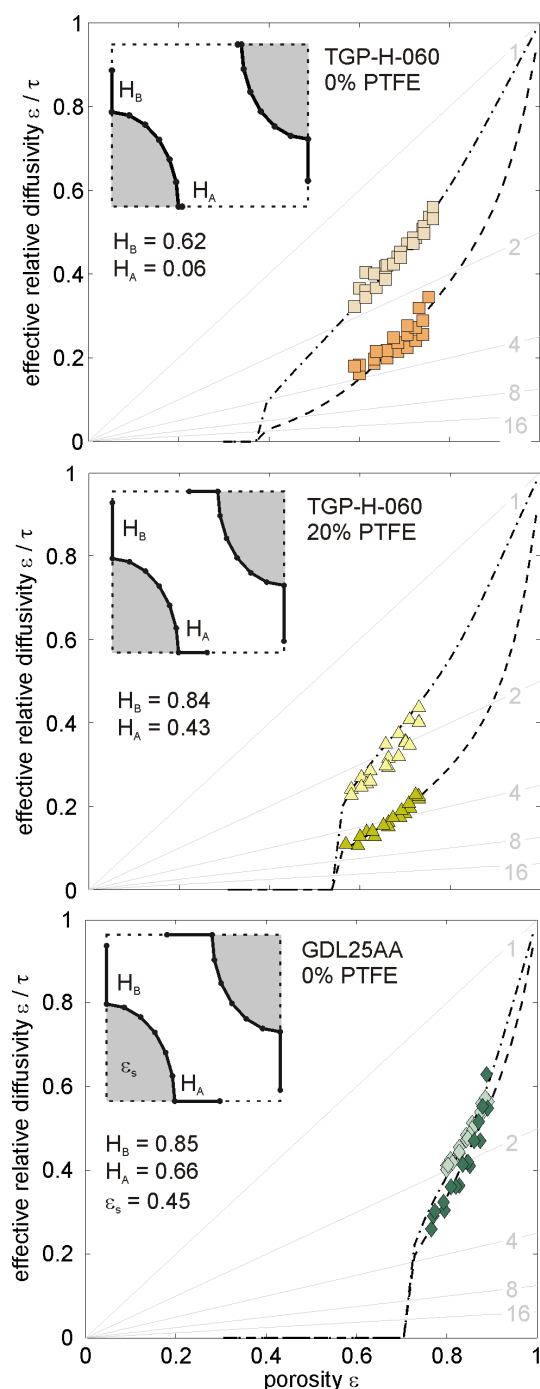
Figure 1. *Unit cell and measured diffusivities as a function of porosity. Dashdoted lines represent ip and dashed lines tp diffusivites of the unit cell. The insets show the real, uncompressed unit cell configuration. The gray lines are iso-tortuosity levels.*

References

[1] R. Flückiger, S.A. Freunberger, D. Kramer, G.G. Scherer, A. Wokaun, F.N. Büchi, PSI Electrochemistry Annual Report 2006, 27, ISSN-1661-5379 (2007).

[2] D. Kramer, S.A. Freunberger, R. Flückiger, I.A. Schneider, A. Wokaun, F.N. Büchi, G.G. Scherer, J. Electroanal. Chem., **612**, 63-77 (2008).

[3] Tobin A. Driscoll, J ACM Trans. Math. Softw., **22**, 168-186 (1996).

HARDWARE IN THE LOOP EMULATION OF FUEL CELL HYBRID VEHICLES

J. Bernard[1], S. Delprat[1], T.M. Guerra[1], R. Kötz, F.N. Büchi
+41 56 310 2411
felix.buechi@psi.ch

In a Fuel Cell Hybrid Vehicle (FCHV), the fuel cell system is power assisted by an energy buffer (battery or supercapacitor). The hydrogen consumption and the vehicle dynamic performances therefore rely on the one hand on the power management strategy and on the other hand on the energy buffer specifications (specific energy, specific power, efficiency). To analyse these aspects, a test bench has been developed to emulate the energy flows in a FCHV and component properties on a reduced scale.

Experimental setup

The hardware-in-the-loop (HiL) test bench is split into two distinct sets as shown in Figure 1:

1. Emulation: the vehicle is simulated by a computer and the motor power demand is reproduced by an electronic load and power supply. Simulation of "kinetic" energy recovery is also possible.

2. Hardware: the core is a 1kW fuel cell system (PowerPac [1]); the energy buffer is either a battery or a supercapacitor.

In the setup, the bus voltage is imposed by the energy buffer and the fuel cell system power is controlled with a DC/DC converter. For the vehicle emulation, the power demand simulated on the computer is scaled according to the power capabilities of the hardware. In addition to the vehicle simulation, the computer is also used for system monitoring (fuel cell system temperature, stack pressure…), data acquisition, and integrates high level controls such as the power management strategy.
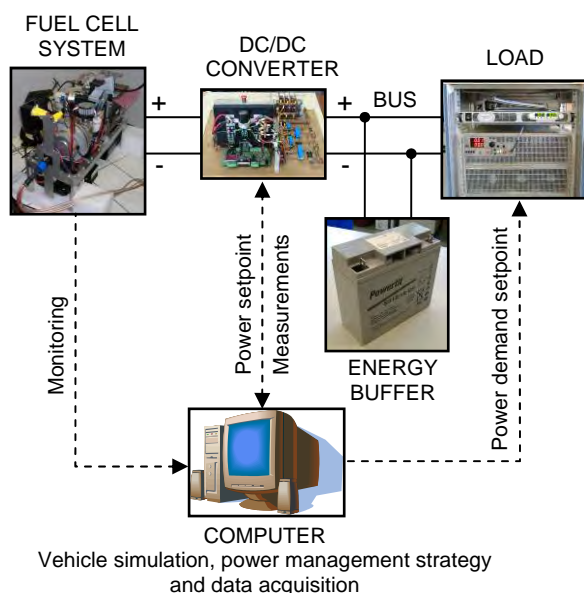
Figure 1. *Experimental setup of the hardware in the loop test bench.*

[1] Laboratoire d'Automatique, de Mécanique et d'Informatique Industrielle et Humaine, UMR CNRS 8530, Université de Valenciennes et du Hainaut-Cambrésis, France

Results

A – Power management strategy

The goal of the control strategy is to define an instantaneous power split between the fuel cell system and the energy buffer; it should fulfil the motor power demand while respecting the hardware constraints and minimizing the hydrogen consumption. The considered strategies are charge sustaining, i.e. the energy buffer is never recharged externally. The results shown in Figure 2 were achieved with a predictive control strategy derived from optimal control theory [2, 3].
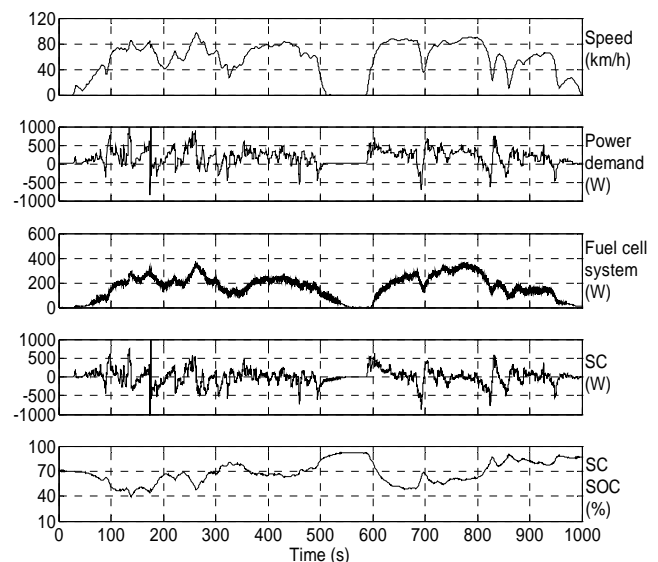
Figure 2. *Simulation of light duty vehicle (1600 kg) driving outer-urban cycle. Scaled HiL powertrain: fuel cell 1 kW and 8 x 2.5V/1200F supercapacitors (SC).*

B – Energy buffer

Two different energy buffers were considered: i) 8x2.5V/1200F supercapacitors and ii) a 12V/18Ah lead acid battery. The two technologies were intensively tested on urban, outer-urban and highway driving cycles with different control strategies.

With respect to the hydrogen consumption, the results achieved with supercapacitors were better than those achieved with the battery. This is related to a better charge/discharge efficiency and a lower mass in the first case. However, the high energy capacity of the battery offers more flexibility in the power management strategy and in the management of the fuel cell system. Considering a battery with better specifications (efficiency, mass) may improve the results.

Conclusions

The hardware in the loop emulation is an interesting rapid-prototyping solution for analysing components, energy flows control strategies and specifications of a FCHV with a fast and low cost set-up.

References

[1] M. Santis, D. Schmid, M. Ruge, G. Paganelli, F.N. Büchi, PSI Scientific Report 2003 V, 118-119 (2004).

[2] J. Bernard, S. Delprat, F.N. Büchi, T.M. Guerra, IREE, **1**, 352-362 (2006).

[3] J. Bernard, PhD Thesis 07-37, Université of Valenciennes et du Hainaut-Cambrésis (2007).

INVESTIGATION OF THE PORE-STRUCTURE OF GAS DIFFUSION LAYERS BY MICRO COMPUTER TOMOGRAPHY

R. Flückiger, M. Stampanoni, F. Marone,
A. Wokaun, F.N. Büchi
+41 56 310 4189
reto.flueckiger@psi.ch

In polymer electrolyte fuel cell (PEFC) research the understanding of mass transport limitations on all scales is of prime importance for the optimization of the involved structures. For collecting current over the channels and to provide access for the gases under the flow field ribs, porous structures, so called gas diffusion layers (GDL), are employed. The anisotropic porosity and high tortuosity of these materials [1] strongly affect and limit the mass transport through the porous structure, which in turn has a strong influence on the current distribution [2] and fuel cell performance.

The GDL materials consist of carbon fibers of typically few micrometers diameter (6–8µm). They are sintered with a carbonaceous binder and have a pore size distribution in the range of tens of micrometers. Due to orientation of the fibers, the pore structure is highly anisotropic. The materials further contain PTFE to increase hydrophobicity, whose inhomogeneous structure and distribution also strongly affects the connectivity of the pores. An additional hydrophobic Microporous Layer (MPL) between catalyst layer (CL) and GDL improves the electric contact to the CL and enhances the water management of the cell. In the PEFC application GDL materials are compressed. Therefore the changes of the pore structure as function of the compression is of high scientific interest.

Experimental

Preliminary Micro Computer Tomography (µ-CT) experiments have been made in 2003 by Andreaus et al. [1]. Their main problem was insufficient resolution and contrast between the different phases. Recently published data with 10 µm resolution was not sufficient to identifiy single carbon fibers [2]. No high resolution measurements have been made investigating compression, PTFE and MPL influence so far. The goal of the present study is to determine the anisotropic pore structure of GDL materials and to correlate with effective transport properties. For this the X02DA TOMCAT beamline at the Swiss Light Source (SLS) was used. Synchotron radiation was required due to sub-µm structures.

Magnification	Field of view / mm^2	Pixel size / µm
1.25x	11.4 x 11.4	5.6 x 5.6
2x	7.15 x 7.15	3.5 x 3.5
4x	3.58 x 3.58	1.75 x 1.75
10x	1.43 x 1.43	0.7 x 0.7
20x	0.72 x 0.72	0.35 x 0.35

Table 1. *Resolutions and field of view at TOMCAT beamline.*
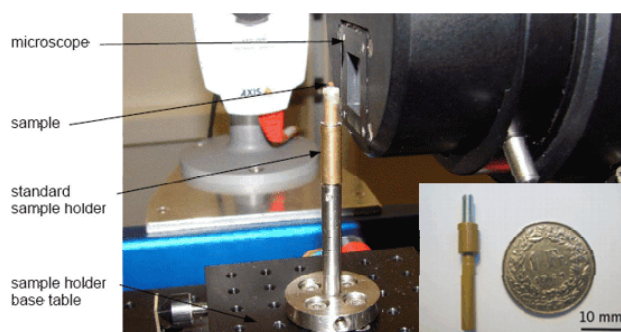
Figure 1. *Endstation of X02DA TOMCAT beamline with sample holder, scintillator and CCD camera. The inset shows the specially designed sample holder.*

Table 1 shows the available resolution and field of view combinations. The resolution of 0.7µm was chosen, resulting in a maximum field of view of 1.43mm x 1.43mm. A special sample holder (inset in Figure 1) was designed to carry a sample with 1.3 mm diameter and allow for compression. The device had to be able to compress the samples with a specific force up to 10 MPa. Furthermore the overall X-ray transmission had to be around 0.3 for an optimum contrast. These requirements were met with TORLON 4203, a polyamide-imide with small x-ray absorption and high tensile strength. The compression was adjusted by a screw and a torque meter. Figure 1 shows the endstation of the TOMCAT beamline where the sample holder is installed.

The GDL samples were exposed to an X-ray beam of 10keV while rotating by 180°. The transmitted radiation was received by a scintillator and recorded by a CCD camera. For one sample 2000 views were taken at different angles and reconstructed to in-plane and through-plane slices. From the 2D information 3D surfaces were generated using the visualization tool Amira®. For the reconstruction every pixel of a slice was asigned to pore-, fiber- or MPL-phase.

Results and Discussion

In Figures 2 and 3 the same section of the basic Toray TGP-H-060 GDL without PTFE is visible at two compression ratios. The comparison reveals that the blocks of binder between the fibers are mechanically stable and do not deform. Instead they shift into neighboring pores if present. This results in highly dense regions with porosity near zero. These regions prevent in-plane mass transport which is essential under the rib. The fibers show an elastic behavior as no broken fibers were found in the compressed sample. Figure 4 shows the segmented 3D surface of an MPL-coated TGP-H-060 paper. The thickness- inhomogeneity and intersection of the MPL with the GDL substrate is cleary visible. Hence the two layers can not be considered separately. In Figure 5 the reconstruction results of the SIGRACET® GDL24 without PTFE are shown. Toray materials contain a low fraction of solid binder with low porosity while GDL24 contain a large amount of highly porous binder. It was possible to reproduce this binder with its thin structures. Due to its high porosity and inhomogeneity, continuous through-plane pores are visible in the top view. Furthermore the fiber distribution is less homogeneous than in Toray papers resulting in larger mean pore diameters of about 50µm as compared to 30µm for Toray material.
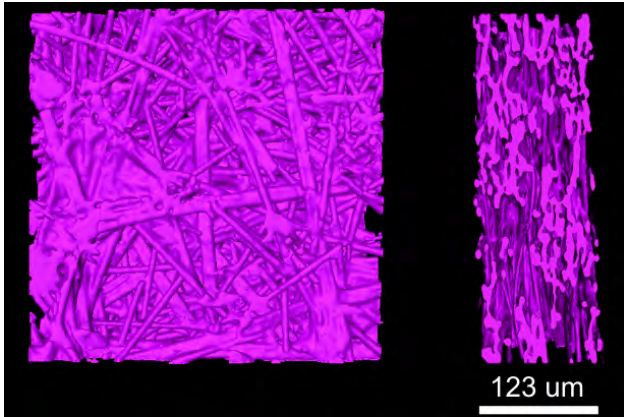
Figure 2. 3D surface of Toray TGP-H-060 without PTFE at a relative thickness of 0.62. The uncompressed thickness was 200 µm.(All figures in color on-line)

Figure 3. 3D surface of TGP-H-060 from Toray without PTFE at a relative thickness of 0.35. The uncompressed thickness was 200 µm.
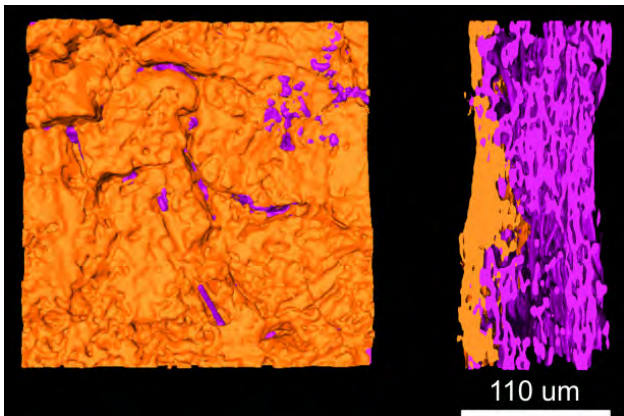
Figure 4. 3D surface of TGP-H-060 with 20% PTFE and MPL (orange phase) at a relative thickness of 0.48. The uncompressed thickness was 230 µm.

Figure 5. 3D surface of GDL24 from SGL without PTFE at a relative thickness of 0.85 The uncompressed thickness was 172 µm.

Conclusion

Micro Computer Tomography images of GDL materials have been successfully measured and analyzed. The important influence of compression, hydrophobic agent distribution and MPL-coating on the pore structure was investigated for the first time with the presented details. A pixel size of 0.7µm was sufficient to capture the smallest structures. However, to reduce the amount of data binning must be considered in future campaigns.

This first campaign was a success as it opened up 3D structural insights into GDLs that could not have been obtained by other means. SEM and light microscopy only resolve the outermost structure. The inner pore-geometry is valuable information for determination of a multitude of effective transport parameters. The data is also of prime importance to GDL manufacturers for optimizations.

References

[1] D. Kramer, S.A. Freunberger, R. Flückiger, I.A. Schneider, A. Wokaun, F.N. Büchi, G.G. Scherer, J. Electroanal. Chem., **612,** 63-77 (2008).

[2] S.A. Freunberger, M. Reum, J. Evertz, A. Wokaun, F.N. Büchi, J. Electrochem. Soc., **153**, A2158-A2165 (2006).

[3] B. Andreaus, H. Kuhn, M. Stampanoni, G.G. Scherer, A. Wokaun, PSI Scientific Report, V, 104 (2003).

[4] P.K. Sinha, P. Halleck, C.Y. Wang, Electrochem. Solid-State Lett., **9**, A344-A348 (2006).

PEFC: INFLUENCE OF FLOW FIELD GEOMETRY ON INTEGRAL PERFORMANCE AND THE CHANNEL-RIB CURRENT DISTRIBUTION

M. Reum, F.N. Büchi
+41 56 310 2127
mathias.reum@psi.ch

In PEFCs, the correlation of integral cell performance to the geometrical flow field structure has been investigated in numerous publications. It was found that sizing of channel and rib dimensions is connected to balancing losses from diffusion- and electrical resistance limitations [1]. At PSI, we are able to gain further insight into these relations by applying our recently developed method for measuring the sub-millimeter current distribution across the channel and rib domains of the flow field structure [2]. Integral cell performance is mainly fostered by a uniform current distribution, which is also coupled to a homogeneous compression of the GDL.

Experimental

12 cells (1.3 cm^2) with different flow field geometries were operated at the same conditions (H$_2$/O$_2$, rh$_{An/Cath}$ = 0.4, T$_{cell}$ = 70°C, p$_{cell}$ = 1.5 bar$_{abs}$, 0.2 l/min$_{constant\ flow}$). The rib- and channel sizes were varied between 3.0 and 0.5 mm, respectively. The rib ratio is thereby defined as the fraction of cell area in a repetitive unit, which is covered by a rib. In the presented experiments, the values range from 20 to 80%. Low values stand for wide channels, and high values stand for wide ribs; a value of 0.5 means that channel and rib have the same size. After measuring the U-I curves, the cells were operated at 0.6 V in order to compare the local current distributions at this point.

a)

b)
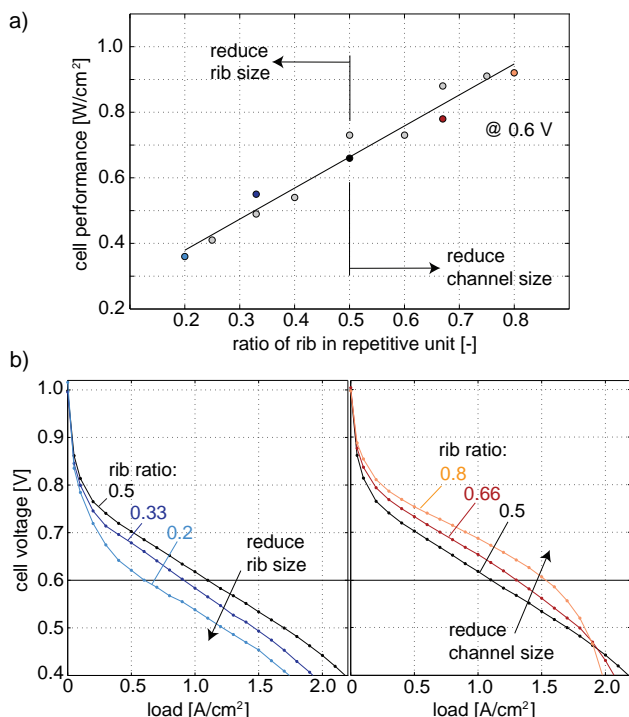
Figure 1. *Correlation of channel-rib sizing and integral cell performance, H$_2$/O$_2$, rh = 0.4, 70°C, 1.5 bar$_{abs}$,*
a) integral cell performance as a function of the rib ratio, potentiostatic operation at 600 mV;
b) U-I-curves for selected flow field geometries with reduced rib sizes (left diagram) and reduced channel sizes (right diagram).

Results and Discussion

Figure 1a) shows the integral cell performance for 12 flow field geometries under potentiostatic operation at 0.6 V. A positive linear correlation can be observed between cell performance and the rib ratio of a repetitive unit, implying a loss reduction when more cell area is covered by a rib. Inspection of the graphs in Figure 1b) confirms this finding for a wider load range. The U-I-curves show 5 selected cells with increasing rib ratio, it can be seen that cell performance rises with wider ribs and smaller channels, respectively. However, this holds true only for the potential range above 0.5 V. At high load, where mass transport limitation is the major overvoltage, the cells with smaller rib ratios reach higher limiting currents in most cases. To understand the behaviour at low and medium load, the local currents are compared at 0.6 V. Figure 2 shows that the difference between the current produced under channel and rib, respectively, is decreasing when the channel size is small compared to the rib size. Nevertheless, it can be noticed that the cell performance is better when the rib ratios are high, which coincides with more uniform current distributions for the respective geometries.
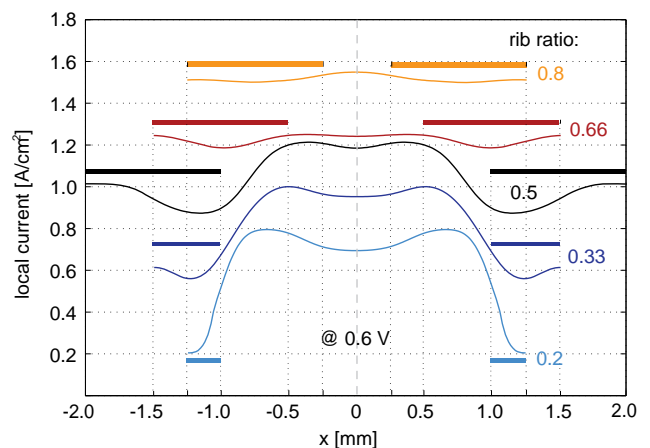
Figure 2. *Locally resolved current distributions across two repetitive flow field units (1 channel and 2 adjacent half-ribs) for the 5 cells from Figure1b), the rib areas are marked with bars, potentiostatic operation at 600 mV.*

These results clearly show a relation between uniform compression and cell performance. By altering the channel- and rib dimensions, the diffusion pathway length, electrical resistance, and water management in the GDL are changed. Unexpectedly, shortening the diffusion pathways leads to a decrease of both, channel and rib currents. The reason for this may be found in the interference of water management and electrical resistance. With a wide channel, the cell is likely to dry out due to increased water removal. In fact, long diffusion pathways towards the reaction layer are avoided, which explains the promotion of channel currents in the case of low rib ratios. The higher ionic resistance may on the other hand cause losses in integral performance. Additionally, the electric resistance in cells with a high relative area of rib-compressed GDL is decreasing. However, this effect alone can not explain the observed improvements.

References

[1] J. Scholta, G. Escher, W. Zhang, L. Küppers, L. Jörissen, W. Lehnert, J. Power Sources **155**, 66-71 (2006).

[2] S.A. Freunberger, M. Reum, A. Wokaun, F.N. Büchi, Electrochem. Commun., **8**, 1435-1438 (2006).

MEASURING THE MEMBRANE RESISTANCE IN PEFCS WITH CHANNEL-RIB RESOLUTION

M. Reum, D. Rätz, F.N. Büchi
+41 56 310 2127
mathias.reum@psi.ch

The recently developed method for measuring the local current distribution on the channel-rib scale using filigree voltage probes [1] allows for obtaining additional information by analyzing the transient cell behaviour. When the distribution of local current is known during an intergral current pulse, locally resolved membrane resistance can be obtained from the ratio of the immediate change in cell voltage and the locally observed shift of the current distribution.

Principle and Experimental

When a cell is operated under stationary conditions, the distribution of local potential (probe signal) $\phi(x)$ is averaged over time and denoted as $\phi(x)^{t1}$. As a current step Δj is applied, the answer of the potential distribution $\phi(x)^{t2}$ as well as the immediate cell voltage change ΔU_{cell} is measured (see Fig.1). In order to fully avoid the regime of other overvoltages than ohmic drop, the rate of the measurement needs to be in the order of few micro-seconds [2].

a)

b)

c)
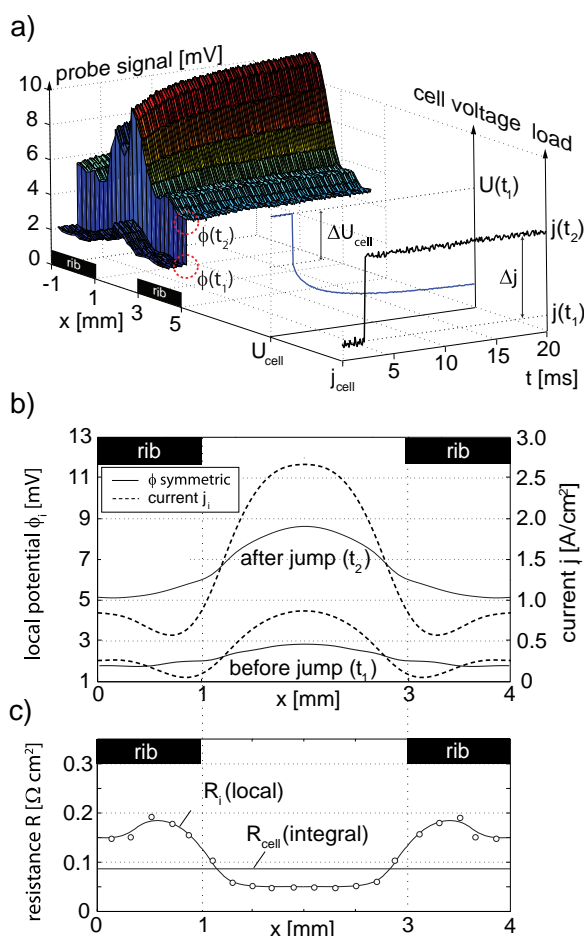
Figure 1. *Principle of local resistance measurement: a) the cannel-rib potential distribution is recorded during a perturbation of cell current, b) the distribution before and after the step is identified and the current is calculated, c) the resistance distribution R_i s obtained from ΔU_{cell} and the local Δj_i during the step.*

According to the formerly introduced principle of the sub-mm current measurement, both potential distributions at $\phi(x)^{t1}$ and $\phi(x)^{t2}$ are transferred into current density distributions (Fig.1b). If the measurement is fast enough, the difference Δj_i at a coordinate i stems solely from the local ohmic resistance. The resistance distribution is finally obtained from division of ΔU_{cell} by the local Δj_i (see Fig.1c). The integral resistance obtained from the sum of the parallel resistors R_i has to match the integral resistance obtained by dividing ΔU_{cell} by the integral current step Δj.

Resistance distributions were measured for a number of operating conditions. The sampling rate of the measurement setup allows for a time resolution of less than 10 μs. However, with the present set-upthe limiting factor is the current switch time of the electronic load, resulting in a time delay of 50-70 μs between t_1 and t_2. The measurement is therefore considered rather "slow" and may lead to slightly overestimated resistances.

Results and Discussion

A cell with a *Nafion®112*-membrane was operated with H_2/Air at different gas humidities (rh = 0.0, 0.1, 0.4, 1.0). Figure 2 shows that the integral cell resistance drops from 0.3 to less than 0.1 Ωcm^2 when the humidity is increased from dry to saturated gases. The corresponding resistance distributions show that the observed changes stem predominantly from the channel area. In the case of dry gases (rh = 0.0), a significant maximum is observed under the channel. Operation on moist or saturated gases on the other hand seems to promote the humidification of the ionomer at this location, leading to a lowered resistance compared to the rib areas.
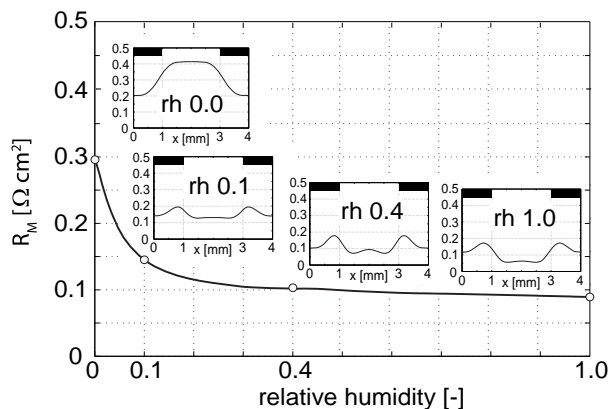
Figure 2. *Integral ohmic resistance and local resistance distributions (insets, ribs pointed out by black bars) for different humidities of both electrodes; cell operated on H_2/Air, 70°C, 1.5 bar_abs.*

These results show that despite certain drawbacks in measurement accuracy, the current step technique can reproduce the behaviour of membrane resistance for *Nafion®* found in literature [3]. Furthermore it provides information on the spatial origin of resistance limitations, i.e. that ionic resistance increases predominantly in the channel area under operation with dry gases.

References

[1] S.A. Freunberger, M. Reum, J. Evertz, A. Wokaun, F.N. Büchi, J. Electrochem. Soc. **153**, A2158 (2006).

[2] F.N. Büchi, A. Marek, G.G. Scherer, J. Electrochem. Soc. **142**, A1895 (1995).

[3] Y. Sone, P. Eckdunge, D. Simonsson, J. Electrochem. Soc. **143**, A1254 (1996).

LOCAL ONLINE GASANALYSIS IN PEFCS

G. Schuler, F.N. Büchi
+41 56 310 5396
gabriel.schuler@psi.ch

Even though some remarkable polymer electrolyte fuel cell (PEFC) durability test results have been published i.e. in [1], degradation is still a major problem for the commercialization of the technology. One critical part of PEFC fuel cells in terms of degradation is the membrane. It is known, that gas permeation lowers membrane lifetime, but the mechanisms are still not fully understood [2,3]. Besides emission rate measurements of membrane constituents, gas permeation data is an indicator of the actual state of the membrane. A novel gas analysis test rig was built for measuring online and *in-situ* the local composition of the fuel cell gas streams. Helium is used as an indicator for the membrane hydrogen permeation characteristics.

Experimental

The cell for local gas analysis has an active area of 200cm^2 and linear graphitic flow field plates. Nafion 112 and E-Tek A6 Elat V2.1 electrodes were used for the membrane electrode assembly. The cell is equipped with 3 heated gas extraction ports along the flow field channels to access the gas at the inlet, mid and outlet of the active area on the cathode side. The extracted gas is conducted through fully heated capillaries and fed to the vacuum chamber of a Pfeiffer Prisma mass spectrometer system. 5.2 % Helium is added to the anode side gas stream in order to characterize online the local permeation characteristics of the membrane by analyzing the helium concentration on the cathode side. Figure 1 shows the gas species concentration along the cathode flow field. Air is fed at port 1 position on the cathode side, while hydrogen flows on the anode side from port 3 to port 1 in counterflow mode.

Results

The concentrations of the cathode side gas species is shown in Figure 1. The dashed lines show reference measurements with air at open circuit conditions. The solid lines show the decrease of oxygen, the associated increase of the nitrogen content and the fraction of argon along the flow field channel under load conditions. Figure 2 illustrates the helium permeation through the membrane under different operating conditions. The dashed curve marks the cathode side helium background without helium addition on the anode side. The solid lines are measurements with 5.2% helium addition to the fuel gas under open circuit and load conditions. The helium accumulation from cathode inlet to the cathode outlet is visible. Under 20A load the helium permeation increase is 40% in comparison to the open circuit case. Reference hydrogen permeation rates of Nafion 112 membranes were electrochemically measured in cells with serpentine flow fields of the same dimension under comparable operating conditions. These measurements showed a hydrogen permeation rate of 0.9 mA/ cm^2 for new membranes under the given operating conditions. This reference value for hydrogen permeation and the given stoichiometries result in an expected virtual hydrogen concentration of 110 ppm at the cathode outlet. If we neglect differences in membrane permeation characteristics of hydrogen and helium, the measured helium permeation rate can serve as an indicator of the hydrogen permeation. The local gas analysis shows a

background corrected helium concentration at the cathode exit of 114 ppm in open circuit and 168 ppm under 20A load condition (see Figure 2). These results show that the online measured helium permeation can serve as a good indicator of the local membrane permeation characteristics and thus for the membrane degradation state.
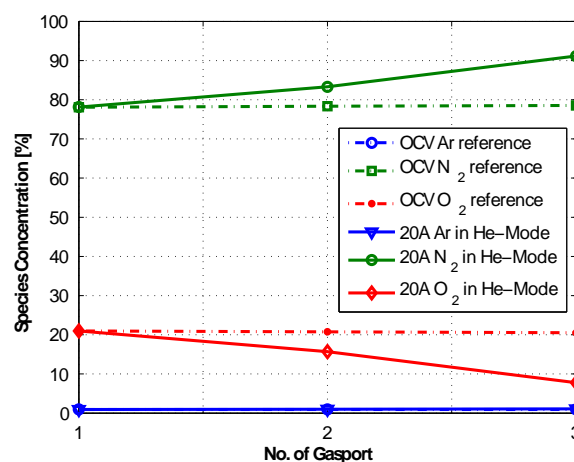
Figure 1. *Species concentration along the cathode channel determined by in-situ mass spectrometry. Cathode: air, T_{dp}=60°C, λ=2, p=1.5 bar; Anode: hydrogen, T_{dp} =60, λ=1.5, p=1.5bar; T_{cell} =75°C.*
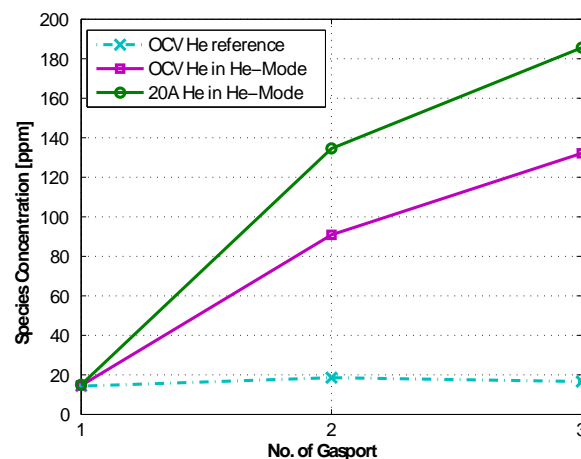
Figure 2. *Helium concentration along the cathode channel determined by in-situ mass spectrometry. Anode side helium addition 5.2%. Cathode: T_{dp}=60°C, λ=2, p=1.5 bar; Anode: T_{dp}=60, λ=1.5, p=1.5bar; T_{cell} =75°C, 5.2% dry helium addition.*

Conclusions

Using a new gas analysis test rig the correlation between helium and hydrogen permeation through Nafion 112 membranes is demonstrated. *In-situ* and online local Helium permeation can serve as a useful indicator of the membrane permeation and therefore of the membrane degradation state. More detailed measurements are planned to investigate the influence of operating conditions on the permeation and the subsequent membrane degradation behaviour.

References

[1] S.J.C. Cleghorn, D.K. Mayfield, D.A. Moore, J.C. Moore, G. Rusch, T.W. Sherman, N.T. Sisofo, U. Beuscher, J. Power Sources, **158**, 446-454 (2006).

[2] V.O. Mittal, H.R. Kunz, J. Fenton, J. Electrochem. Soc. **9**, A299-302 (2006).

[3] M. Inaba, T. Kinumoto, M. Kiriake, R. Umebayashi, A. Tasaka, Z. Ogumi, Electrochim. Acta, **51**, 5746–5753 (2006).

BATTERIES & SUPERCAPACITORS

MATERIALS

$Li_4V_3O_8$: A POSSIBLE CANDIDATE AS HIGH CAPACITY POSITIVE ELECTRODE MATERIAL FOR LITHIUM-ION BATTERIES

S.H. Ng, N. Tran, K.G. Bramnik[1], H. Hibst[1], P. Novák

+41 56 310 4406

see-how.ng@psi.ch

Today lithium-ion batteries are the power sources of choice for popular portable electronics, such as cellular phones and notebooks [1]. However, despite their outstanding commercial success, these batteries are still open to improvements. In particular, improvements on the positive electrode are critical for the progress of lithium-ion batteries. Indeed, considerable efforts are presently directed to the replacement of the high cost, partially toxic $LiCoO_2$ with more affordable and sustainable materials.

Vanadium oxides such as V_2O_5, V_6O_{13}, and LiV_3O_8, appeared to be promising candidates as positive electrode materials due to the advantages of higher capacity, lower cost, and better safety features [2-4]. However, for use in lithium-ion batteries, these materials are not suitable, since they contain no extractable lithium-ions during the first charge. Chemical lithiation of vanadium oxides for producing viable positive electrodes at an economical scale is indeed a scientific challenge. Previous methods based on lithiation with LiI (in acetonitrile) [5] and *n*-BuLi (in hexane) [6] have proven to be economically not attractive.

Herein, we report on an industrially scalable method for producing $Li_4V_3O_8$ via the spray-drying method [7] followed by chemical lithiation with Li_2S [8]. Systematic characterization of the lithiated vanadates in terms of their physical properties as well as their electrochemical performance will be discussed in detail here.

Experimental

$Li_4V_3O_8$ was prepared via reduction of a $Li_{1.1}V_3O_8$ precursor compound by Li_2S (Alfa-Aesar) in an argon-filled glove box (H_2O < 1 ppm, O_2 < 1 ppm). The reactants, with molar ratio of Li/V (1.45/1) were refluxed in anhydrous acetonitrile (Merck, Germany) at 80 °C for 24 hrs [8]. The by-product, S, was afterward washed out by a warm, ethanol/toluene solvent mixture. The $Li_{1.1}V_3O_8$ precursor compound was synthesized via a spray-drying process in air using a Mobile Minor 2000 type device, followed by heat treatment in air at 320 °C for 1 hr [7].

The as-synthesized $Li_4V_3O_8$ compound was analyzed for lithium content using the atomic absorption spectroscopy (AAS) technique in the emission mode. The vanadium content was determined by a potentiometric titration technique [8]. Scanning electron microscopy (SEM) images were obtained using a JEOL JSM 6400F microscope.

The $Li_4V_3O_8$ positive electrodes were prepared by a solvent route where acetonitrile (99.9 %, Aldrich) was used as the dispersing medium. The $Li_4V_3O_8$ active material, carbon black (CB), and polymeric binder mixture (PVdF-HFP and PEO) were dispersed in the solvent under magnetic stirring for 1 hour. The solvent quantity was 4 mL for every 500 mg of the composite materials. The as-prepared slurry was doctor-bladed on an aluminium foil and dried in the argon-filled glove box. After drying,

[1] BASF Aktiengesellschaft, Performance and Chemical Research, Ludwigshafen, Germany

electrode disks (1.3 cm^2) were punched for test cell assembly. The working electrodes now consist of 50 wt.% $Li_4V_3O_8$, 43 wt.% carbon black (Super P, TIMCAL), and 7 wt.% of a polymeric binder mixture (1:1 by weight) of PVdF-HFP (Kynar 2801, Atochem) and PEO (M_w = 300000, Aldrich). The mass loading of the positive electrodes was typically 4-6 mg of active material per cm^2. Hermetically sealed laboratory test cells were used in which the working and counter electrodes (the latter from metallic lithium for a half-cell, and from LBG1025 graphite for a full cell) were slightly pressed together against a glass fiber separator soaked with a standard battery electrolyte (1M $LiPF_6$ in EC:DMC (1:1), Ferro).

The electrochemical cycling was performed between 2.0-4.0 V (half-cell, vs. Li metal) or 1.6-4.0 V (full cell, vs. LBG1025 graphite) in the galvanostatic mode immediately followed by a potentiostatic mode until the specific current decreased to 10 % of the current used in the galvanostatic mode. For determining the C-rate, a theoretical specific capacity of 350 mAh g^{-1} of the oxide was assumed for all cases. For the air sensitivity tests, the exposure time was calculated based on the duration of time for the doctor-bladed electrode exposed under ambient air. For the long term cycling tests, the charge and discharge rates in the galvanostatic mode were equal to C/3 rate. For the rate capability tests, the specific current was varied from C/10 to 8C rates. For each C-rate an average value was calculated for the first 10 cycles.

Results and Discussion

The determined Li/V ratio was 3.80(5)/3.00(5) for the as-synthesized $Li_4V_3O_8$ compound, which is in good agreement with the nominal value (4/3) when considering the accuracy of the analytical method for each element. Figure 1 shows the SEM image of the as-synthesized $Li_4V_3O_8$ compound, which is mainly dense, macro-sized (up to 20 μm), spherical agglomerates consist of rod-like nanostructures (100-150 nm wide) as their building blocks (see inset of Figure 1).
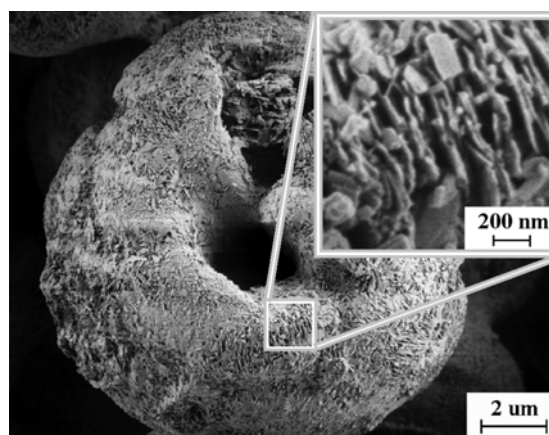
Figure 1. *SEM image of the as-synthesized $Li_4V_3O_8$ material, with the inset showing the presence of rod-like nanostructures as the building block for the spherical agglomerates.*

In order to test the stability of the as-synthesized $Li_4V_3O_8$ compound when exposed to ambient air, the $Li_4V_3O_8$ positive electrodes were dried in air after doctor-blading for various duration of time. Figure 2 shows that the $Li_4V_3O_8$ positive electrodes could maintain almost 100 % of its average charge capacities over 10 cycles (at C/3 rate) when exposed to ambient air for approximately 5 hrs. This should provide ample of handling time for practical industrial applications in ambient atmosphere.
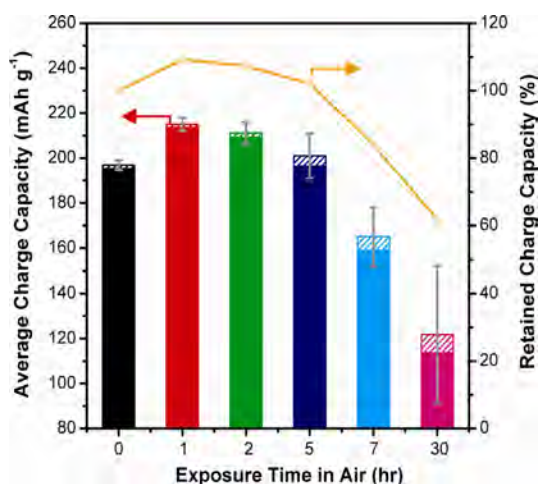
Figure 3. The average (over 10 cycles) specific capacities of the $Li_4V_3O_8$ electrodes cycled between 2.0 and 4.0 V at different specific currents (C-rate). Note that 1C rate is assumed to be 350 mA g^{-1} in all cases.

Meanwhile, as demonstrated in Figure 3, when applied in half-cell (vs. Li metal), the $Li_4V_3O_8$ positive electrode exhibited rather high average specific capacities, retaining 279 mAh g^{-1} (Li$^+$ extraction) and 283 mAh g^{-1} (Li$^+$ insertion), respectively, at a reasonable specific current of 117 mA g^{-1} (C/3 rate). Furthermore, the $Li_4V_3O_8$ positive electrode also demonstrated excellent rate capabilities, matching those of the $Li_{1.1}V_3O_8$ precursor material, retaining an average specific charge capacity of 205 mAh g^{-1} at 2800 mA g^{-1} (8C rate), when cycled in the potential range of 2.0-4.0 V vs. Li metal. The capacity contribution from the galvanostatic part decreased significantly with increasing C-rate during insertion of Li-ions. This could be attributed to the slower Li$^+$ migration from the surface to the inside of the electrode when the concentration of Li$^+$ on the electrode-electrolyte surface is high at higher C-rate.
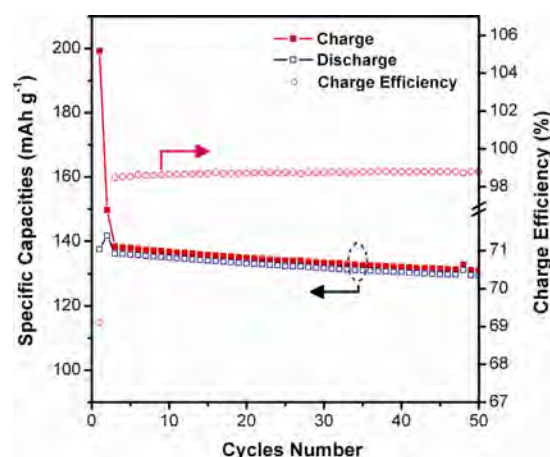
Figure 4. Cycle life behaviour of the $Li_4V_3O_8$ cathode in a full cell (vs. graphite LBG1025), where cycling took place between 1.6 and 4.0 V at 117 mA g^{-1}.

When applied in a non-optimized full cell system (vs. LBG1025 graphite), the $Li_4V_3O_8$ positive electrode showed promising cycling behaviour (see Figure 4), retaining specific charge capacity above 130 mAh g^{-1} beyond 50 cycles, when cycled in the voltage range of 1.6-4.0 V, at a specific current of 117 mA g^{-1} (C/3 rate). The lower specific capacity shown by the full cell system was due to the excess mass of the graphite negative electrode.

Conclusions

$Li_4V_3O_8$ compounds have been successfully prepared via chemical lithiation of spherical-shaped $Li_{1.1}V_3O_8$ precursor materials obtained from the spray-drying technique with Li_2S. The $Li_4V_3O_8$ materials are stable in air up to 5 hours, with almost no capacity drop. We believe that with further synthetic optimization and better balancing of the electrodes' masses, $Li_4V_3O_8$ should be a viable candidate as high capacity positive electrode material in commercial lithium-ion batteries.

References

[1] B. Scrosati, Nature **373**, 557-558 (1995).

[2] S.H. Ng, S.Y. Chew, J. Wang, D. Wexler, Y. Tournayre, K. Konstantinov, H.K. Liu, J. Power Sources **174**, 1032-1035 (2007).

[3] D.W. Murphy, P.A. Christian, F.J. Disalvo, J.N. Carides, J. Electrochem. Soc. **126**, 497-499 (1979).

[4] T.J. Patey, S.H. Ng, R. Büchel, N. Tran, F. Krumeich, J. Wang, H.K. Liu, P. Novák, Electrochem. Solid-State Lett., in press (2007).

[5] C. Satto, P. Sciau, E. Dooryhee, J. Galy, P. Millet, J. Solid State Chem. **146**, 103-109 (1999).

[6] M.S. Whittingham, M.B. Dines, J. Electrochem. Soc. **124**, 1387-1388 (1977).

[7] N. Tran, K.G. Bramnik, H. Hibst, J. Prölss, N. Mronga, M. Holzapfel, W. Scheifele, P. Novák, J. Electrochem. Soc., in press (2007).

[8] B. Chaloner-Gill, D.R. Shackle, T.N. Andersen, J. Electrochem. Soc. **147**, 3575-3578 (2000).

THE INFLUENCE OF SURFACE PROPERTIES TO THE IRREVERSIBLE CAPACITY OF GRAPHITE DURING THE FIRST ELECTROCHEMICAL LITHIUM INSERTION

S.H. Ng, N. Tran, C. Vix-Guterl[1], R. Gadiou[1],
J. Dentzer[1], E. Spahr[2], D. Goers[2], H. Wilhelm[2],
J. Ufheil, H. Buqa, P. Novák
+41 56 310 4406
see-how.ng@psi.ch

Recent developments in the field of hybrid electric vehicles have been the main driving force behind the search for lithium-ion batteries with high energy density and power density, without compensating on the safety aspects [1]. Graphitic carbons are currently the most often employed material for the negative electrode due to their low cost, excellent cyclability and reliability, and non-toxicity [2].

One of the key areas where improvement on the graphite is of great importance is with regards to the reduction of the irreversible capacity measured during the first electrochemical Li$^+$ insertion. This irreversible capacity is attributed to the electrolyte decomposition on the graphite surface during the first reduction cycle, forming a passivation layer, also known as the solid electrolyte interphase (SEI). On the contrary, this SEI layer also avoids electrochemical exfoliation of the graphite [2-5]. Therefore, more research works are needed in order to identify key parameters influencing the SEI formation and its corresponding efficiency.

Herein, we report on the role played by the active surface area (ASA) [6], and also by the surface functional groups on graphite towards the SEI formation efficiency and tendency to exfoliate, which will result in different first cycle irreversible capacity for the surface-modified graphite. Note that only physical treatments on the graphite surface are studied here.

Experimental

The highly crystalline, synthetic graphite material, TIMREX® SLX50 (TIMCAL SA, Bodio, Switzerland) is used as the parent material in the negative electrode for this study. Variation of the graphite surface properties can be easily obtained after thermal modifications under various gas atmospheres without significantly changing the bulk properties (especially the total surface area) and the particle size distribution of the treated-samples. The graphite surface modification treatments are summarized in the footnote of Table 1. For example, in the "SLX50 - Vacuum" case, the as-received SLX50 graphite was heated at 950 °C. After the heat treatment, the graphite sample was cooled to 25 °C in vacuum, and finally, was exposed to air.

The active surface area (ASA) measurement was adapted from the method developed by Walker and his co-workers, which is based on di-oxygen chemisorption [7-8]. The graphite samples are first outgassed under vacuum (10^{-4} Pa) at 950 °C for 2 hrs to release the active sites. Subsequently, oxygen is chemisorbed at 300 °C over a period of 15 hrs (with an initial oxygen pressure of 66.5 Pa), leading to the formation of surface oxygenated complexes. The amount of oxygen complexes formed was determined by mass spectrometry by measuring the

amount of CO and CO$_2$ resulting from the decomposition of the oxygen complexes at temperatures higher than their formation by performing a temperature-programmed desorption (TPD) step between 300 and 950 °C. Knowing the number of each mole for each gas desorbed, and taking the area of an edge carbon site that chemisorbed an oxygen atom as 0.083 nm^2, the surface area occupied by chemisorbed oxygen can be determined. Detailed information can be found elsewhere [6, 8].

Graphite negative electrodes were prepared by doctor-blading slurries consisting the graphite active material (90 wt.%) and the poly(vinylidene fluoride) binder (10 wt.%, SOLEF 1015, Solvay SA) in a N-methylpyrrolidinone (NMP) solvent, onto the copper foil. The electrodes were vacuum dried at 120 °C for overnight. After drying, electrode disks (1.3 cm^2) were punched for test cell assembly in the argon-filled glove box. The mass loading of each working electrode was typically 4-5 mg of active material per cm^2. Hermetically sealed laboratory test cells were used in which the working and counter electrodes (the latter from metallic lithium) were slightly pressed together against a glass fiber separator soaked with a standard battery electrolyte (1M LiPF$_6$ in EC:DMC (1:1), Ferro). Both the oxygen and water contents were less than 1 ppm in the argon-filled glove box.

Galvanostatic measurements were performed at a specific current of 10 mA g^{-1} (of graphite) in order to complete the SEI formation in the first electrochemical Li$^+$ insertion. When a potential of 5 mV vs. Li/Li$^+$ was reached, the discharge step was continued until the current dropped below 5 mA g^{-1}. The charge step was performed at a constant specific current of 10 mA g^{-1} until a cut-off potential of 1.5 V vs. Li/Li$^+$ was reached. All measurements were carried out at room temperature.

Results and Discussion

From our previous study [6] on the importance of ASA during the first electrochemical Li$^+$ insertion in a 1 M LiPF$_6$, EC:DMC (1:1) electrolyte system, we could summarize that the SLX50 graphite materials tend to exfoliate when the ASA value is much lower than 0.10 m^2 g^{-1}. This has led to a very high first cycle irreversible capacity (> 50 %), as shown in Figure 1.

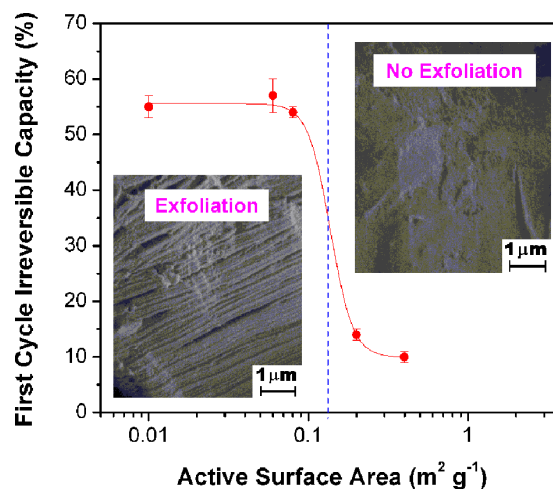**Figure 1.** *Irreversible capacities (C$_{irr}$) for the first electrochemical Li$^+$ insertion into TIMREX® SLX50 negative electrodes as a function of the active surface area (ASA) measured at 10 mA g^{-1} in a 1 M LiPF$_6$, EC:DMC (1:1) electrolyte. Experimental data points and modified SEM images were obtained from Ref. [6].*

---

[1] Institut de Chimie des Surfaces et Interfaces, Mulhouse, France
[2] TIMCAL SA, Bodio

Table 1. *The active surface area (ASA), amount of CO gas desorbed (from TPD measurements), and the first cycle irreversible capacity of various surface-modified TIMREX® SLX50 graphite materials.*

Graphite Samples	ASA ($m^2 g^{-1}$)	CO Gas Desorbed ($\mu mole\ g^{-1}$)	1st Cycle Irreversible Capacity (%)
SLX50 - As - received	0.20	12.2	14
SLX50 - Argon	0.06	1.8	57
SLX50 - Vacuum	0.30	30.6	15
SLX50 - O$_2$	0.40	54.2	14
SLX50 - H$_2$	0.20	2.2	25

"SLX50 - As - received": TIMREX® SLX50 graphite material provided by TIMCAL; "SLX50 - Argon": as-received SLX50 sample heat-treated at 1300 °C for 1 hr under an argon flow; "SLX50 - Vacuum": as-received SLX50 sample heat-treated at 950 °C followed by cooling to 25 °C in vacuum, and finally, contact with air; "SLX50 - O$_2$": as-received SLX50 sample heat-treated at 950 °C, followed by cooling to 500 °C in oxygen (1 Torr) for 15 mins, and finally, contact with air; "SLX50 - H$_2$": as-received SLX50 sample heat-treated at 950 °C under hydrogen flow, followed by cooling under hydrogen flow, and finally, contact with air.

When comparing the "SLX50 - Argon" sample with the "SLX50 - Vacuum" sample, although they have huge difference in their ASA values (0.06 vs. 0.30 $m^2 g^{-1}$), both exhibited a similar specific functional group (see Figure 2, with a peak between 350 - 400 °C) after air contact. However, from their electrochemical performance, we can conclude that ASA played a more important role in the tendency to exfoliate when the ASA value is much lower than 0.10 $m^2 g^{-1}$.

When the ASA value of the treated graphite is much higher than 0.10 $m^2 g^{-1}$, as in the case of "SLX50 - Vacuum" where the ASA value is 0.30 $m^2 g^{-1}$, only slight increase in the first C_{irr} is observed in comparison to the oxygen-treated sample. One of the possible reason for the slight increase in C_{irr} for the vacuum-treated graphite is due to slight exfoliation (see inset of Figure 3).
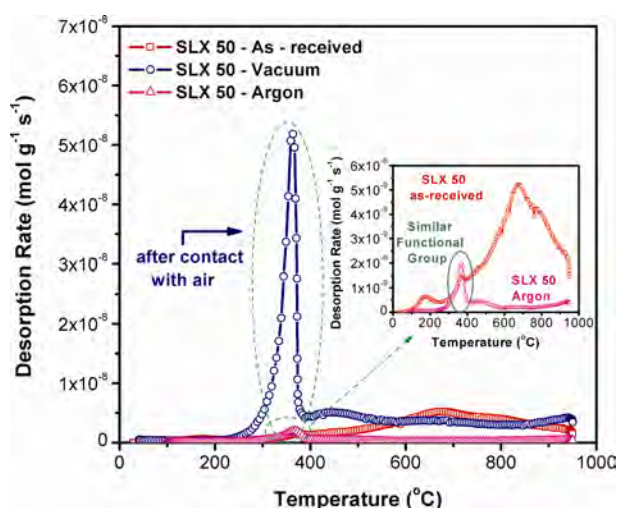
Figure 2. *Desorption rate of CO gas as a function of temperature measured after oxygen chemisorption by temperature-programmed desorption (TPD) experiments for graphite samples of "SLX50 - As - received", "SLX50 - Vacuum", and "SLX50 - Argon". An enlarged plot of the circled dashed line is shown in the inset. A specific surface functional group is observed at 350 °C for all treated samples.*
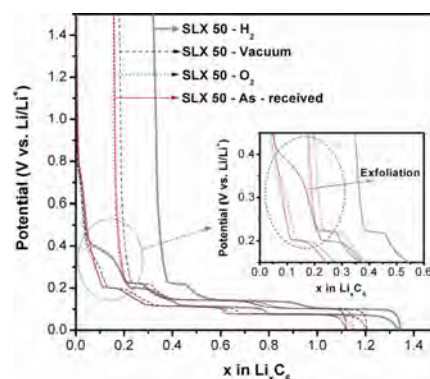
Figure 3. *First electrochemical Li⁺ insertion/de-insertion into TIMREX® SLX50 negative electrodes measured at 10 mA g^{-1} in a 1 M LiPF$_6$, EC:DMC (1:1) electrolyte. An enlarged plot of the circled dashed line is shown in the inset. Exfoliation was observed for both hydrogen- and vacuum-treated graphite samples.*

As can be seen in Figure 3, no exfoliation is observed with graphite electrodes having a surface chemistry enriched with oxygen functional groups. Therefore, oxygen functional groups seem to be of prime importance for the SEI formation since they could act as nucleation sites for an effective SEI formation during the first reduction process. This importance is confirmed by testing a hydrogen-treated graphite electrode. In this case, the oxygen functional groups were removed by the heat treatment and were replaced by C-H bonds formed during the hydrogen treatment. As can be seen from Figure 3, the presence of the C-H bonds is detrimental to the SEI formation, which led to the exfoliation of graphite.

Conclusions

We have successfully shown that by controlling the active surface area (ASA) of the surface-modified graphite to a certain extent (in this case >> 0.10 $m^2 g^{-1}$), it was possible to minimize the tendency for the graphite to exfoliate. In addition, we have found that oxygen functional groups are in favour of a stable SEI formation, whereas the passivation of the surface by C-H bonds is detrimental for the SEI formation. Finally, the nature of specific functional groups that are present at specific temperature range should be identified and quantified in future works.

References

[1] J.-M. Tarascon, M. Armand, Nature **414**, 359-367 (2001).

[2] M. Winter, J.O. Besenhard, M.E. Spahr, P. Novák, Adv. Mater. **10**, 725-763 (1998).

[3] M.E. Spahr, H. Wilhelm, F. Joho, J.-C. Panitz, J. Wambach, P. Novák, N. Dupont-Pavlovsky, J. Electrochem. Soc. **149**, A960-A966 (2002).

[4] M.E. Spahr, H. Wilhelm, T. Palladino, N. Dupont-Pavlovsky, D. Goers, F. Joho, P. Novák, J. Power Sources **119-121**, 543-549 (2003).

[5] M.E. Spahr, H. Buqa, A. Würsig, D. Goers, L. Hardwick, P. Novák, F. Krumeich, J. Dentzer, C. Vix-Guterl, J. Power Sources **153**, 300-311 (2006).

[6] P. Novák, J. Ufheil, H. Buqa, F. Krumeich, M.E. Spahr, D. Goers, H. Wilhelm, J. Dentzer, R. Gadiou, C. Vix-Guterl, J. Power Sources **174**, 1082-1085 (2007).

[7] N.R. Laine, F.J. Vastola, P.L. Walker Jr., J. Phys. Chem. **67**, 2030-2034 (1963).

[8] C. Vix-Guterl, P. Ehrburger, World of Carbon, P. Delhaes (Ed.), Taylor and Francis, **2**, 188 (2003).

ELECTROCHEMISTRY OF LITHIUM MANGANATE NANOPARTICLES MADE BY FLAME SPRAY PYROLYSIS

T.J. Patey, R. Büchel[1], S.E. Pratsinis[1], P. Novák
+41 56 310 4071
timothy.patey@psi.ch

$LiMn_2O_4$ spinel material has become an attractive alternative to $LiCoO_2$ because of its safer performance, low cost, and low toxicity due to intensive research efforts over the past two decades [1-2]. Use of nano-sized cathode materials has shown promise when higher power densities are required [3]. Flame spray pyrolysis (FSP) is a rapid and industrially scalable route to produce lithium manganate nanoparticles for use in lithium-ion batteries [4].

Experimental

The experimental setup of FSP is described elsewhere in literature [5]. Specific surface area of the FSP-made particles is controlled by the oxidant flow rate and the precursor/fuel composition. The flexibility of FSP for producing various transition metal oxides is rooted in the variety of precursors which can be prepared; if the transition metal can be dissolved into the liquid precursor, then a metal oxide containing that transition metal can usually be synthesized. For the synthesis of $LiMn_2O_4$ powder, 1.0 M solution of Li-t-butoxide in tetrahydrofuran and Mn(III)-acetylacetonate (Aldrich) are mixed into xylene to form the flammable precursor with a Li:Mn stoichiometric ratio of 1:2. For electrochemical cycling, $LiMn_2O_4$ powders are prepared into electrodes with mass ratios of 7:2:1 for $LiMn_2O_4$ nanoparticles : carbon black : polymer binder.

Results

A powder with a Brunauer-Emmett-Teller specific surface area (BET SSA) of 142 m^2 g^{-1} is synthesized by FSP. For monodisperse spherical particles, a particle diameter of 10 nm is calculated (d_{BET}). Analysis of a transmission electron micrograph (TEM, Figure 1) confirms this is a good calculation of particle diameter and the powder is crystalline.
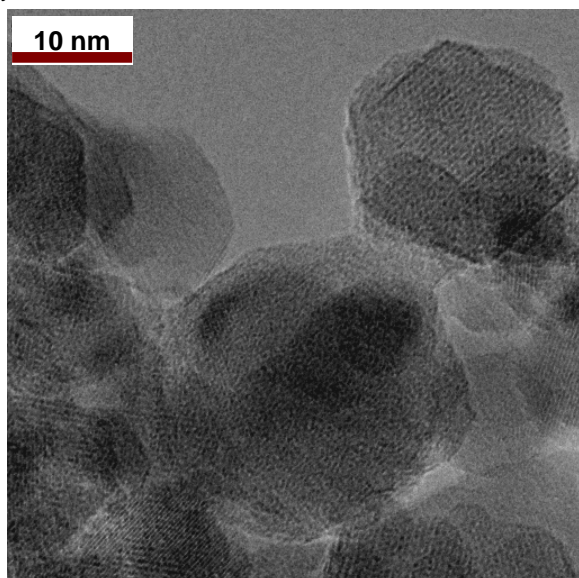
Figure 1. *TEM of FSP-produced $LiMn_2O_4$ nanoparticles.*

The same powder is annealed for 10 hours at 700°C, decreasing the BET SSA to 25 m^2 g^{-1}, corresponding to a d_{BET} of 56 nm. Figure 2 displays the cycling capacity of the two powders at various C-rates.
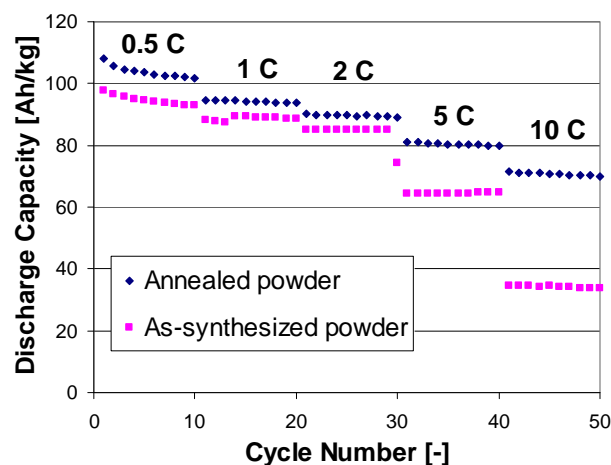
Figure 2. *Galvanostatic cycling capacity of the FSP-produced $LiMn_2O_4$ nanoparticles at various C-rates between 3.5 and 4.3 V vs Li. Capacity is expressed per kg of $LiMn_2O_4$. 1C = 148 A kg^{-1}.*

The annealed powder has a higher discharge capacity than the as-synthesized material, particularly for currents greater than or equal to 5 C. This result contradicts the maxim that smaller particles means higher power [3], but particle size is not the sole parameter for electrochemical energy storage. The increase in crystallinity caused by annealing likely improves lithium insertion into the crystal structure. Furthermore, carbon black / $LiMn_2O_4$ powder contact may be optimized for the larger nanoparticles.

Annealing improves electrochemical performance of the material and is closer to performing as well as a commercial material does [2]. Further optimization by particle coating or use of dopants or electrode engineering – or all three – may allow for $LiMn_2O_4$ nanoparticles to become a commercial replacement of $LiCoO_2$ powders for use in high-powered, lithium-ion batteries.

References

[1] M.M. Thackeray, W.I.F. David, P.G. Bruce, J.B. Goodenough, Mater. Res. Bull. **18**, 461-472 (1983).

[2] M. Lanz, C. Kormann, H. Steininger, G. Heil, O. Haas, P. Novák, J. Electrochem. Soc. **147**, 3997-4000 (2000).

[3] A.S. Arico, P. Bruce, B. Scrosati, J. M. Tarascon, W. Van Schalkwijk, Nat. Mater. **4**, 366-377 (2005).

[4] F.O. Ernst, H.K. Kammler, A. Roessler, S.E. Pratsinis, W.J. Stark, J. Ufheil, P. Novák, Mater. Chem. Phys. **101**, 372-378 (2007).

[5] L. Madler, H.K. Kammler, R. Mueller, S.E. Pratsinis, J. Aerosol Sci. **33**, 369-389 (2002).

---

[1] Particle Technology Laboratory, ETH Zürich

INFLUENCE OF THE ELECTROLYTE ON THE ELECTROCHEMICAL INTERCALATION OF PF$_6^-$ IN GRAPHITE

W. Märkle, N. Tran, D. Goers[1], M.E. Spahr[1], P. Novák

+41 56 310 2474

wolfgang.maerkle@psi.ch

Metal oxides are used as positive electrode materials in Li-ion batteries. As the electronic conductivities of these oxides are low, conductive additives are needed. Graphite is a common material for this purpose. During the charging process at high potentials, anions, e.g., PF$_6^-$ from the electrolyte can intercalate into the graphite additive. This might be accompanied by changes in the graphite structure and properties, which can also have an influence on the contact between graphite and oxide particles and, thus, may determine the overall electrode stability. It was reported that in sufficient oxidative stable electrolytes like ethyl methyl sulfone, PF$_6^-$ intercalates and deintercalates reversibly in graphite in staged phases similar to Li$^+$ ions in the negative electrode [1]. To get information about the influence of the solvent on the reversible anion intercalation we investigated the high potential cycling of graphite with different electrolyte mixtures.

Experimental

The electrodes for the electrochemical experiments were prepared by a mixture of 90% (w/w) TIMREX® SFG6 graphite (TIMCAL) and 10% binder (SOLEF PVDF 1015, Solvay), both suspended in N-methylpyrrolidone (NMP, Fluka). The slurry was applied onto a titanium current collector, vacuum dried at 80 °C to remove the NMP, and finally heated at 120 °C for 12 h in vacuum. Mass loading was 8-9 mg/cm^2 active material. Standard laboratory cells described elsewhere [2] were used for the experiments. Lithium foil (Alfa Aesar) was used as counter electrode. The two electrodes were separated by a glass fiber separator soaked with electrolyte and pressed against each other with a spring (pressure 2 kg/cm^2). Electrolyte mixtures were made from ethylene carbonate (EC, Ferro), propylene carbonate (PC, Ferro), dimethyl carbonate (DMC, Ferro), ethyl methyl carbonate (EMC, Merck) and ethyl methyl sulfone (EMS, TCI), all used as received. Each mixture contained 1 M LiPF$_6$ as conducting salt.

Results

An electrochemical charging/discharging curve from 3.0 to 5.5 V vs. Li/Li$^+$ in EC:DMC electrolyte is shown in Figure 1. In the high potential region, potential plateaus can be observed during the charging step. This points to staged intercalation of PF$_6^-$ in graphite similar to Li$^+$ ions in the negative graphite electrode at low potentials. The higher charge in the charging step compared to the discharging step is most probably due to some electrolyte decomposition.

A comparison of different electrolytes in the electrochemical cycling process at high potentials shows that in EMS the specific charge remains constant throughout 10 cycles (Figure 2) and is in the range of the theoretical calculated value of 140 Ah/kg [1].
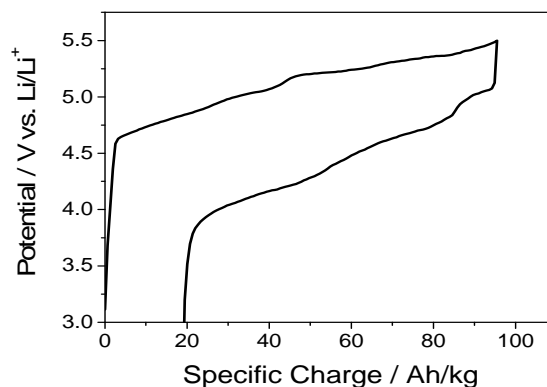
Figure 1. *Electrochemical cycling of graphite in 1 M LiPF$_6$, EC:DMC (1:1) electrolyte.*

Cycling in EC:DMC exhibits a lower specific charge. An increase can be observed in the 8th and 9th cycle which points to enhanced electrolyte decomposition, nevertheless the potential plateaus were observed throughout all cycles and thus, PF$_6^-$ can be intercalated and deintercalated even in this electrolyte. The other investigated electrolytes show a very large first charge value indicating massive electrolyte decomposition. In tendency, the higher the first charge, the lower is the specific charge in the subsequent cycles, except for EMS. For all electrolytes the discharge values were observed to be lower than the charge values which points to partial electrolyte decomposition even in the more stable solvents.
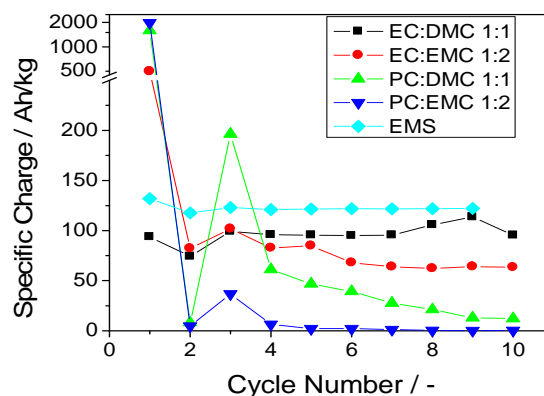
Figure 2. *Cycling behavior (charging steps only) of graphite in the high potential region (3.0 – 5.5 V vs. Li/Li$^+$) in different electrolytes.*

PC containing electrolytes show less stable behavior than EC based ones and DMC is superior than EMC related to oxidation stability. Most probably the less oxidation stable the electrolyte, the more the graphite structure is deteriorated during the high potential cycling, preventing the anions from reversible intercalation/deintercalation. Possibly this occurs by solvated cointercalation accompanied with solvent oxidation, leading to exfoliation of the graphite.

References

[1] J. A. Seel, J. R. Dahn, J. Electrochem. Soc. **147**, 892-898 (2000).

[2] P. Novák, W. Scheifele, F. Joho, O. Haas, J. Electrochem. Soc. **142**, 2544-2540 (1995).

---

[1] TIMCAL SA, Bodio TI

THE INFLUENCE OF LITHIUM EXCESS IN THE TARGET ON THE PROPERTIES AND COMPOSITIONS OF THE $Li_{1+x}Mn_2O_{4-\delta}$ THIN FILMS PREPARED BY PLD

F. Simmen, T. Lippert, P. Novák,
B. Neuenschwander[1], M. Döbeli[2], M. Mallepell[2],
A.Wokaun
+41 56 310 4144
franziska.simmen@psi.ch

Rechargeable lithium-ion batteries utilizing a lithium metal oxide as positive electrode are nowadays commonly used in mobile applications such as cameras, laptop computers, and mobile phones. The alternative electroactive material to the currently used layered $LiCoO_2$ could be the nontoxic cheaper spinel $LiMn_2O_4$ (space group Fd3m).

$LiMn_2O_4$ can be synthesized by different methods, e.g., spray pyrolysis [1], and in the form of thin films by pulsed laser deposition (PLD) [2-4]. The advantage of thin films as cathode materials is the possibility to study the lithium insertion process and the electrode/electrolyte interface reactions during cycling of pure $Li_xMn_2O_4$. This means that, differently to powder based electrodes, additives such as conductive carbon and binder materials are not present.

Pulsed laser deposition has one disadvantage, consisting in the control of the composition, which is difficult for volatile light elements [2], such as lithium. It was suggested by Julien et al. to overcome the loss of lithium by applying targets with lithium excess [4].

Experimental

Thin films of $Li_{1+x}Mn_2O_{4-\delta}$ on stainless steel substrates (T ~ 500 °C) were prepared by PLD (KrF laser, Lambda Physik, 248 nm, 20 ns, 10 Hz, 4.0 – 4.3 Jcm^{-2}, 18000 pulses, d_{t-s} = 4 cm, p_{O2} = 0.2 mbar). Different target compositions ($Li_{1.03}Mn_2O_4$ + x Li_2O, x= 0, 2.5, 7.5, 12.5 Mol%) were used. The targets ($Li_{1.03}Mn_2O_4$ + x Li_2O) were prepared by mixing $Li_{1.03}Mn_2O_4$ (99.7 % purity, Honeywell, Li/Mn = 0.515) and Li_2O (99.5 % purity, Alfa Aesar) powders and subsequent pressing and sintering.

The thin films were cycled in the potential range of 3.5 - 4.4 V versus Li/Li$^+$ (cyclic voltammetry at 0.05 mV s^{-1}) using Li foil (Aldrich) as anode and a solution of 1 M $LiPF_6$ (Ferro) in 1:1 EC:DMC (Ferro, EC: ethylene carbonate, DMC: dimethyle carbonate) as electrolyte.

Results and discussion

The prepared polycrystalline thin films showed a dependency between the used target composition and the film composition. The oxygen content is below the stoichiometric content of 2 which most probably results in the formation of oxygen vacancies in the spinel. The target with 7.5 Mol% of added Li_2O results in films with the desired lithium content of ca. 1.04. The loss of lithium, comparing the target and the film compositions, is decreasing from 24.3 % to 11.7 % with increasing lithium content in the target. This could be due to a higher probability for lithium to reach the substrate without collisions. The depth profile showed a homogenous distribution of Li, Mn, and O in the film.

The measured cyclic voltammograms of the thin films (see Figure 1) show the characteristic two redox peak pairs of $LiMn_2O_4$.
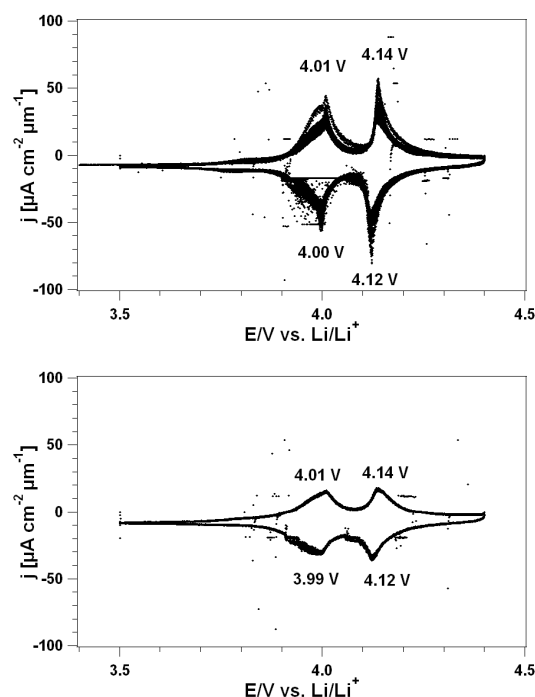
Figure 1. Typical cyclic voltammograms at 0.05 mV s^{-1} of thin films of $Li_{0.87}Mn_2O_{3.47}$ after 20 (top) and 140 (bottom) cycles; 20 cycles are shown.

After 120 cycles the normalized current density is decreasing, which is most probably due to degradation of the films during cycling. A significant shift of the redox peaks with the cycle number is not observed, suggesting that the insertion and deinsertion mechanism does not change.

Conclusion

The present work confirms that the preparation of polycrystalline thin Li-Mn-O films with PLD with a desired lithium content is possible. The target with a composition of $Li_{1.03}Mn_2O_4$ + 7.5 Mol% Li_2O yielded films with the desired Li/Mn ratio of about 1.04. All prepared thin films exhibit a good electrochemical cycle stability confirming their applicability for detailed studies of the lithium insertion/deinsertion processes.

References

[1] D. Y. K. Seo Hee Ju, Eun Byul Jo, Yun Chan Kang, J. Ceram. Soc. Jap. **115,** 241-244 (2007).

[2] C. Ouyang, H. Deng, Z. Ye, M. Lei, L. Chen, Thin Solid Films **503,** 268-271 (2006).

[3] T. Dumont, T. Lippert, M. Dobeli, H. Grimmer, J. Ufheil, P. Novak, A. Würsig, U. Vogt, A. Wokaun, Appl. Surf. Sci. **252,** 4902-4906 (2006).

[4] C. Julien, E. Haro-Poniatowski, M.A. Camacho-Lopez, L. Escobar-Alarcon, J. Jimenez-Jarquin, Mater. Sci. Eng., B **72,** 36-46 (2000).

---

[1] Berner Fachhochschule, Burgdorf
[2] Paul Scherrer Institut and ETH Zürich

SINGLE-WALLED CARBON NANOTUBES AS A MODEL SYSTEM FOR SUPERCAPACITOR ELECTRODES

P. Ruch, A. Foelske, R. Kötz, A. Wokaun
+41 56 310 4131
patrick.ruch@psi.ch

Activated carbon electrodes in supercapacitors exhibit complex structural properties on the nanometer-scale regarding both crystallinity and porosity. These parameters dictate the electrochemical charge storage performance of supercapacitors.

As a step towards understanding the charging behaviour of activated carbon in supercapacitors, single-walled carbon nanotubes (SWCNTs) were investigated as a model electrode with well-defined structural and chemical properties.

Experimental

SWCNTs prepared by the HiPco® process were obtained from Carbon Nanotechnologies Inc. The as-received powder was used as a working electrode in electrochemical cells enabling the *in situ* measurement of Raman spectra [1] and height change [2], respectively. The counter and reference electrodes consisted of PTFE-bound activated carbon, and the electrolyte used was 1M Et_4NBF_4 in acetonitrile (AN). All materials were dried at 120°C under a vacuum better than $3 \cdot 10^3$ Pa for at least 24 hours and then assembled in the sealed cells in an argon-filled glove-box with < 1 ppm O_2 and H_2O.

The SWCNT electrode was cycled between 0 and ±1.5 V vs. carbon, respectively, at a sweep rate of 1 mV/s. The Raman spectra of the SWCNTs were obtained using a Labram series Raman microscope (Jobin Yvon SA) with a HeNe-laser (E_{laser} = 1.96 eV).

Results

The height change of the SWNT electrodes during electrochemical cycling is plotted in Figure 1, showing an initial irreversible swelling followed by reversible height changes.
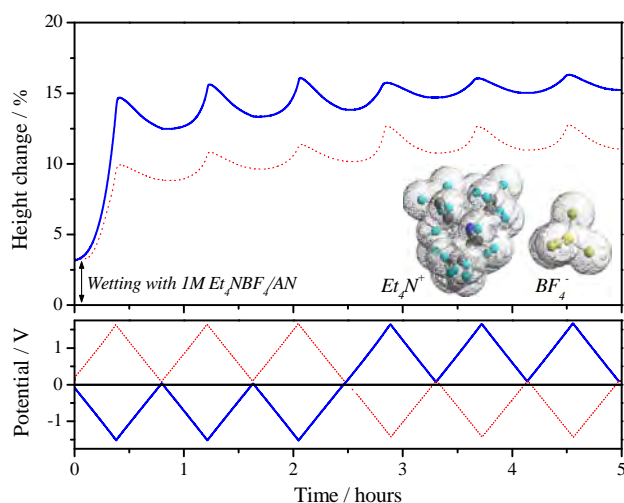
Figure 1. In situ dilatometry of SWCNTs during potential sweeps.

The SWCNTs are capped at the ends and form bundles containing many individual SWCNTs [3]. Any observed expansion must therefore be due to a widening of the pore channels between the SWCNTs.

The pronounced expansion upon the first charging process indicates that bundles are irreversibly loosened. The attractive forces between ions and charged SWCNTs thus appear sufficiently strong to overcome the forces which hold together individual SWCNTs. The reversible swelling observed is due to changes in ion concentration within the pore channels during charging and discharging. The difference in magnitude of the swelling can be explained by the different sizes of the corresponding counter-ions involved in balancing the charge on the SWCNT network.

The band intensities of the radial breathing modes (RBM) of the SWCNTs are shown in Figure 2. The inset shows the four most prominent RBM bands observed in the Raman spectrum. These are associated with SWCNTs of specific diameters and chiralities which are in resonance with the laser energy [4].
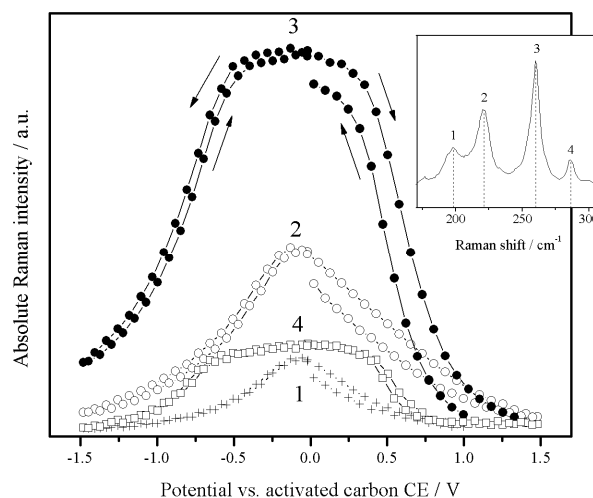
Figure 2. Intensity variation of RBM bands during cycling.

Upon positive or negative charge injection into the SWCNT network, it can be seen that bands 1 and 2 experience a decrease in intensity due to reduced transition probabilities between occupied and empty electronic states. These bands can be assigned to metallic SWCNTs. The intensity maximum corresponds to the half-filling potential between the valence (π) and conduction (π^*) bands [5].

Bands 3 and 4 are expected to belong to semi-conducting SWCNTs. Indeed, Figure 2 reveals intensity plateaus for these bands due to the fact that no charge injection can take place within the band gap. These results provide a basis for the electrochemical charging behaviour of a sp^2-hybridized, aromatically bound carbon system in which no ion intercalation can take place.

References

[1] L.J. Hardwick, M. Hahn, P. Ruch, M. Holzapfel, W. Scheifele, H. Buqa, F. Krumeich, P. Novák, R: Kötz, Electrochim. Acta. **52**, 675-680 (2006).

[2] M. Hahn, O. Barbieri, R. Gallay, R. Kötz, Carbon **44**, 2523-2533 (2006).

[3] P. Nikolaev, M.J. Bronikowski, R.K. Bradley, F. Rohmund, D.T. Colbert, K.A. Smith, R.E. Smalley, Chem. Phys. Lett. **313**, 91-97 (1999).

[4] A. Jorio, M.A. Pimenta, A.G.S. Filho, R. Saito, G. Dresselhaus, M.S. Dresselhaus, New J. Phys. **5**, 139.1-17 (2003).

[5] I. Heller, J. Kong, K.A. Williams, C. Dekker, S.G. Lemay, J. Am. Chem. Soc. **128**, 7353-7359 (2006).

BATTERIES & SUPERCAPACITORS

DIAGNOSTIC

A NOVEL ELECTROCHEMICAL CELL FOR *IN SITU* NEUTRON DIFFRACTION STUDIES OF ELECTRODE MATERIALS FOR LITHIUM-ION BATTERIES

F. Rosciano, M. Holzapfel, W. Scheifele,
H. Kaiser, P. Novák
+41 56 310 5426
fabio.rosciano@psi.ch

Lithium-ion batteries (Li-ion) are the most widely used energy source for many daily applications, from consumer electronics to power tools. Their strengths mainly lie in the high energy density, highly reversible nature of their cycling and the long shelf life. Nonetheless, in order to improve these systems to make their use possible in more advanced applications like in hybrid vehicles, further enhancements are necessary.

Li-ion batteries work on the principle of reversible insertion ("intercalation") and extraction ("de-intercalation") of lithium ions from host insertion materials. In general, the negative electrodes are based on carbonaceous materials, while the positive electrodes use various transition metals compounds such as layered oxides (e.g. $LiCoO_2$), olivine type phosphates (e.g. $LiFePO_4$) or spinel type oxides (e.g. $LiMn_2O_4$). In order to improve the energy density of Li-ion batteries, it is needed to find new materials that would enable either higher reversible capacity or wider potential windows: the practical charge that can be extracted from the cathode is roughly the half of the one of the anode (~150 mAh/g vs. ~350 mAh/g) and additionally many compounds show a high reactivity with the electrolyte at potentials positive to 4.3 V vs. Li^+/Li.

The development of these much needed innovative materials triggers the need for advanced analysis techniques, among which powder diffraction is a key player: both X-ray and neutron diffraction offer a powerful and well established platform to study phase transitions and other transformations occurring in the electrode materials. Different information can be derived from the use of these radiations, among which the most important for Li-ion studies is the ability of neutrons to directly investigate lithium atoms in the crystalline structures. Furthermore, given the metastable nature of electrode materials in their charged states and their sensitivity to oxygen and moisture, the need for *in situ* techniques is extremely important in this field of application.

In situ X-ray diffraction is a well established technique, both at conventional laboratory sources [1] and at synchrotron facilities [2]. Neutron diffraction, on the other hand, is still in its pioneering stage, and only one attempt to create an electrochemical cell that would effectively couple electrochemistry and diffraction has been undertaken until now [3]. It has to be noted that the use of neutrons for diffraction represents a quite hostile environment that poses additional challenges when planning the geometry of the device. For example, given the low interaction of neutrons with matter, it is needed to have a large amount of active material in the sample: this leads to thick electrodes and high currents that can result in large overpotentials and inhomogeneities in the electrode. Furthermore, many elements can absorb the radiation and become radioactive: among the most dangerous is cobalt, often a key component in positive electrode materials. Additionally, today's electrolytes are based on organic solvents that contain many hydrogen atoms: these have to be substituted with deuterium in

order to avoid the strong incoherent scattering that would dramatically lower the signal to noise ratio of the diffraction experiments.

After considering all these possible sources of difficulties, a new cell for *in situ* neutron diffraction experiments on electrode materials for Li-ion batteries was designed and it is hereby presented.

Experimental

A schematic representation of the *in situ* cell is shown in Figure 1.
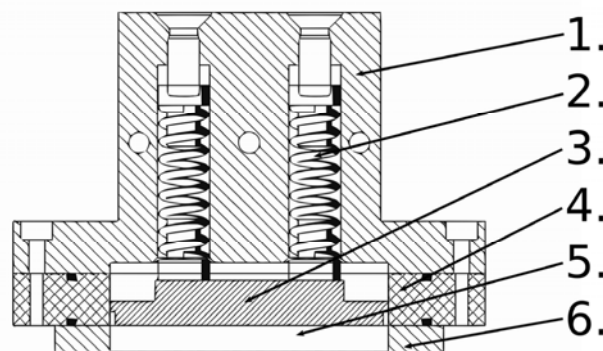
Figure 1. *Schematic view of the in situ electrochemical cell. The elements of the device are: 1. Cell top, 2. Spring, 3. Negative current collector, 4. PEEK cell body, 5. Cavity for the electrode material, 6. Positive current collector.*

Six elements constitute the device: the cell top (1.) is made out of aluminum and contains two springs (2.) that push on the copper negative current collector (3.) in order to achieve the best possible contact between the electrodes. The cell body is made out of polyetheretherketone (PEEK, 4.), a polymer inert to the solvents present in the electrolyte. The cavity in which the electrode material is pressed (5.) is machined in the aluminum positive current collector (6.) that serves as sample holder.

The electrode assembly is shown in Figure 2 and demonstrates in detail the various layers that form the lower part of the device.
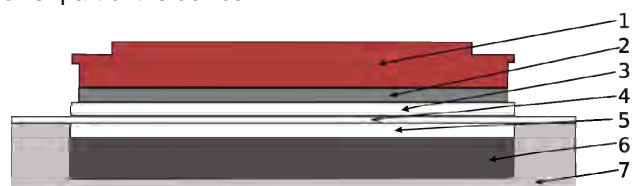
Figure 2. *Schematic view of the electrode assembly. 1. Copper current collector, 2. Metallic lithium strip, 3. Glass fiber separator, 4. Polymeric separator, 5. Glass fiber separator, 6. Active material powder, 7. Positive current collector.*

Under the negative current collector (1.) the anodic material is placed (metallic lithium strip, 2.). This sits on a glass fiber separator (3.) that can easily be soaked with electrolyte. Underneath there is a thin polymeric separator (4.) providing protection against lithium dendrite formation. Going further down another glass fiber separator (5.) is placed on the active material powder (6.) contained in the positive current collector (7.). The positive electrode is prepared by dry mixing of active material powder and carbonaceous materials, used as filler for the cavity and to enhance the electronic conductivity of the whole electrode.

Results

In order to test the performance of the cell for both electrochemical and diffraction suitability $LiNiO_2$ was chosen as model material. This choice was not dictated by the particularly interesting properties of this material but because it is well known and has been extensively studied before [4]. Additionally, nickel is stable when irradiated with neutrons, allowing for a safe removal of the cell prototypes after the tests.

In order to test the electrochemical performance, a $LiNiO_2$ electrode was cycled between 4.5 V and 3.0 V vs. Li^+/Li, and then compared to a similar electrode included in a normal coin-like cell used for routine experiments. The resulting potential profiles are shown in Figure 3.
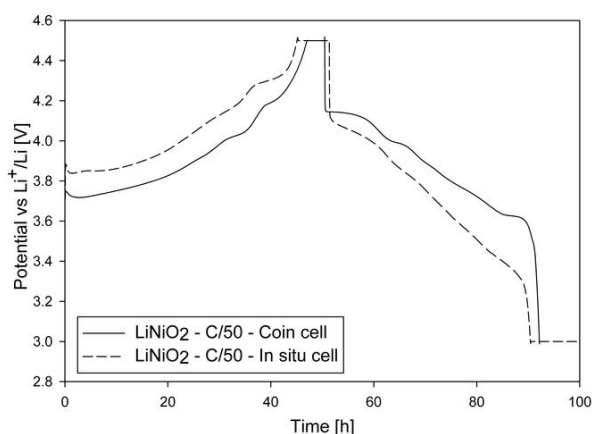
Figure 3. *Comparison between the electrochemical performance of the neutron cell (dashed line) and a coin-like cell (solid line). Both cells were cycled at a C/50 rate against a metallic lithium counter electrode. The electrolyte was a 1:1 (wt.%) mixture of ethylene carbonate and dimethylcarbonate with 1M $LiPF_6$.*

The curve obtained for the neutron cell shows similar features ("plateaus") to the one relative to the conventional cell. A well defined overpotential in the order of 150 mV is also observable.

To verify the suitability of the cell to obtain clear powder diffraction data, the device was tested at the HRPT powder diffractometer at the SINQ neutron source at PSI. A cell was assembled as described and the positive electrode was a mixture of 2:1 in weight between $LiNiO_2$ and carbonaceous materials.

The resulting diffraction pattern is shown in Figure 4.
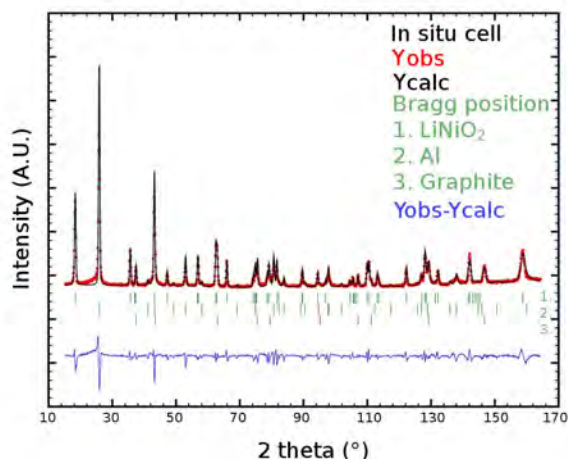
Figure 4. *Neutron diffraction pattern of a $LiNiO_2$ electrode measured in the in situ cell. The measurement was performed at a wavelength of 1.5 Å.*

Along with the $LiNiO_2$ pattern it is possible to observe the peaks relative to the aluminum current collector and those relative to the graphite contained in the electrode.

From the results it is clear that the new cell satisfies in both, electrochemical and diffraction experiments. Thus, *in situ* experimental campaigns at various neutron sources are now possible.

Conclusions

A new electrochemical cell allowing for *in situ* neutron diffraction measurements was presented. The cell was tested for both electrochemical and diffraction capabilities: it demonstrated its suitability to sustain full charge-discharge cycles and to obtain diffraction patterns with very high signal to noise ratio.

References

[1] G.G. Amatucci, J.M. Tarascon and L.C. Klein, J. Electrochem. Soc **143** (3), 1114-1123 (1996).

[2] F. Rosciano, M. Holzapfel, H. Kaiser, W. Scheifele, P. Ruch, M Hahn, R. Kötz, P. Novák, J. Synch. Rad. **14**, 487-491 (2007).

[3] O. Bergstöm, A. M. Andersson, K. Edström, T. Gustafsson, J. Appl. Cryst. **31**, 823-825 (1998).

[4] A. Hirano, R. Kanno, Y. Kawamoto, Y. Takeda, K. Yamaura, M. Takano, K. Ohyama, M. Ohashi, Y. Yamaguchi, Solid State Ionics **78**, 123-131 (1995).

DIRECT EVIDENCE OF OXYGEN EVOLUTION FROM $Li_{1+x}(Ni_{1/3}Mn_{1/3}Co_{1/3})_{1-x}O_2$ AT HIGH POTENTIALS

F. La Mantia, F. Rosciano, N. Tran, P. Novák
+41 56 310 2161
fabio.lamantia@psi.ch

The lithium-ion battery possesses the greatest energy density of all known rechargeable battery systems and has a power density close to the nickel-cadmium battery [1]. The major challenge of lithium-ion battery research is to develop systems with even higher power and energy densities.

The oxide family with the general formula $Li_{1+x}(Ni_{1/3}Mn_{1/3}Co_{1/3})_{1-x}O_2$ called NMC is believed to be among the most promising positive electrode materials to substitute the current industrial standard, $LiCoO_2$.

NMC compounds show higher thermal stability [2,3], a good cycling stability, and a higher specific charge with respect to $LiCoO_2$ [4] (ca. 150 mAhg^{-1} for the NMC compound with x = 0 when cycling in the potential window from 2.5 to 4.4 V vs. Li/Li$^+$). A voltage "plateau" is observed on the first galvanostatic charging curve in the high voltage region (>4.5 V vs. Li/Li$^+$) for overlithiated NMC compounds [5]. Dahn's group suggested to explain this plateau with structural changes associated with oxygen loss from the oxide and a simultaneous Li$^+$ extraction [2].

Two representative NMC compounds with nominal values of overlithiation degree x = 0 and x = 0.1, respectively, were therefore synthesized and compared. We confirmed the differences between the two compounds in the charge/discharge curves at high potentials, as reported in the literature. The high voltage region was then examined for both NMC compounds with Differential Electrochemical Mass Spectrometry (DEMS).
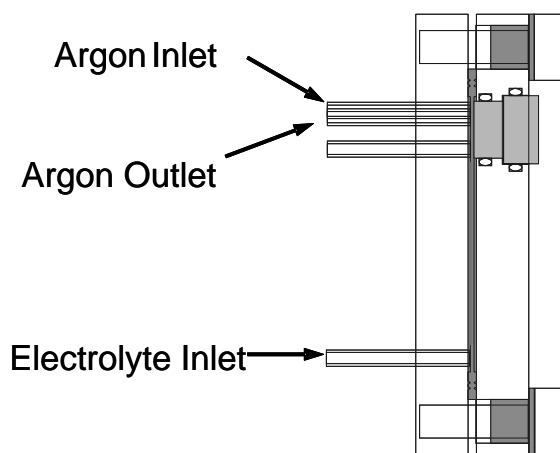
Figure 1. Cell design for Differential Electrochemical Mass Spectrometry experiments.

Experimental

NMC oxides with different degree of overlithiation were obtained by soft chemistry synthesis in an aqueous-ethanol solution. A subsequent thermal treatment at 850 °C was necessary to obtain the desired oxide.

The Differential Electrochemical Mass Spectrometry (DEMS) experiments were performed at 25 °C in a separator-free cell accommodating metallic lithium counter and oxide working electrode, respectively, on titanium current collectors (see Figure 1). Cyclic voltammetry was performed between 5.3 and 2.5 V at a sweep rate of 0.2 mV s^{-1} in a 1:1 by wt. mixture of ethylene carbonate (EC) and dimethyl carbonate (DMC) containing 1 M LiPF$_6$.

Results

Figure 2 shows the differential plot of dQ/dE vs. E of the galvanostatic experiments for the first cycle. It revealed that at high potentials (above 4.5 V) the stoichiometric NMC (x = 0) shows a small irreversible oxidative peak, while the overlithiated sample (x = 0.1) shows an intense irreversible oxidative peak, which disappears in the following cycles (see Figure 3).
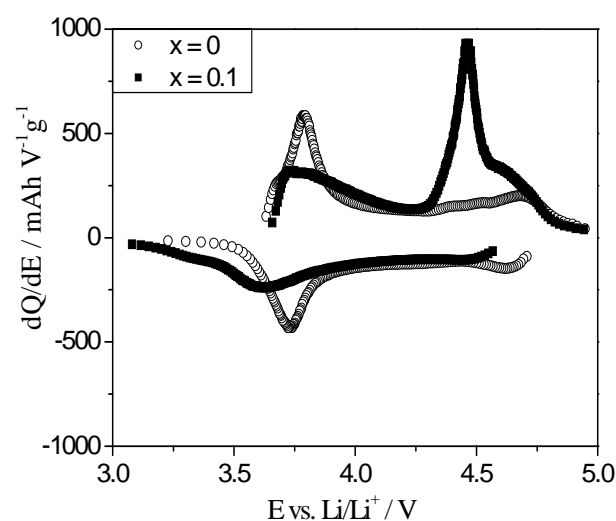
Figure 2. Differential plot for the $Li_{1+x}(Ni_{1/3}Mn_{1/3}Co_{1/3})_{1-x}O_2$ (x = 0 and x = 0.1, respectively) materials in the high voltage experiment in EC:DMC, 1 M LiPF$_6$ (1st cycle).
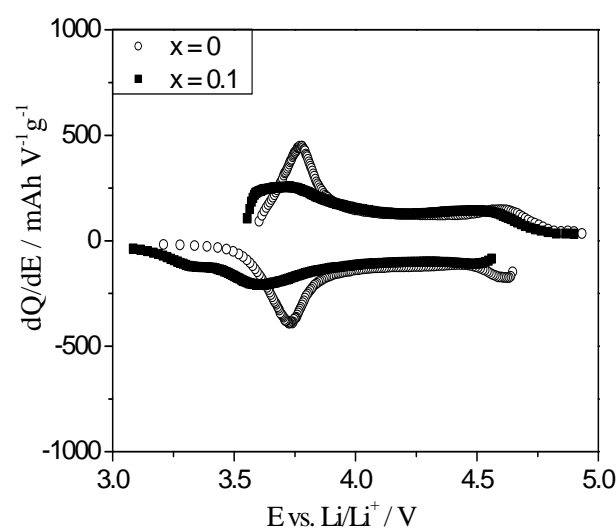
Figure 3. Differential plot for the $Li_{1+x}(Ni_{1/3}Mn_{1/3}Co_{1/3})_{1-x}O_2$ (x = 0 and x = 0.1, respectively) materials in the high voltage experiment in EC:DMC, 1 M LiPF$_6$ (2nd cycle).

The high voltage region was further investigated with the DEMS technique, which analyzes *on-line* the electrochemically generated gases and volatile compounds. Structural changes were anticipated for the overlithiated NMC compounds in this voltage region.
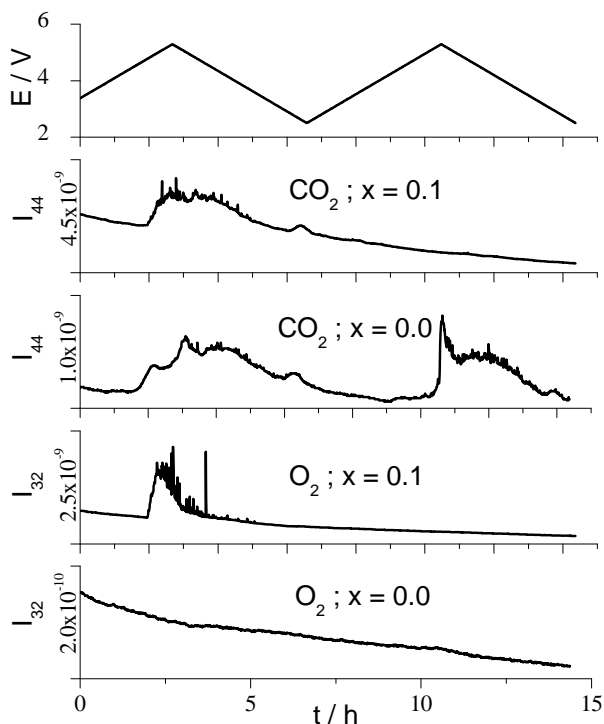
Figure 4. Plot of mass signal intensities $I_{m/z}$ $[A\ g^{-1}]$ for $Li_{1+x}(Ni_{1/3}Mn_{1/3}Co_{1/3})_{1-x}O_2$ (x = 0 and x = 0.1, respectively) normalized in respect to the oxide mass; E is the potential vs. Li/Li^+ [V].

Figure 4 compares the intensities of the relevant mass signals $I_{m/z}$ from electrodes containing the two NMC materials. On the top the applied potential E (vs. Li/Li^+) is also given. The m/z = 32 signal is assigned to oxygen and m/z = 44 to CO_2, respectively. Clearly, for the stoichiometric sample no oxygen evolution is detected while CO_2 is evolved during the first and further cycles in the high voltage region. The CO_2 evolution is due to the electrolyte oxidation, as evidenced by us for a number of electroactive oxides elsewhere [6,7]). In contrast, for the overlithiated NMC oxide, both CO_2 and O_2 evolution is observed in the high voltage region but only during the first cycle.

This result strongly supports the hypothesis that, (i) during the first delithiation the overlithiated NMC compounds irreversibly lose oxygen at high potentials (as proposed by the Dahn's group [6]) and (ii) in the case of the overlithiated NMC materials, the oxidation of the electrolyte (evidenced by the CO_2 evolution) is somehow inhibited, in contrast to the stoichiometric material. A surface film composed of electrolyte oxidation products and/or changed surface properties of the NMC oxide due to the oxygen loss is believed to block the further oxidation of the electrolyte and consequently the CO_2 development in the second cycle.

Conclusion

Using the DEMS technique we observed oxygen development from the overlithiated NMC oxide in the first cycle at potentials positive to 4.5 V vs. Li/Li^+, which proves

a previous hypothesis assuming oxygen loss from the positive electrode material's crystal lattice.

References

[1] M. Winter, J.O. Besenhard, M.E. Spahr, P. Novák, Adv. Mater. **10,** 725-763 (1998).

[2] Z.H. Lu, D.D. MacNeil, J.R. Dahn, Electrochem. Solid State Lett. **4,** A191-A194 (2001).

[3] N. Tran, L. Croguennec, C. Labrugere, C. Jordy, P. Biensan, C. Delmas, J. Electrochem. Soc. **153,** A261-A269 (2006).

[4] T. Ohzuku, Y. Makimura, Chem. Lett. 642-643 (2001).

[5] Z.H. Lu, J.R. Dahn, J. Electrochem. Soc. **149,** A815-A822 (2002).

[6] A. Würsig, W. Scheifele, P. Novák, J. Electrochem. Soc. **154,** A449-A454 (2007).

[7] J. Vetter, M. Holzapfel, A. Würsig, W. Scheifele, J. Ufheil, P. Novák, J. Power Sources **159,** 277-281 (2006).

VIBRATIONAL SPECTRA OF NITROXIDE MATERIALS FOR ORGANIC RADICAL BATTERIES

P. Maire, P. Nesvadba[1], T. Hintermann[1], P. Novák

+41 56 310 5810
pascal.maire@psi.ch

Lithium-ion batteries are widely used in portable electronic devices and are promising power sources for future hybrid electric vehicles. They combine high energy density and power density with long cycle life. A drawback is the fact that the cathode materials of these batteries consist of late transition metal compounds. These metals - cobalt is the most often used among them - are expensive, toxic, and of limited availability. There is thus a need to develop alternative cathode materials, e.g. on the basis of organic molecules. Nakahara and co-workers [1] were the first to describe cathodes for lithium-ion batteries made from polymeric nitroxide material (Figure 1). Upon charging of battery, the nitroxide group is oxidized at a potential of 3.7 V vs. Li/Li$^+$, while lithium is intercalated into the anode material.
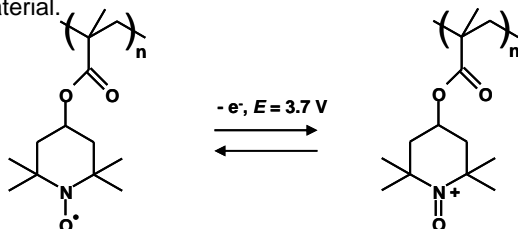
Figure 1. *Reversible one-electron oxidation of PTMA at a potential E = 3.7 V vs. Li/Li$^+$ leading to oxoammonium cation.*

To get more insight into the processes in organic radical batteries, an electrochemical cell allowing in-situ characterization of the cathode material by infrared spectroscopy was developed.

Experimental

Poly(4-methacryloxy-tetramethylpiperidine-*N*-oxyl) (PTMA) prepared by group transfer polymerization was used as model electrode material [2]. Cathodes were made by pressing a mixture of active nitroxide material (PTMA, 74%), vapour grown carbon fibres as conductive agent (VGCF, 13%) and polyvinylidene difluoride binder (PVDF, 13%) onto an aluminium mesh. Li$_4$Ti$_5$O$_{12}$ was used as counter/reference electrode. A solution of 1M LiClO$_4$ in acetonitrile was used as electrolyte, ensuring a large free spectral window. Cells were assembled in polypropylene casing on top of a diamond ATR unit. A hole in the casing permits to press the cathode material directly onto the ATR prism (Figure 2).

Results

Infrared spectra of a cathode made from organic active material were acquired while the cell was charged and discharged (Figure 3). The initial spectrum of the uncharged electrode (on top) shows the expected bands for alkyl C-H stretching vibrations (2950 cm^{-1}), C≡N stretching of the electrolyte solvent (2249 cm^{-1}) and the C=O function
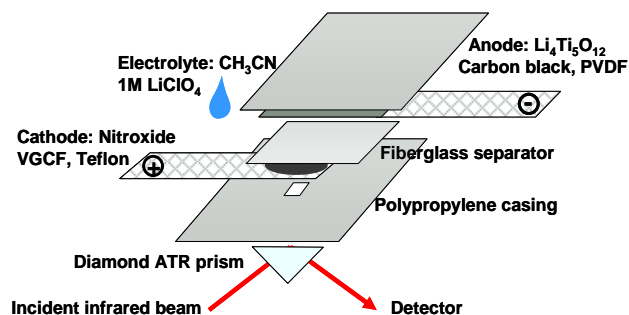
Figure 2. *In-situ infrared cell on diamond ATR device.*

of the ester linkage between TEMPO and the polymer backbone (1725 cm^{-1}). The N-O$^•$ vibration would be expected around 1360 cm^{-1}, but the band is usually weak and is not clearly resolved in this case. Upon charging of the cell a new signal at 1625 cm^{-1} emerges, which is assigned to the stretching vibration of the newly formed N=O double bond. The reaction depicted in Figure 1 is thus confirmed by these spectra. This redox process involves no major structural changes of the nitroxide, which is a prerequisite for fast electron transfer, and explains the high rate capability of organic radical batteries [3].
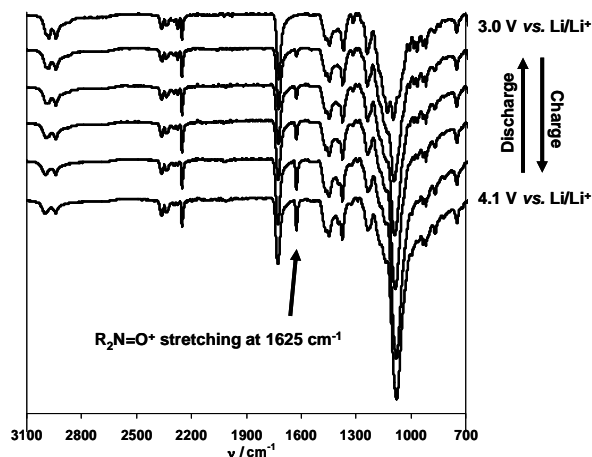
Figure 3. *Infrared spectra of a cathode made from PTMA as a function of state of charge.*

Future work aims at increasing the energy density of organic radical batteries. Nitroxides with lower molecular mass and more positive redox potential are now being tested, but their long term stability is not yet sufficient. In-situ infrared spectroscopy could help revealing degradation mechanisms and thus lead the way to improved battery materials.

References

[1] K. Nakahara, S. Iwasa, M. Satoh, Y. Morioka, J. Iriyama, M. Suguro, E. Hasegawa, Chem. Phys. Lett. **359**, 351-354 (2002).

[2] L. Bugnon, C. J. H. Morton, P. Novák, J. Vetter, P. Nesvadba, Chem. Mater. **19**, 2910-2914 (2007).

[3] Y. Yonekuta, K. Oyaizu, H. Nishide, Chem. Lett. **36**, 866-867 (2007).

[1] Ciba, Basel

COLORIMETRIC DETERMINATION OF LITHIUM CONTENT IN GRAPHITE ANODES

W. Scheifele, P. Maire, P. Novák
+41 56 310 2471
werner.scheifele@psi.ch

Today's lithium-ion batteries still suffer from capacity fading upon prolonged storage and intense cycling. Much effort has been devoted to the understanding of this capacity fading [1], and loss of mobile lithium has been proposed as a main reason [2]. Besides loss of active lithium, an uneven distribution of lithium in the active materials was also reported to affect cycle life of lithium-ion cells. This has been observed in graphite anode materials [3], as well as in metal oxide cathode materials.

Graphite is known to undergo a color change upon intercalation of lithium from black in the pristine state to golden yellow in the fully lithiated material of composition LiC_6. Intermediate compounds are of dark blue and reddish color. Colorimetry might thus be a straightforward method to determine the state of charge of a graphite electrode.

Experimental and Results

To correlate the state of charge with color, a series of model graphite electrodes were fully charged in coin cells and then discharged to a defined state of charge (SOC). The coin cells were opened in the inert atmosphere of a glove box. The color of the electrodes clearly indicates the state of charge as shown in Figure 1.

100% SOC, 32 mV   90% SOC, 93 mV   80% SOC, 94 mV

70% SOC, 94 mV   60% SOC, 126 mV   50% SOC, 133 mV
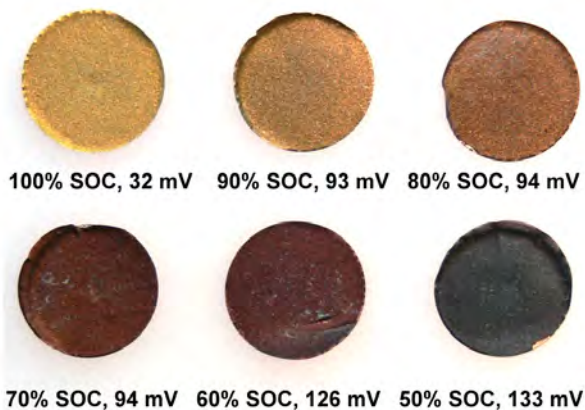
Figure 1. Graphite electrodes harvested from coin cells after intercalation of different amounts of lithium.

The charge/discharge curves obtained for lithium intercalation in graphite show distinct plateaus indicative of different staging states. As a consequence, the open circuit voltage for cells charged to 90%, 80% and 70% respectively is almost equal, i.e. about 93-94 mV.

The surface color composition of the anodes was measured using a commercial color analyzer. The color, expressed in values of red, green, and blue was plotted vs. SOC. Figure 2 shows the strong correlation between red and green color components and the state of charge.
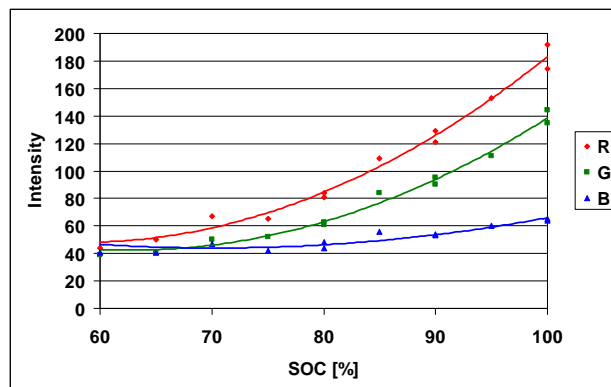
Figure 2. Calibration curves for electrodes made from graphite LBG1025 (90%) and PVDF (10%).

Commercial high power cells for consumer applications were cycled at a rate of 6C. After the capacity had dropped to 60% of the initial value, the cells were fully charged to 4.2 V, and opened in an argon filled glove box. Figure 3 shows one of these anodes with bright yellow, lithium-rich regions close to darker, lithium deficient areas.
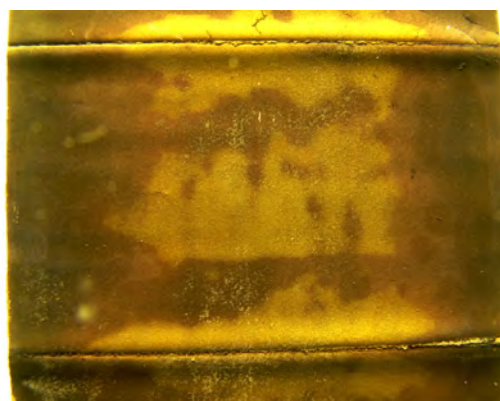
Figure 3. Anode of a commercial high-power cell after 1500 cycles at 6C rate.

The inhomogeneous distribution of active lithium is likely to lead to an accelerated degradation of cell performance due to local overcharge or overdischarge of active materials and lithium plating on the anode side. This problem seems to be of particular importance for high power cells, designed for fast charging rates.

References

[1] P. Arora, R.E. White, M. Doyle, J. Electrochem. Soc. **145**, 3647-3667 (1998).

[2] J. Christensen, J. Newman, J. Electrochem. Soc. **152**, A818-A829 (2005).

[3] Y. Reynier, R. Yazami, B. Fultz, J. Power Sources **165**, 616-619 (2007).

VOLTAGE BALANCING OF MANY SUPERCAPACITORS IN SERIES

R. Kötz, P. Ruch
+41 56 310 2057
ruediger.koetz@psi.ch

Supercapacitors (SC) are characterized by a rather small single cell voltage of 2.7 V. For many applications where higher voltages are required, such as for the drive train of an electric vehicle, several single cells have to be connected in series. In such a SC module, only the overall voltage is controlled by the power electronics and thus individual SC cells may acquire a voltage above the nominal voltage. Therefore, manufacturers recommend the use of active or passive voltage balancing devices.

Basically, the imbalance of single cell voltages within a module is caused by two effects: a distribution of (i) the capacitance C_i and (ii) leagake resistance R_i. Manufacturers typically guarantee a 10 % accuracy of these parameters. A sketch of a number of capacitors in series is shown in Figure 1.
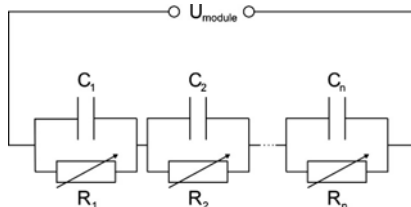
Figure 1. *Sketch of a series connection of supercapacitors.*

After Okamura [1] the spread in capacitance can be overcome by a so-called initialization process where all capacitors are adjusted to the same voltage at the upper operation voltage of the module. While the distribution of capacitance is important during dynamic charge/discharge processes, the different values of parallel resistances causing different degrees of self-discharge play an important role also during floating voltage periods of the module.

Model Calculation

In order to understand the evolution of single cell voltages in a SC module, a model calculation was performed based on an iterative discharge of the capacitors through the parallel resistors and a subsequent recharge of the capacitors to keep the module voltage constant in infinitesimal steps.
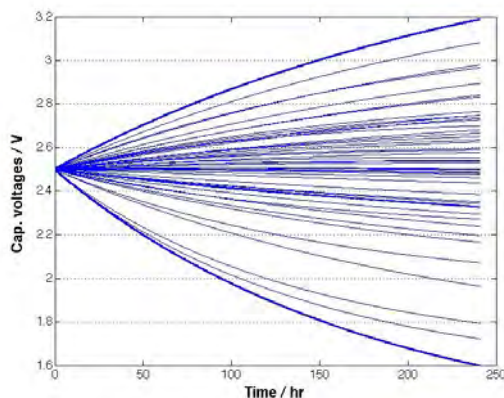
Figure 2. *Evolution of single cell voltages in a SC module with 50 capacitors in series; $C_i = 350 \pm 70$ F, $R_i = 2500 \pm 500$ Ω. R_i is assumed to be constant.*

The voltage evolution for 50 capacitors in series with a capacitance of 350 F and a parallel resistor with 2.5 kΩ after an initialization at 2.5 V is shown in Figure 2. For both, the capacitance and the parallel resistance, a normal distribution of 20 % was assumed.

With the above assumptions the highest voltage in the module approaches 3.3 V after 250 hours. Such a high voltage is detrimental for the respective capacitor and would require voltage balancing measures.

However, the result of Figure 2 is in clear contradiction to the experience made in the HY-LIGHT project [2], where a SC module in a hybrid fuel cell vehicle was used without any voltage balancing measures for more than two years without problems.

To understand this contradiction we investigated the leakage current of BCAP350 supercapacitors from Maxwell Technologies in more detail. It turned out that the parallel resistances are not constant, but decrease exponentially with increasing cell voltage. Typically, for an increase in cell voltage of 600 mV the leakage current increases 10-fold. Recalculation of the voltage evolution under these conditions results in a significantly different behaviour (Figure 3).
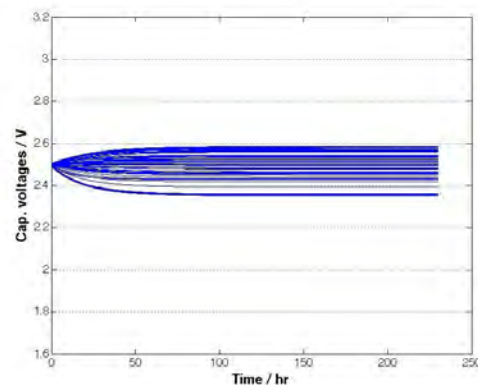
Figure 3. *Evolution of single cell voltages in a SC module with 50 capacitors in series; $C_i = 350 \pm 70$ F, $R_i = 2500 \pm 500$ Ω. R_i is a function of the cell voltage. Same scale as Figure 2.*

In contrast to Figure 2, the highest voltage in the module is now below 2.6 V, which corresponds to a <100 mV deviation from the nominal voltage. Obviously, the exponential dependence of the leakage currents on the cell voltage has a self-regulating effect. A voltage deviation <100 mV which will reduce the lifetime of the capacitor by less than a factor of 2 can be tolerated for many applications.

Conclusions

Voltage balancing measures, which introduce weight, volume and additional unreliability to the SC module, are not absolutely necessary to guarantee stable behaviour of a SC module. Monitoring of the individual cell voltages, however, is strongly recommended to detect malfunctioning cells in due time.

References

[1] M. Okamura, Proceedings of the 13th International Seminar on Double Layer Capacitors and Hybrid Energy Storage Devices, Deerfield Beach, Florida, 205 (2003).

[2] F.N. Büchi, G. Paganelli, P. Dietrich, D. Laurent, A. Tsukada, P. Varenne, A. Delfino, R. Kötz, S.A. Freunberger, P.-A. Magne, D. Walser, D. Olsommer, Fuel Cells 07, **4**, 329 (2007).

CATALYSIS & INTERFACES

EXPERIMENTAL AND THEORETICAL INVESTIGATIONS OF NICKEL DEPOSITION ON γ-AL$_2$O$_3$

F. Loviat, I. Czekaj, J. Wambach, A. Wokaun
+41 56 310 4464
izabela.czekaj@psi.ch

Recently, surface modifications of a commercial Ni/Al$_2$O$_3$ catalyst during the production of methane from synthesis gas [1] were investigated by *quasi in-situ* X-ray photoelectron spectroscopy (XPS). The effect of the synthesis gas on the surface properties of the catalyst and on its activity under methanation conditions was studied on an atomic level [2]. The conclusion was that the stability of different Ni clusters on the γ-Al$_2$O$_3$ support can be influenced by the type of deposition, which influences size and distribution of metal particles. Supplementary experimental and theoretical studies of nickel deposition on γ-Al$_2$O$_3$ have been used to help understanding further details about surface modifications during methanation and possible reasons of nickel particles detachment. .

Technical details

The metal deposition and XPS characterisation of model catalyst were carried out in a VG ESCALAB 220i XL (VG Scientific) setup, which is equipped with an additional preparation chamber and a home-made Metal Evaporator (ME). In parallel, the molecular structure of the model Ni/γ-Al$_2$O$_3$ catalyst used during methanation of synthesis gas was investigated using the DFT method (program code StoBe) with a cluster model and non-local functional approximation (RPBE). The cluster Al$_{15}$O$_{40}$H$_{35}$ has been selected for the investigation, representing the predominantly naturally-formed (100) surface of the γ-Al$_2$O$_3$ support. Ni clusters with different sizes were cut from Ni (100) surface and deposited at the Al$_{15}$O$_{40}$H$_{35}$ cluster in order to validate the deposition model determined by XPS analysis.

Nickel deposition (three different clusters Ni$_x$, x=2,7,9) on Al$_{15}$O$_{40}$H$_{35}$ clusters is shown in Figure 1.
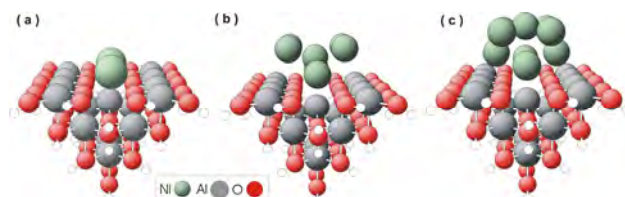
Figure 1. *Ni$_x$ model clusters: (a) Ni$_2$, (b) Ni$_7$, (c) Ni$_9$ deposited at (100) γ-Al$_2$O$_3$ represented by Al$_{15}$O$_{40}$H$_{35}$ cluster.*

Results and Discussion

Our experimental studies suggest that in case of room-temperature deposition of Ni on the Al$_2$O$_3$ support a kind of "modified" Stranski-Krastanov growth model can explain our observations. Firstly, a fraction of a Ni metal mono-layer (ML), presumably 0.5 ML with every second row missing, is deposited and, secondly, on top of this layer three-dimensional islands of Ni metal are growing (see Figure 2).
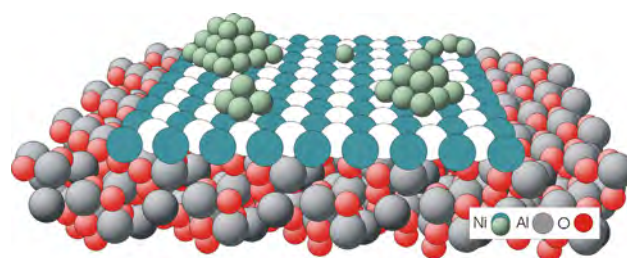
Figure 2. *Suggested model of nickel deposition at the γ-Al$_2$O$_3$ support with the "missing row" first layer*

Taking into account theoretical predictions of intensity together with the observed changes in Ni2p$_{3/2}$/Al2s ratio as well as Ni2p$_{3/2}$ binding energies (Figure 3), it becomes evident that up to about 0.5 ML the deposited nickel atoms are strongly bound to the oxygen of the γ-Al$_2$O$_3$ support (binding energy typical for NiO).
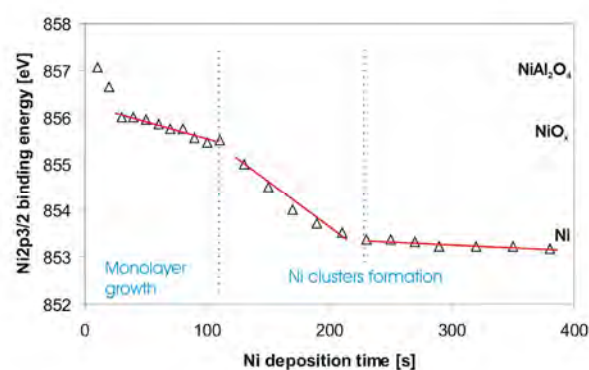
Figure 3. *Changes of BE Ni 2p$_{3/2}$ during nickel deposition on Al$_2$O$_3$ model catalysts: XPS studies.*

Our DFT calculations indicate that at first nickel adsorbs in hole positions of the γ-Al$_2$O$_3$ (100) surface between surface oxygen centres stabilised by -0.9 eV/Ni atom and influencing the electronic properties of the newly formed surface by modification of both oxygen and aluminium centres. The visible asymmetry suggests that Ni prefers being localized in AlO$_4$ tetrahedrons between rows of AlO$_5$, which quite accurately corresponds with the 0.5 ML coverage of nickel found experimentally as maximum of the first deposition stage.

Conclusions

Nickel is stabilized at the γ-Al$_2$O$_3$ surface and influences the electronic properties of the newly formed surface. Our DFT results correspond astonishing well with the 0.5 ML coverage found experimentally as maximum of the first deposition stage.

References

[1] F. Raimondi, M. Seemann, S. Biollaz, J. Wambach, A. Wokaun, PSI Scientific Reports 2003, **V**, 116 (2004).

[2] I. Czekaj, F. Loviat, F. Raimondi, J. Wambach, S. Biollaz, A. Wokaun, Appl. Catal., A, **329**, 68-78 (2007).

CORE LEVEL SHIFTS INDUCED BY ELECTROCHEMICAL INTERCALATION OF $(C_2H_5)_4N^+$ AND BF_4^- INTO HOPG

A. Foelske, P. Ruch, R. Kötz

+41 56 310 4193

annette.foelske@psi.ch

The electrochemical intercalation of lithium ions into graphite has been extensively studied for many years as this process is responsible for charging and discharging of lithium ion batteries (LIB) [1].

Like LIBs, Supercapacitors (SC) utilize carbon electrodes and non-aqueous electrolytes with the important differences that the carbons used in SCs provide a very high surface area and that the electrolyte contains quaternary ammonium salts like tetraethylammonium tetrafluoroborate (Et_4NBF_4) for charge storage. So far film formation and intercalation processes which might affect the aging of these devices were hardly investigated using surface analytical tools. Herein, we report on Fermi and core level shifts that have been observed after intercalation of the ions into a graphitic host structure using X-ray Photoelectron Spectroscopy (XPS).

Experimental

Highly oriented pyrolytic graphite (HOPG) was used as a working electrode in an electrochemical cell in which the counter and reference electrodes consisted of PTFE-bound activated carbon. The electrolyte used was 1M Et_4NBF_4 in propylene carbonate (PC). All materials were dried at 120°C under a vacuum better than $3 \cdot 10^3$ Pa for at least 24 hours, then assembled in the sealed cells and, subsequently, electrochemically prepared in an argon filled glove box with < 1 ppm O_2 and H_2O. The HOPG was cleaved with adhesive tape prior to each electrochemical experiment.

After electrochemical preparation, the HOPG electrode was removed from the electrochemical cell under potential control, rinsed with PC and blown dry with N_2 gas, and, subsequently, investigated by X-ray Photoelectron Spectroscopy (VG ESCALAB 220iXL).

Results

The typical current density potential curves of HOPG in 1M Et_4NBF_4 / PC electrolyte are shown in Figure 1.
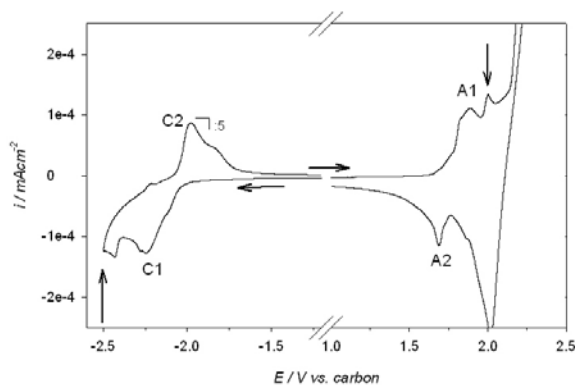
Figure 1. *Current density potential curves of HOPG in 1M Et_4NBF_4/PC; dE/dt = 10mV/s, anodic and cathodic scans were recorded separately, scan direction as indicated*

The processes that correspond to the cathodic (C1/C2) and in the anodic (A1/A2) redox couples can be mainly attributed to intercalation and deintercalation which has been recently proven by *in situ* XRD measurements [2]. In the negative potential range, however, the current density is one order of magnitude lower, than in anodic direction, which may be due to a low diffusion coefficient of the large cation in HOPG inhibiting the intercalation process into the bulk material. In order to compare both, the charged and the discharged state of the positive and the negative electrode, two experiments have been performed at E_{pos} = +2.0 V and at E_{neg} = -2.5 V, respectively. In the first experiment the electrode has been removed after 30 min at the corresponding potential, and in the second experiment it has been removed after scanning back from that potential to 0 V.

For the positively polarized electrode which is intercalated by the BF_4^- anions one would expect a positive shift of binding energy of the C 1s signal and no shift of the signals resulting from anionic species. Interestingly, however, the C 1s, B 1s and F 1s XP-spectra of the intercalated sample all show a shift to lower binding energies (BE) in comparison with the discharged sample, which is shown in Figure 2 for the C 1s and F 1s spectra. The C 1s signal is shifted by ΔE = 0.7 eV, and the B 1s and F1s peaks are both shifted by ΔE = 2.0 eV.
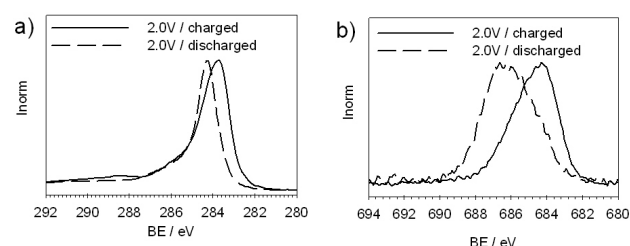
Figure 2. *Comparison of the XP spectra obtained from the positive electrode in its charged and discharged state. a) C 1s signal $\Delta E = 0.7$ eV; b) F 1s $\Delta E = 2.0$ eV*

Similar shifts have already been measured for perchlorate intercalation into HOPG in aqueous electrolyte [3] and explained by displacement of the Fermi level of the intercalated layers according to Wertheim et al. [4]. According to these models the binding energy of the B 1s and the F 1s level is constant as the anion does not change its valence state. The work function of the BF_4^- intercalated graphene layers, however, is increased by the measured energy shift of ΔE = 2.0 eV which means that the Fermi level is shifted by the same value. The resulting shift of the C 1s core level amounts 1.3 eV in comparison to the discharged sample. Deconvolution of the B 1s and F 1s signals verifies that after discharging of the sample 20-25 % of the graphene layers are still intercalated.

For the negatively polarized HOPG electrodes the screening effects described above are less pronounced. The main reason might be that much less intercalation takes place which leads to in a significant decrease of this effect.

References

[1] J.R. Dahn, T. Zheng, Y. Liu, J.S. Xue, Science **270,** 590 (1995).

[2] P.W. Ruch, M. Hahn, F. Rosciano, M. Holzapfel, H. Kaiser, W. Scheifele, B. Schmitt, P. Novak, R. Kötz, A. Wokaun, Electrochim. Acta, **53**, 1074-1082 (2007).

[3] B. Schnyder, D. Alliata, R. Kötz, H. Siegenthaler, Appl. Surf. Sci. **173**, 221-232 (2001).

[4] G.K. Wertheim, P.M.Th.M. Van Attekum, S. Basu. Solid State Commun. **33,** 1127 (1980).

ACTIVITY AND STABILITY OF PLATINUM-COBALT CORE-SHELL NANOPARTICLES AS ELECTROCATALYSTS FOR OXYGEN REDUCTION

H. Schulenburg, T. Roser, G. Khelasvili[1],
H. Bönnemann[1], G.G. Scherer
+41 56 310 2125
hendrik.schulenburg@psi.ch

The sluggish kinetics of the oxygen reduction reaction at Pt/C electrocatalysts limits the efficiency of PEFCs. According to the DOE goals for 2010, the activity for oxygen reduction catalysts should increase by a factor 4, if a Pt/C catalyst serves as benchmark [1]. Commercial $PtCo_x$/C catalysts already show a mass activity, which is about twice as high [1, 2]. An explanation of this effect is the facilitated desorption of oxygen species from the catalyst particles [3]. $PtCo_x$/C catalysts usually consist of alloy nanoparticles supported on carbon black. One attempt to further increase the mass activity are $PtCo_x$ core-shell nanoparticles, which consist of a Co-core and a Pt-shell.

Experimental

The reaction scheme for the preparation of $PtCo_3$/C core-shell catalysts is given in Figure 1. Thermolysis of Co-precursors leads to the formation of Co-nanoparticles, which are supported on carbon black. Subsequential treatment and reduction of Pt-precursors lead to the formation of core-shell $PtCo_3$/C.
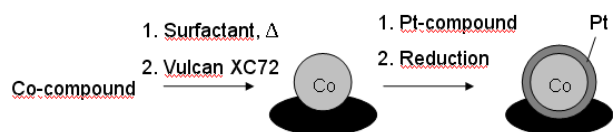
Figure 1. *Preparation of core-shell $PtCo_3$/C catalysts*

Results

The mean particle size of core-shell $PtCo_3$/C is about 4.3nm (Figure 1, Table1). Few particles are larger than 10-20nm, a fact also observed with commercial $PtCo_x$/C catalysts. Core-shell particles, however, should not contain Pt inside these large particles. Therefore, in core-shell particles less Pt would be lost for the catalytic reaction.
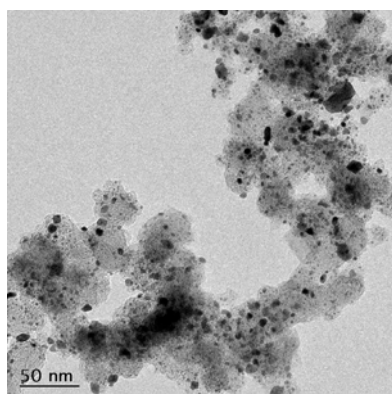
Figure 2. *TEM image of core-shell $PtCo_3$/C*

Cyclic voltammograms show that commercial Pt/C and $PtCo_{0.4}$/C have higher H_{upd} areas than the core-shell

[1] Forschungszentrum Karlsruhe, Eggenstein, Germany

$PtCo_3$/C catalyst. Therefore the electrochemically active surface area seems to be lower. On the other hand the Pt-O reduction peak of the core-shell $PtCo_3$/C is more positive than $PtCo_{0.4}$/C and especially Pt/C. This indicates a facilitated oxygen desorption, which is preferable for oxygen reduction. The mass activity of core-shell $PtCo_3$/C is slightly better than $PtCo_{0.4}$/C, both are clearly higher active than Pt/C (Table 1).
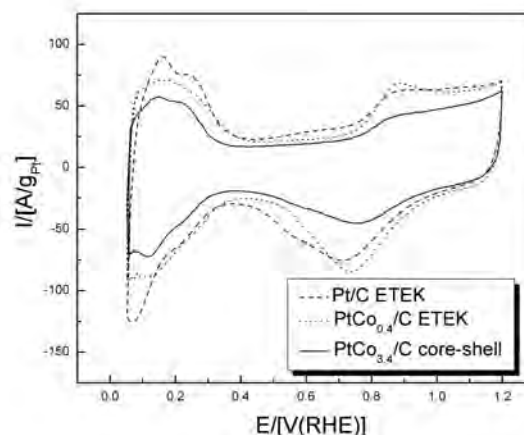
Figure 3. *Cyclic voltammogramms of commercial and $PtCo_3$/C core-shell catalysts; Ar-saturated 0.1M $HClO_4$, v=100mV/s, RT.*

For PEFC applications high catalyst stability under varying load conditions is crucial. This was investigated with an accelerated ageing test. Catalysts were cycled 4000 times within the potential range from 0.6 to 1.2V (RHE). The core-shell $PtCo_3$/C shows 37% activity loss, which is significantly higher than the activity loss of the commercial catalysts. Sintering effects may explain the ageing of Pt/C, since the particle size increases. Cobalt leaching may explain the ageing of the $PtCo_x$/C catalyst, since sintering is not observed (Table 1).

	Mass activity[a] BOL[b] [A/mg_Pt]	Mass activity loss EOL[c] [%]	Particle size[d] BOL[b] [nm]	Particle size[d] EOL[c] [nm]
Pt/C (ETEK)	0.087	22	3.4	4.1
PtCo/C(ETEK)	0.140	23	4.6	4.4
$PtCo_3$/C	0.146	37	4.3	3.9

Table 1 *Catalytic activity and stability of catalysts for oxygen reduction. a: determined by rotating disc electrode measurements, 0.9V (RHE), O_2-saturated 0.1M $HClO_4$, v=5mV/s,1600rpm, RT; b: beginning of life, c: end of life (after 4000 cycles from 0.6 to 1.2V(RHE), v=50mV/s, RT); d: determined by TEM.*

References

[1] H.A. Gasteiger, S.S. Kocha, B. Sompalli, F.T. Wagner, Appl. Cat. B: Environ. **56,** 9-35 (2005).

[2] U.A. Paulus, A. Wokaun, G.G. Scherer, T.J. Schmidt, V. Stamenkovic, N.M.Markovic, P.N. Ross, Electrochim. Acta **47,** 3787-3798 (2002).

[3] V. Stamenkovic, B.S. Mun, K.J.J. Mayrhofer, P.N. Ross, N.M. Markovic, J. Rossmeisl, J. Greeley, J.K. Nørskov, Angew. Chem. Int. Ed. **45,** 2897-2901 (2006).

CONSTRUCTION OF A XENON EXCIMER LAMP FOR THE PHOTOASSISTED ACTIVATION OF METHANE

F. Loviat, S. Stutz, M. Isler[1], U. Kogelschatz[1],
T. Jung, T. Lippert, J. Wambach, R. Kötz,
A. Wokaun
+41 56 310 4396
francois.loviat@psi.ch

The transformation of methane (CH_4) into other useful chemical species is currently subject to a growing interest. The enormous reserves of methane and its ease of purification make of this gas a very interesting feedstock for the production of a large variety of chemicals.

CH_4 activation, commonly admitted to be the rate limiting step for the conversion of methane, and the formation of surface methyl groups is therefore pivotal. For that, we plan to overcome the activation barrier of CH_4, i.e. the abstraction of one hydrogen atom to form a methyl radical, by using highly energetic photons produced by an excimer lamp [1].

In order to ensure controlled preparation conditions and the unhampered application of surface science techniques like XPS, AFM, SEM, TPD and LEED, these experiments must be carried out in UHV. However, as no UHV suitable excimer lamp is commercially available, a unique setup fitting our needs had to be developed at PSI. The main features of this lamp are its narrow emission band centred at 172 nm (~ 7 eV, Figure 1), an internal water cooling and a small size allowing an installation at a DN63CF port.
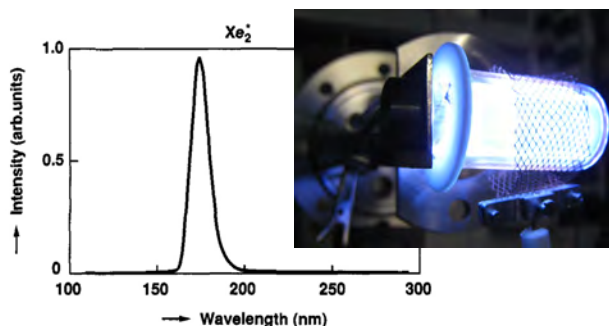
Figure 1. *Emission spectrum and image of xenon excimer lamp*

Experimental

The lamp was entirely built at PSI. The xenon compartment is made of two concentric tubes, the outer one being special high grade quartz called Suprasil®, which is partially transparent to 172 nm and the inner one a VUV resistant, opaque quartz (Figure 2).
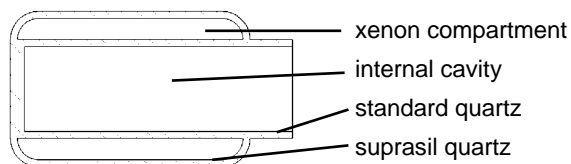
Figure 2. *Cross section of excimer lamp tube*

After a well defined cleaning procedure the tube was filled with xenon 5.0 on a filling station. The tube is then sealed, detached from the filling station, and installed on the support as well as equipped with the electrodes.

The lamp is operated by a HPG-2 power generator delivering tension from 0 to 10 kV at 125 to 325 kHz with a maximum power of 150 Watts. The radiation intensity was measured with a calibrated photodiode form Gigahertz-Optik after filtration trough a 172 nm optical filter (ARC).

Results

The intensity of the lamp was found to increase with the xenon pressure in the gas compartment as shown in Figure 3. However, a small vacuum in the tube is needed for a convenient sealing of the lamp. A pressure of 700 mbar was found to be a good compromise between lamp intensity and sealing problems.
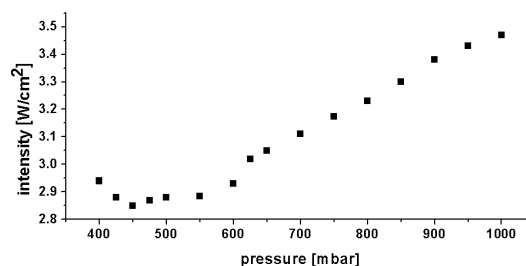
Figure 3. *Lamp intensity versus xenon pressure*
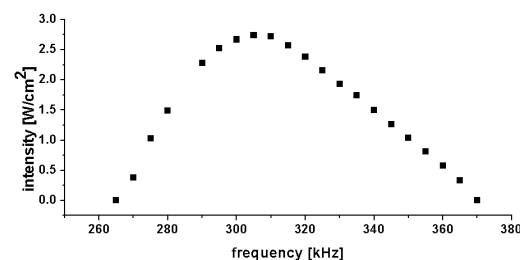
Figure 4. *Lamp intensity versus frequency at 3 kV*

The optimum frequency was found to be 305 kHz as shown on Figure 4. This frequency corresponds to the maximum intensity of the lamp at 3 kV.

Cooling of the lamp is a serious issue. A decrease of the intensity by quenching was observed as the temperature was building up. For this reason, the lamp has to run as cool as possible. Operated in a gaseous atmosphere, these lamps do not need water cooling as the small amount of heat produced can be dissipated by convection. This cooling mechanism does not exist any more in vacuum and an efficient cooling is therefore required. The most efficient cooling would be a direct water flow in the internal cavity of the tube, but attempts to do so failed due to tightness problems connected with the different expansion coefficients of the materials in contact. Quartz has indeed an expansion coefficient which is 20 to 50 times lower than most metal and polymers (glues). On the other hand, an indirect cooling by inserting a water cooled copper rod in the internal cavity of the lamp showed not to be efficient enough. The reason is that the walls of the lamp are not perfectly cylindrical and the contact with the cooled copper rod is therefore not optimal. This problem was solved by melting a very soft and well conducting material between the quartz and the copper rod, indium in this case, in order to ensure a sufficient contact and therefore remove heat more efficiently. With this system the excimer lamp can be operated at low temperature with a stable intensity for extended time period.

References

[1] U. Kogelschatz, Applied Surf. Sci., **54**, 410-423 (1991).

THE ELECTROCHEMISTRY LABORATORY

Electrochemistry Laboratory

G.G. Scherer *(head)*
R. Kötz *(deputy head)*
I. Kalt *(secretary)*

Fuel Cells

G.G. Scherer

Clean Energy Conversion
with high efficiency
Optimized components
and cells

Batteries

P. Novak

High energy density
Compact 4V cells

Interfaces and Capacitors

R. Kötz

Physical, chemical and
structural analysis of inter-
facial processes
Internal & external support

High power density com-
plementary storage device
with high capacitance and
cycle life

Fuel Cell Systems

F. Büchi

Optimisation of system
efficiency
Novel stack concepts

IR Beamline SLS & Nanocat Project

*Synchrotron radiation as IR source, model
catalysts for energy processes*

J. Wambach

ECL-PERSONNEL

Staff

Alkan Gürsel Selmiye, Dr. (until August) ♦ Arcaro Manuel (until February)

Büchi Felix, Dr.

Czekaj Izabela, Dr.

Foelske Annette, Dr.

Geiger Friederike ♦ Gloor Thomas ♦ Gubler Lorenz, Dr.

Hahn Matthias, Dr. (until April)

Kaiser Hermann ♦ Kalt Isabella ♦ Kötz Rüdiger, Dr.

Maire Pascal, Dr. ♦ Märkle Wolfgang, Dr. (since September) ♦ Marmy Christian

Ng Desmond, Dr. (since August) ♦ Novák Petr, Dr.

Sauter Jean-Claude (until October) ♦ Scheifele Werner ♦ Scherer Günther G., Dr. ♦ Schneider Ingo, Dr. ♦ Schulenburg Hendrik, Dr.

Tran Nicolas, Dr. (until September) ♦ Tsukada Akinori

Ufheil Joachim, Dr. (until February)

von Roth Fritz

Wambach Jörg, Dr. ♦ Wei Xun, Dr. (until August)

PhD Students

Bayer Michael (since June) ♦ Ben Youcef Hicham ♦ Boillat Pierre

Chew Sophie (since August)

Dockheer Sindy

Farquet Patrick

Hintennach Andreas (since October)

Kramer Denis (until March)

La Mantia Fabio ♦ Loviat François

Patey Timothy

Reum Mathias ♦ Rosciano Fabio ♦ Ruch Patrick

Schuler Gabriel ♦ Seyfang Bernhard ♦ Simmen Franziska

Wallasch Frank

Zaglio Maurizio (since November) ♦ Zellweger Hans (since May)

AWARDS

**P. Boillat, D. Kramer,
B.C. Seyfang, G. Frei,
E. Lehmann, G.G. Scherer,
A. Wokaun, Y. Tasaki,
Y. Ichikawa, K. Shinohara**

Best poster
Application of high resolution neutron imaging in polymer electrolyte fuel cell (PEFC) diagnostics.
From Physical Understanding to Novel Architectures of Fuel Cells, Trieste, Italy,
May 21 - 25, 2007.

**H. Ben youcef, S. Alkan
Gürsel, L. Gubler,
A. Wokaun, G.G. Scherer**

Best poster
Effect of crosslinker concentration on performances and properties of styrene grafted onto ETFE based membranes
REACT 2007, Dresden, September 23 – 26, 2007.

THESE PHD STUDENTS FROM ECL GRADUATED IN 2007

Dr. Denis Kramer

Mass transport aspects of polymer electrolyte fuel cells under two-phase flow conditions

Ph.D. Thesis, Technische Universität Bergakademie Freiberg, March 2007

Advisors   Prof. Dr.-Ing. habil., Gerd Walter, TU Freiberg
                 Prof. Dr.-Ing. Helmut Eichert, FH Zwickau
                 Dr. rer. nat. Günther G. Scherer, PSI Villigen

Dr. Andreas Reiner

Die Platinkatalysatorschicht in Polymerelektrolyt-Brennstoffzellen Beiträge zum Verständnis und zur Optimierung

Ph.D. Thesis, No. 17127, ETH Zürich, March 2007

Advisors   Prof. Dr. A. Wokaun, PSI/ETH Zürich
                 Prof. Dr. K. Hungerbühler, ETH Zürich
                 Prof. Dr. D. Kolb, Universität Ulm
                 Dr. rer. nat. Günther G. Scherer, PSI Villigen

Dr. Markus Kuhnke

Fabrication and characterization of micro-structured glassy carbon electrodes for miniaturized fuel cells

Ph.D. Thesis, No. 17309, ETH Zürich, June 2007

Advisors   Prof. Dr. A. Wokaun, PSI/ETH Zürich
                 Prof. Dr. V Sandoghdar, ETH Zürich
                 Prof. Dr. T. Lippert, PSI Villigen
                 Dr. rer. nat. G.G. Scherer, PSI Villigen

EXCHANGE STUDENTS, DIPLOMA THESES, SUMMER STUDENTS

Benjamin Breiten

ETFE based radiation grafted membranes for the DMFC
Heinrich Heine Universität, Düsseldorf, DE, September 2006 – March 2007.

Martin Kohl

Katalysatoren für die Sauerstoffreduktion in Polymerelektrolyt-Brennstoffzellen: Platinfilme auf Cobaltpartikeln
Fachhochschule Amberg-Weiden, DE, October 2006 – March 2007.

See How Ng

Nanostructured materials for electrodes in lithium-ion batteries
University of Wollongong, AU, October 2006 – April 2007.

Antonio José Martin Fernández

In situ characterization of fuel cell cathodes prepared by the electrospray technique
CIEMAT, Madrid, ES, November 2006 – February 2007

Jérôme Bernard

Optimization of hydrogen consumption in hybrid electric powertrains
University of Valenciennes, FR, February – August 2007.

Martin Schisslbauer

Untersuchungen zur Degradation von strahlengepfropften Membranen in der Polymerelektrolyt-Brennstoffzelle
Fachhochschule Amberg-Weiden, DE, March – September 2007.

Cyrill Lohri

Parametric study of a polymer electrolyte fuel cell
ETH Zürich, March – June 2007.

Anne Buisson

Characterization of mechanical properties of radiation grafted films and membranes for fuel cells
INP Grenoble, FR, May – August 2007.

Rémi Desvignes

Effect of temperature on the properties of radiation grafted ETFE based films and membranes.
INP Grenoble, FR, May - August 2007.

Maria Rodriguez Rius

FTIR spectroscopic investigations of alpha-methylstyrene based radiation grafted films
University of Manchester, GB, June – September 2007.

Andrei Diatlov

Investigation of anisotropic transport properties of gas diffusion layer materials under compression
Technical University Aachen (RWTH), June – August 2007.

Gregor Hammer

Einfluss der Kanalbreite auf die Performance einer Mikro-Polymerelektrolytbrennstoffzelle
Technische Universität Wien, DE, July – September 2007.

Thomas Roser

Katalysatoren für die Sauerstoffreduktion in Polymerelektrolyt-Brennstoffzellen: Aktivität und Stabilität von Core-shell PtCo3/C-Katalysatoren
Fachhochschule beider Basel (Nordwestschweiz), September – December 2007.

Prof. Helmut Bönnemann Forschungszentrum Karlsruhe, DE	*Colloidal design of fuel cell catalysts* February 19, 2007.	
Prof. A. Robert Hillman University of Leicester, GB	*Effect of salvation phenomena on polymer film structure and dynamics* March 12, 2007.	
Dr. Jürgen Schumacher ZHW Winterthur	*Wassertransport in PEM-Brennstoffzellen: Ein zweiphasiges Modell und Bestimmungen von Transportparametern* March 26, 2007.	
Dr. Johannes Herrmann Collini-Flühmann AG, Dübendorf	*Oberflächentechnik aus der Sicht der Industrie* April 16, 2007.	
Dr. Thomas Wandlowski Research Center Jülich, DE	*An electrochemical approach to functional nanostructures* May 18, 2007.	
Prof. John W. Weidner South Carolina University, USA	*Electrochemical generation of hydrogen via thermochemical cycles* September 17, 2007.	
Dr. Jan Van herle EPF Lausanne	*Modeling, validation and testing solid oxide fuel cell stacks and materials at EPFL – LENI* October 1, 2007.	
Salvador Pané I Vidal ETH Zürich	*Electrodeposition: An alternative way for the preparation of magnetic sheets* October 8, 2007.	
Prof. Alexei Khokhlov Universität Ulm, DE	*Polymer electrolyte membranes for fuel cells: Computer modeling and new experimental developments* October 15, 2007.	
Gérard Gebel CEA, Grenoble, FR	*Structure, transport properties and water management in fuel cell membranes studied by X-ray and neutron scattering* October 22, 2007.	
Dr. Daniel Chartouni ABB Baden	*Battery energy storage system for electric utilities* November 12, 2007.	
Dr. Wolfgang Bessler Universität Heidelberg, DE	*Elektrochemische Impedanz von Chemie und Transport in der Festoxid-Brennstoffzelle* November 26, 2007.	
Dr. Ravindranathan Thampi EPF Lausanne	*Electrochemical research related to energy conversion in SOFC and Dye sensitized solar cells* December 3, 2007.	
Prof. Gregory Jerkiewicz Queens University, Kingston, CA	*Interfacial electrochemistry of platinum: Something old, something new, and something unexpected* December 10, 2007.	

CONFERENCES – WORKSHOPS

Electrocatalysis	23rd One-Day-Symposium May 3, 2007 Organizers: G.G. Scherer and R. Kötz, PSI Contributions from: Holger Kuhn, MTU CFC Solutions GmbH, Munich, DE Brian E. Hayden, University of Southampton, GB Timo Jacob, Fritz-Haber-Institut der MPG, Berlin, DE Elena R. Savinova, University of Novosibirsk, RU & University of Strasbourg, FR Thomas J. Schmidt, PEMEAS GmbH, Frankfurt/M, DE Gunther Wittstock, University of Oldenburg, DE

**Swiss "Impuls-Day"
Hydrogen & Fuel Cell**
	Swiss Federal Office of Energy SFOE
	November 30, 2007
	Organizers: Andreas Luzzi, Michael Spirig, HSR, SPF,
	               Rapperswil
	               Günther G. Scherer, PSI
	
	More than 40 contributions addressing
	Business
	Innovation
	Enabling Factors

REVIEW ACTIVITIES OF THE LABORATORY

Journals

Applied Physics A, Materials: Science & Processing

Carbon

Dalton Transactions

Electrochimica Acta ♦ Electrochemistry Communications ♦ Electrochemical and Solid-State Letters

International Journal of Hydrogen Energy

Journal of the Electrochemical Society ♦ Journal of Fuel Cell Science and Technology (ASME) ♦ Journal of New Materials for Electrochemical Systems ♦ Journal of Physical Chemistry ♦ Journal of Physics and Chemistry of Solids ♦ Journal of Power Sources

Langmuir

Macromolecules ♦ Measurement Science and Technology

Physical Chemistry Chemical Physics

Simulation Modelling Practice and Theory

Organisations

Christian Doppler Forschungsanstalt, Wien, Austria

Deutsche Forschungsgesellschaft

Fonds zur Förderung der wissenschaftlichen Forschung (FWF), Wien, Austria

National Research Council, Canada

PSI FOKO, Switzerland

Technische Universität Bergakademie Freiberg, Germany

Co-Referee's Report for Dissertations

D. **K**ramer, PSI/TU Freiberg ♦ M. Kuhnke, PSI/ETH Zürich

A. **R**einer, PSI/ETH Zürich

INDUSTRIAL PARTNERS

The Laboratory had the pleasure to collaborate with the following industrial partners during the year 2007:

BASF AG, Ludwigshafen, Germany

Ciba ♦ Construction Développement Michelin SA (CDM), Givisiez, Switzerland ♦ CEKA Elektrowerkzeuge AG, Wattwil, Switzerland

MES DEA, Stabio, Switzerland

Nissan Motors Co., Ltd. Yokosuka, Japan

Oerlikon Stationary Batteries Ltd., Switzerland

TIMCAL AG, Bodio, Switzerland
/

**PROJECT COLLABORATIONS
WITH EXTERNAL PARTNERS**

CCEM

F.N. Büchi
Project Leader PSI

hy.muve: Development of **hy**drogen powered **mu**nicipal **ve**hicle
with EMPA Dübendorf and Industrial Partners

BFE

F.N. Büchi, G. Schuler
Project Leader

Lokale Gasphasenanalyse an PE-Brennstoffzellen

F.N. Büchi
Project Leader

*Cal.PEF-CH: Modelbased investigation of PE fuel cell performance with
focus on porous layer properties*
with ZHAW, Winterthur

L. Gubler, G.G. Scherer
Project Leader

*Lebensdauer Limitierungen von Brennstoffzellen-Membranen:
Mechanismen, Methoden und Innovationen*
since 1.9.2007

L. Gubler, I.A. Schneider,
G.G. Scherer
Project Leader

*go.PEF-CH: Enhancing PEFC durability and reliability under application-
relevant conditions*
since 1.10.2007

R. Kötz
Project Leader

Integrated Micro-Supercapacitor
with NTB, Buchs

G.G. Scherer, L. Gubler
Project Leader

*Protonen-Leitende Polymermembranen für Brennstoff- und
Elektrolysezellen*

EU

I.A. Schneider
Project Leader

EU-Project *Nanoglowa (Nano Membranes against Global Warming)*
(Diagnostics workpackage)

Gebert Ruef Stiftung

F.N. Büchi
Project Leader PSI

*SIMPEM (Simulation von Polymer Elektrolyt Brennstoffzellen und
Stapeln)*
with ZHAW, Winterthur

KTI

F.N. Büchi
Project Leader PSI

Brennstoffzellenstapel mit erweiterter Funktionalität
with CEKA AG, Wattwil and FH Bern

Industry

F.N. Büchi, M. Reum
Project Leader

Diagnostics of polymer electrolyte fuel cells
Automotive Industry

N. Tran, W. Märkle
Project Leader

Graphite für die negative Elektrode der Lithiumionen-Batterie
TIMCAL SA, Bodio

P. Maire
Project Leader

Electrochemical characterization of polymeric organic active materials
Ciba, Basel

J. Ufheil
Project Leader

Rechargeable magnesium batteries
Nissan Motor Co. Ltd., Yokohama, Japan

| G.G. Scherer | *Diagnostics of polymer electrolyte fuel cells* |
| Project Leader | Automotive industry |

| G.G. Scherer | *Diagnostics of polymer electrolyte fuel cells* |
| Project Leader | Nissan Motor Co. Ltd., Yokohama, Japan |

NATIONALFONDS

| P. Novák | *Advanced materials for efficient portable energy supplies* |
| Project Leader | PSI und ETHZ |

P. Novák	*Synthesis and characterization of advanced electroactive materials for*
Project Leader	*electrodes of rechargeable lithium-ion batteries*
	PSI

SBF

P. Novák	*ALiSTORE (Advanced lithium energy storage systems based on the use*
	of nano-powders and nano-composite electrodes/electrolytes)
	EU-Project (Network of Excellence)

TEACHING ACTIVITIES

University Level Teaching

| PD Dr. P. Novák, | *Technische Elektrochemie* |
| Prof. Dr. A. Wokaun | ETH Zürich, HS 2007 |

Prof. Dr. A. Wokaun,	*Renewable Energies Technologies II*
Dr. G.G. Scherer,	ETH Zürich, SS 2007
Prof. Dr. K. Boulouchos	

Dr. G.G. Scherer	*Brennstoffzellen*
	Contributions to the lecture „Energie und Klima", Prof. Dr. G. Gänteför,
	Universität Konstanz, SS 2007

PUBLICATIONS

Peer Reviewed Papers

S. Alkan Gürsel,
H. Ben youcef, A. Wokaun,
G.G. Scherer

Influence of reaction parameters on grafting of styrene into poly(ethylene-alt-tetrafluoroethylene) films
Nucl. Instr. and Meth. in Phys. Res. B. **265**, 198-203 (2007).

F. Atchison, T. Brys[1,4],
M. Daum, P. Fierlinger[1,3],
A. Foelske, M. Gupta,
R. Henneck, S. Heule[1,3]
M. Kasprzak[1,5], K. Kirch,
R. Kötz, M. Kuzniak[1,6],
T. Lippert, C. F. Meyer[2],
F. Nolting, A. Pichlmaier,
D. Schneider[2], B. Schultrich[2],
P. Siemroth[2], U. Straumann[3]

Structural characterization of diamond-like carbon films for ultracold neutron applications
Diamond & Relat. Mater. **16**, 334-341 (2007).
[1] Paul Scherrer Institut, Villigen PSI, Switzerland
[2] Fraunhofer Institut, Dresden, Germany
[3] Universität Zürich, Switzerland
[4] ETH Zürich, Switzerland
[5] Austrian Academy of Sciences, Vienna, Austria
[6] Jagellonian University, Cracow, Poland

C.N. Borca, S. Canulescu,
F. Loviat, T. Lippert,
D. Grolimund, M. Döbeli,
J. Wambach, A. Wokaun

Analysis of the electronic configuration of the pulsed laser deposited $La_{0.7}Ca_{0.3}MnO_3$ thin films
Appl. Surf. Sci. **254,** 1352-1355 (2007).

F.N. Büchi,
S.A. Freunberger, M. Reum,
G. Paganelli[1], A. Tsukada,
P. Dietrich, A. Delfino[1]

On the efficiency of an advanced automotive fuel cell system
Fuel Cells **7**, 159-164 (2007).
[1] Conception et Devéloppment Michelin, Givisiez, Switzerland

F.N. Büchi, G. Paganelli[1],
P. Dietrich, D. Laurent[1],
A. Tsukada, P. Varenne[1],
A. Delfino[1], R. Kötz,
S.A. Freunberger,
P.-A. Magne[1], D. Walser[1],
D. Olsommer[1]

Consumption and efficiency of a passenger car with a hydrogen/oxygen PEFC based hybrid electric drivetrain
Fuel Cells **7,** 329-335 (2007).
[1] Conception et Devéloppment Michelin, Givisiez, Switzerland

L. Bugnon[1], C.J.H. Morton[1],
P. Novák, J. Vetter,
P. Nesvadba[1]

Synthesis of poly(4-methacryloyloxy-TEMPO) via group transfer polymerization and its evaluation in organic radical battery
Chem. Mater. **19**, 2910-2914 (2007).
[1] Ciba, Basel

T.A. Centeno[1], M. Hahn,
J.A. Fernández[1], R. Kötz,
F. Stoeckli[2]

Correlation between capacitances of porous carbons in acidic and aprotic EDLC electrolytes
Electrochem. Commun. **9**, 1242-1246 (2007).
[1] Instituto Nacional del Carbón-C.S.I.C., Oviedo, Spain
[2] Université de Neuchâtel, Switzerland

A.M. Chaparro[1], R. Benítez[1],
L. Gubler, G.G. Scherer,
L. Daza[2]

Study of membrane electrode assemblies for PEMFC, with cathodes prepared by the electrospray method
J. Power Sources **169**, 77-84 (2007).
[1] Centro de Investigaciones Energéticas, Medioambientales y Tecnológicas (CIEMAT), Madrid, Spain
[2] Instituto de Catáalisis y Petroleoquímica (CSIC), Madrid, Spain

I. Czekaj, F. Loviat,
F. Raimondi, J. Wambach,
S. Biollaz, A. Wokaun

Characterization of surface processes at the Ni-based catalyst during the methanation of biomass-derived synthesis gas: X-ray photoelectron spectroscopy (XPS)
Appl. Catal. A: General **329**, 68-78 (2007).

F.O. Ernst[1], H.K. Kammler[1],
A. Roessler[1], S.E. Pratsinis[1],
W.J. Stark[1], J. Ufheil,
P. Novák

Electrochemically active flame-made nanosized spinels: $LiMn_2O_4$, Li_4TiO_{12} and $LiFe_5O_8$
Mater. Chem. Phys. **101**, 372-378 (2007).
[1] ETH Zürich

P. Farquet, A. Kunze,
C. Padeste, H.H. Solak,
S. Alkan Guersel,
G.G. Scherer, A. Wokaun

Influence of the solvent viscosity on surface graft-polymerization reactions
Polymer **48**, 4936-4942 (2007).

P. Farquet, C. Padeste,
H.H. Solak, S. Alkan
Guersel, G.G. Scherer,
A. Wokaun

EUV lithographic radiation grafting of thermo-responsive hydrogel nanostructures
Nucl. Instrum. Methods Phys. Res. B *265*, 187-192 (2007).

R. Flückiger, A. Tiefenauer[1],
M. Ruge[2], C. Aebi[3],
A. Wokaun, F.N. Büchi

Thermal analysis and optimization of a portable, edge-air-cooled PEFC stack
J. Power Sources **172**, 324-333 (2007).
[1] Center for Computational Physics, Zurich University of Applied Sciences, Winterthur, Switzerland
[2] Fuel Cell Laboratory, Berne University of Applied Sciences, Biel, Switzerland
[3] CEKA Elektrowerkzeuge AG, 9630 Wattwil, Switzerland

L. Gubler, D. Kramer,
J. Belack[1], Ö. Ünsal[1],
T.J. Schmidt, G.G. Scherer

Celtec-V: A polybenzimidazole based membrane for the direct methanol fuel cell
J. Electrochem. Soc. **154**, B981-B987 (2007).
[1] BASF Fuel Cell GmbH, Frankfurt am Main, Germany

L.J. Hardwick, M. Holzapfel,
P. Novák, L. Dupont[1],
E. Baudrin[1]

Electrochemical lithium insertion into anatase-type TiO_2: An in situ Raman microscopy investigation
Electrochim. Acta **52**, 5357-5367 (2007).
[1] Université de Picardie Jules Verne, Amiens, France

L.J. Hardwick, H. Buqa,
M. Holzapfel, W. Scheifele,
F. Krumeich[1], P. Novák

Behavior of highly crystalline graphitic materials in lithium-ion cells with propylene carbonate containing electrolytes: An in situ Raman and SEM study
Electrochim. Acta **52**, 4884-4891 (2007).
[1] ETH Zürich

L.J. Hardwick, M. Holzapfel,
A. Wokaun, P. Novák

Raman study of lithium coordination in EMI-TFSI additive systems as lithium-ion battery ionic liquid electrolytes.
J. Raman Spectrosc. **38**, 110-112 (2007).

S. Heule[1,2], F. Atchison,
M. Daum, A. Foelske,
R. Henneck, M. Kasprzak[1,3],
K. Kirch, A. Knecht[1,2],
M. Kuzniak[1,4], T. Lippert,
M. Meier, A. Pichlmaier,
U. Straumann[2]

Diamond-like carbon coatings for ultracold neutron guides
Appl. Surf. Sci. **253**, 8245-8249 (2007).
[1] Paul Scherrer Institut, Villigen PSI, Switzerland
[2] Universität Zürich, Switzerland
[3] Austrian Academy of Science, Vienna, Austria
[4] Jagellonian University, Cracow, Poland

M. Holzapfel, A. Würsig,
W. Scheifele, J. Vetter,
P. Novák

Oxygen, hydrogen, ethylene and CO_2 development in lithium-ion batteries
J. Power Sources **174**, 1156-1160 (2007).

R. Kötz, J.-C. Sauter,
P. Ruch, P. Dietrich,
F.N. Büchi, P.A. Magne[1],
P. Varenne[1]

Voltage balancing: Long-term experience with the 250 V supercapacitor module of the hybrid fuel cell vehicle HY-LIGHT
J. Power Sources **174,** 264-271 (2007).
[1] Conception et Développement Michelin SA, 1762 Givisiez, Switzerland

H. Kuhn, A. Wokaun,
G.G. Scherer

Exploring single electrode reactions in polymer electrolyte fuel cells
Electrochim. Acta **52**, 2322-2327 (2007).

E.H. Lehmann, G. Frei,
G. Kühne, P. Boillat

The micro-setup for neutron imaging: A major step forward to improve the spatial resolution
Nuc. Instrum. Methods Phys. Res., Sect. A **576**, 389-396 (2007).

F. Loviat, H M. Rønnow[1,2],
Ch. Renner[3], G. Aeppli[3],
T Kimura[4], Y. Tokura[5,6]

The surface layer of cleaved bilayer manganites
Nanotechnology **18**, 044020 (2007).
[1] PSI, Villigen
[2] ETH Zürich, Switzerland
[3] University College London, London, UK
[4] Lucent Technologies, Murray Hill, USA
[5] University of Tokyo, Tokyo, Japan
[6] Japan Science and Technology Corporation (JST), Tsukuba, Japan

P. Novák, J. Ufheil, H. Buqa,
F. Krumeich[1], M. E. Spahr[2],
D. Goers[2], H. Wilhelm[2],
J. Dentzer[3], R. Gadiou[3],
C. Vix-Guterl[3]

The importance of the active surface area of graphite materials in the first lithium intercalation
J. Power Sources **174**, 1082-1085 (2007).
[1] ETH Zürich
[2] TIMCAL SA, Bodio
[3] Institut de Chimie des Surfaces et Interfaces, CNRS, Mulhouse, France

J. Reim[1], H. Rentsch[1],
W. Scheifele, P. Novák

Synthesis and characterization of doped $Li[Mn_{0.5-x/2}Ni_{0.5-x/2}Co_x]O_2$ positive electrode materials
J. Power Sources **174**, 584-587 (2007).
[1] Ferro GmbH, Frankfurt am Main, Germany

A. Reiner, H. Kuhn,
A. Wokaun, G.G. Scherer

Hydrogen adsorption on activated platinum electrodes – an electrochemical impedance spectroscopy study
Z. Phys. Chem. **221**, 1319-1341 (2007).

F. Rosciano, M. Holzapfel,
H. Kaiser, W. Scheifele,
P. Ruch, M. Hahn, R. Kötz,
P. Novák

A multi-sample automatic system for in situ electrochemical X-ray diffraction synchrotron measurements
J. Synchrotron Rad. **14**, 487-491 (2007).

P. W. Ruch, M. Hahn,
F. Rosciano, M. Holzapfel,
H. Kaiser, W. Scheifele,
B. Schmitt, P. Novák,
R. Kötz, A. Wokaun

In situ X-ray diffraction of the intercalation of $(C_2H_5)_4N^+$ and BF_4^- into graphite from acetonitrile and propylene carbonate based supercapacitor electrolytes
Electrochim. Acta **53**, 1074-1082 (2007).

I.A. Schneider,
S.A. Freunberger,
D. Kramer, A. Wokaun,
G.G. Scherer

Oscillatons in gas channels
Part I. The forgotten player in impedance spectroscopy in PEFCs
J. Electrochem. Soc. **154**, B383-B388 (2007).

I.A. Schneider, D. Kramer,
A. Wokaun, G.G. Scherer

Oscillations in gas channels
Part II. Unraveling the characteristics of the low frequency loop in air-fed PEFC impedance spectra
J. Electrochem. Soc. **154**, B770-B782 (2007).

I.A. Schneider, D. Kramer,
A. Wokaun, G.G. Scherer

Effect of inert gas flow on hydrogen underpotential deposition measurements in polymer electrolyte fuel cells
Electrochem. Commun. **9**, 1607-1612 (2007).

B. Schnyder, T. Rager

Surface modification of radiation-grafted polymer films and membranes by crosslinking
J. Appl. Polym. Sci. **104**, 1973-1978 (2007).

M. Schnippering, M. Carrara,
A. Foelske, R. Kötz,
D.J. Fermín

Electronic properties of Ag nanoparticle arrays. A Kelvin probe and high resolution XPS study
Phys. Chem. Chem. Phys. **9**, 725-730 (2007).

B.C. Seyfang, M. Kuhnke,
T. Lippert, G.G. Scherer,
A. Wokaun

A novel, simplified micro-PEFC concept employing glassy carbon micro-structures
Electrochem. Commun. **9**, 1958-1962 (2007).

J. Vetter, L.J. Hardwick,
A. Würsig, M. Holzapfel,
O.D. Schneider, J. Ufheil,
P. Novák

Application of in situ techniques for investigations in lithium-ion battery materials
ECS Transactions **3**, 29-43 (2007).

A. Würsig, W. Scheifele,
P. Novák

CO_2 gas evolution on cathode materials for lithium-ion batteries
J. Electrochem. Soc. **154**, A449-A454 (2007).

Other Papers

L. Gubler, H. Ben youcef,
S. Alkan Gürsel, A. Wokaun,
G.G. Scherer

Crosslinker Effect in ETFE Based Radiation Grafted Membranes
212th Meeting of the Electrochemical Society, Washington DC, USA, October 7-12 (2007).
Electrochem. Soc. Trans. **11**, 27-34 (2007).

R. Kötz, J-C. Sauter,
P. Ruch, P. Dietrich,
F.N. Büchi, P.A. Magne,
P. Varenne

Voltage balancing of a 250 Volt supercapacitor module for a hybrid fuel cell vehicle.
Proc. 17th International Seminar on Double Layer Capacitors and Hybrid Energy Storage Devices, Deerfield Beach, Florida, USA, December 10-13 (2007).

R. Kötz, M. Hahn,
P.W. Ruch, A. Foelske

Carbon-based Electrochemical Capacitors – Drawbacks and Opportunities
2007 International Conference on Advanced Capacitors (ICAC2007) Kyoto, Japan
Extended Abstracts 36-39, May 28-30 (2007).

I.A. Schneider, M.H. Bayer,
P. Boillat, A. Wokaun,
G.G. Scherer

Formation of low frequency inductive loops in polymer electrolyte fuel cell impedance spectra under sub-saturated conditions
212th Meeting of the Electrochemical Society, Washington DC, USA, October 7-12 (2007).
Electrochem. Soc. Trans. **11**, 461-472 (2007).

TALKS

Invited Talks

F.N. Büchi   *Neue Treibstoffe und Antriebe - Aussichten für eine effiziente individuelle Mobilität*
EMPA Dübendorf, Wissensapéro, July 9, 2007.

F.N. Büchi   *Inhomogeneous cell polarization*
From Physical Understanding to Novel Architectures of Fuel Cells, Trieste, Italy, May 23, 2007.

F.N. Büchi   *Insights from sub-mm current density measurements in PEFC*
Workshop on Fuel Cell Modeling, Aachen, Germany, March 7, 2007.

I. Czekaj   *Electronic structure of the Ni/γ-Al$_2$O$_3$ Catalyst: DFT cluster model study*
Swiss Chemical Society - Fall Meeting, Computational Chemistry Session, EPFL, Switzerland, September 12, 2007.

P. Farquet   *Nanostructured polymer brushes by EUV-radiation grafting*
International Nano Student Conference (INASCON), Silkeborg, Denmark, July 7-10, 2007.

L. Gubler   *Strategy for aging tests of fuel cell membranes*
US DoE High Temperature Membrane Working Group Meeting (joint session with CARISMA), October 10, 2007.

R. Kötz   *Carbon-based electrochemical capacitors – drawbacks and opportunities*
Plenary Lecture, 2007 International Conference on Advanced Capacitors (ICAC2007) Kyoto, Japan, May 28-30, 2007.

R. Kötz   *Supercapacitors*
Umicore Materials for Sustainable Energy Workshop, Mechelen / Brüssel, Belgium, June 27, 2007.

R. Kötz   *Fuel cell – supercapacitor hybrids*
f-cell, Die Brennstoffzelle / 7. Forum für Produzenten und Anwender, Stuttgart, Germany, September 24-26, 2007.

R. Kötz   *A 250 V supercapacitor module for a hybrid fuel cell supercapacitor vehicle*
Advanced Energy Storage Technologies Symposium 2007, Euro Capacitors 2007, Cologne, Germany, November 5-8, 2007.

R. Kötz   *Supercaps – Elektrochemische Doppelschichtkondensatoren*
Hoppecke Batterien, F&E Kolloquium, Brilon, Germany, November 26, 2007.

P. Novák   *Interface electrochemistry - the scientific key to long-lasting lithium-ion batteries*
Seminar at the Department of Chemistry, Seoul National University, Seoul, Korea, June 14, 2007.

P. Novák   *In situ Raman spectroscopy of insertion electrodes for lithium-ion batteries and supercapacitors*
The 14th International Symposium on Intercalation Compounds ISIC-14, Seoul, Korea, June 12, 2007.

P. Novák   *Materials and interfaces in lithium-ion batteries*
National Institute of Advanced Industrial Science and Technology, Osaka, Japan, June 8, 2007.

G.G. Scherer	*Electrochemical conversion and storage systems - chances and obstacles on the way to the market place* Swiss Physical Society, Annual Meeting 2007, Session 7 *Challenges of Future Energies,* Universität Zürich, February 23, 2007.
G.G. Scherer	*Polymermembranen als Festelektrolyte für Brennstoffzellen* FHNW, Windisch-Brugg, March 28, 2007.
G.G. Scherer	*Polymer membranes as solid electrolytes for fuel cells* Workshop on Fuel Cells, ICCMP, University of Brasilia, Brasil, April 9-13, 2007.
G.G. Scherer	*Combined in situ characterization methods for polymer electrolyte fuel cells* Workshop on Fuel Cells, ICCMP, University of Brasilia, Brasil, April 9–3, 2007.
G.G. Scherer	*Materials research for polymer electrolyte fuel cells - activities at Paul Scherrer Institut* NRC Institute for Fuel Cell Innovation , Vancouver, Canada, September 5, 2007.
G.G. Scherer	*What can we learn from combined locally resolved in situ diagnostic methods for PEFCs?* NRC Institute for Fuel Cell Innovation, Vancouver, Canada, September 5, 2007.
G.G. Scherer	*Combined locally resolved in situ diagnostic methods for PEFCs – our approach at Paul Scherrer Institut* Ballard Power Systems, Vancouver, Canada, September 6, 2007.
G.G. Scherer	*Combined locally resolved in situ diagnostic methods for polymer electrolyte fuel cells* University of Victoria, Institute for Integrated Energy Systems, Victoria, Canada, September 7, 2007.
G.G. Scherer	*Influence of crosslinking on irradiated ETFE based grafted membranes* 58th Annual Meeting, International Society of Electrochemistry, Banff, Canada, September 9–14, 2007.
G.G. Scherer	*Elektrochemische Wandler- und Speichersysteme für automobile Anwendungen* Plenary lecture, GDCH-Wissenschaftsforum Chemie 2007, Universität Ulm, Germany, September 17–19, 2007.
G.G. Scherer	*From Hy-Light to Hupd platinum nanoparticles for electrochemical energy conversion* Electrochemistry in the Nanoregime, Bunsen Kolloquium dedicated to Prof. Dr. Dieter M. Kolb on the occasion of his 65th birthday, Kloster Roggenburg, Germany, December 12-14. 2007.
I.A. Schneider	*The low frequency impedance response of polymer electrolyte fuel cells* Workshop on Fuel Cell Modeling, Aachen, Germany, March 6, 2007.
I.A. Schneider	*Insights into phenomena caused by convective gas flow in PEFC diagnostics* University of Florida Electrochemical Society, Gainesville, USA, May 21, 2007
J. Wambach	*Molekülspektroskopie an Oberflächen: Einblick in die Dynamik der Moleküle* Oberflächen- und Beschichtungstechniken - Schicht- und Oberflächenanalytik, SVMT, EMPA Akademie, Dübendorf, Switzerland, May 30-June 1, 2007.

Other Talks

S. Biollaz, T. Schildhauer, J. Wambach
Science and development aspects of the PSI fluidised bed methanation technology
International Seminar on Gasification and Methanation, Gothenburg, Sweden, September 20-21, 2007.

P. Boillat, D. Kramer, G. Frei, G.G. Scherer, A. Wokaun, Y. Tasaki[1], Y. Ichikawa[1], K. Shinohara[1]
Application of high resolution neutron radiography in fuel cell diagnostics
SINQ-User Meeting, Paul Scherrer Institut, Villigen, PSI, Switzerland, June, 2007.
[1] Nissan Motor Co., Ltd., Yokosuka-shi, Japan

P. Farquet
Microstructured proton conducting membranes by synchrotron radiation induced grafting
Reactive Polymers in Inhomogeneous Systems, in Melts and at Interfaces (REACT), Dresden, Germany, September 23-26, 2007.

R. Flückiger
Material and cell characterizations for channel-rib models
BMBF Meeting PEMDesign, Berlin, Germany, March 11-13, 2007.

L. Gubler
Meaningful fuel cell membrane aging tests
CARISMA Degradation Workshop, Grenoble, France, July 5, 2007.

L. Gubler
Locally resolved degradation analysis of aged fuel cell membranes
CARISMA Workshop on Ionomer Membranes for Medium and High Temperature PEM Fuel Cells, Stuttgart, Germany, October 11-14, 2007.

R. Kötz, J-C. Sauter, P. Ruch, P. Dietrich, F.N. Büchi, P.A. Magne, P. Varenne
Voltage balancing of a 250 Volt supercapacitor module for a hybrid fuel cell vehicle.
Proc. 17th International Seminar on Double Layer Capacitors and Hybrid Energy Storage Devices, Deerfield Beach, Florida, USA, December 10-13, 2007.

F. La Mantia, P. Novák
Impedance spectroscopy on graphite electrodes for lithium-ion batteries
58th Annual Meeting of the International Society of Electrochemistry, Banff, Canada, September 10, 2007.

F. La Mantia, F. Rosciano, N. Tran, P. Novák
Direct evidence of oxygen evolution from $Li_{1+x}(Ni_{1/3}Mn_{1/3}Co_{1/3})_{1-x}O_2$ at high potentials
Giornate dell' Elettrochimica Italiane, Cagliari, Italy, July 17, 2007.

P. Maire, P. Nesvadba[1], T. Hintermann[1], C. Morton[1], P. Novák
Electrochemistry of novel nitroxide materials
58th Annual Meeting of the International Society of Electrochemistry, Banff, Canada, September 12, 2007.
[1] Ciba, Basel

S.H. Ng
Li-ion batteries @ Paul Scherrer Institut (PSI), Switzerland
Institute for Superconducting and Electronic Materials, University of Wollongong, Australia, July 2, 2007.

T.J. Patey
Nano-sized LiV_3O_8 powders as cathode material in Li-ion batteries
Particle Technology Laboratory of the ETH Zürich, April 20, 2007.

T.J. Patey
Co-synthesis of $LiMn_2O_4$ nanoparticles and carbon black: an insight into the electrode engineering of nanoparticles for Li-ion batteries
Particle Technology Laboratory of the ETH Zürich, December 7, 2007.

T.J. Patey, R. Büchel[1], S.E. Pratsinis[1], P. Novák
Synthesis, characterization, and processing of lithium manganese oxide nanoparticles for lithium-ion batteries
Empa PhD Symposium, November 21, 2007.
[1] ETH Zürich

M. Reum
High resolution current measurements in PEFC
ASME 5th Int. Conference of Fuel Cell Science and Technology, New York, USA, June 17-20, 2007.

F. Rosciano	*X-ray and neutron diffraction methods for in-situ studies of electrochemical systems* Laboratoire de Réactivité et de Chimie des Solides, Université de Picardie Jules Verne, Amiens, France, October 10, 2007.
P. Ruch, M. Hahn, R. Kötz	*The increase of supercapacitor energy density by utilizing insertion type reactions* The 2nd International Conference on Carbon for Energy Storage and Environment Protection (CESEP'07), Krakow, Poland, September 2-6, 2007.
P. Ruch, M. Hahn, A. Foelske, R. Kötz	*In situ Raman spectroscopy and electrochemical dilatometry of sp²-hybridized carbons during charging in supercapacitors* GDCh Wissenschaftsforum Chemie 2007, Ulm, Germany, September 16-19, 2007.
I.A. Schneider, D. Kramer, A. Wokaun, G.G. Scherer	*What determines the low frequency impedance response of polymer electrolyte fuel cells?* 7th International Symposium on Electrochemical Impedance Spectroscopy, Argelès-sur-Mer, France, June 3-8, 2007.
B.C. Seyfang, P. Boillat, M. Kuhnke, T. Lippert, G.G. Scherer, A. Wokaun	*Ein neues, vereinfachtes Konzept für eine Mikro Polymer Elektrolyt Brennstoffzelle* GDCh Wissenschaftsforum Chemie 2007, Ulm, Germany, September 16-19, 2007.
J. Ufheil, J. Dentzer[1], N. Tran, P. Novák, M.E. Spahr[2], D. Goers[2], H.A. Wilhelm[2], R. Gadiou[1], C. Vix-Guterl[1]	*The importance of surface properties of graphite to the first lithium intercalation* CARBON 2007, Seattle, USA, July 20, 2007. [1] Institut de Chimie des Surfaces et Interfaces, CNRS, Mulhouse, France [2] TIMCAL SA, Bodio
F. Vogel, M. Nachtegaal, J. Wambach	*Advanced in-situ instrumentation for catalysis research at PSI* Defining the Future, OPERANDO Meeting, München, Germany, September 24-26, 2007.
F. Wallasch	*Development of proton conducting membranes for PEFC: The system FEP-g-(AMS-co-MAN)* 9th Network Young Membrains Meeting (NYM9), Thessaloniki, Greece, September 26-28, 2007.
J. Wambach	*Surface processes on Ni-based catalysts during methanation of biomass-derived synthesis gas* Symposium on current trends in physics and chemistry, CAMD, DTU, Lyngby, Denmark, June 8, 2007.
X. Wei, A. Reiner, E. Müller, G.G. Scherer, A. Wokaun	*Morphological evolution of polycrystalline Pt during electrochemical roughening* 5th Spring Meeting of the International Society of Electrochemistry, Dublin, Ireland, May 1-4, 2007.

POSTERS

S. Alkan Gürsel, H. Ben youcef, L. Gubler, A. Wokaun, G.G. Scherer	*Effect of crosslinker concentration on performances and properties of styrene grafted onto ETFE based membranes* 3rd International Symposium on Reactive Polymers in Inhomogeneous Systems, in Melts and at Interfaces, Dresden, Germany, September 23-26, 2007.
P. Boillat, D. Kramer, B.C. Seyfang, G. Frei, E. Lehmann, G.G. Scherer, A. Wokaun, Y. Tasaki[1], Y. Ichikawa[1], K. Shinohara[1]	*Application of high resolution neutron imaging in polymer electrolyte fuel cell (PEFC) diagnostics.* From physical understanding to novel architectures of fuel cells, Trieste, Italy, May 21-25, 2007. [1] Nissan Motor Co., Ltd., Yokosuka-shi, Japan

P. Boillat, D. Kramer, G. Frei, G.G. Scherer, A. Wokaun, Y. Tasaki[1], Y. Ichikawa[1], K. Shinohara[1]

Application of high resolution neutron radiography in fuel cell diagnostics
4th European Conference Neutron Scattering, Lund, Sweden, June 25-29, 2007.
[1] Nissan Motor Co., Ltd., Yokosuka-shi, Japan

C.N. Borca, S. Canulescu, F. Loviat, D. Grolimund, T. Lippert, J. Wambach, A. Wokaun

Electronic configuration of the pulsed laser deposited $La_{0.7}Ca_{0.3}Mn_{0.8}Fe_{0.2}O_3$ thin films
Correlated Electron Materials, 6th PSI Summer School on Condensed Matter Research, Lyceum Alpinum, Zuoz, Switzerland, August 18-25, 2007.

I. Czekaj, F. Raimondi, J. Wambach, S. Biollaz, A. Wokaun

Modifications of Ni/Al_2O_3 catalyst structure during methanation on nanoscopic level
23rd SAOG-GSSI Conference, Université de Fribourg - Institut de Physique Pérolles, Fribourg, January 26, 2007.

I. Czekaj, J. Wambach, A. Wokaun

DFT modeling of the Ni-compounds and Ni deposited at γ-Al_2O_3 (100) surface
Swiss Physical Society Meeting, University of Zürich, Zürich, Switzerland, February 20-21, 2007.

I. Czekaj, F. Loviat, F. Raimondi, J. Wambach, S. Biollaz, A. Wokaun

Modification of Ni/Al_2O_3 catalyst structure during methanation by biomass-derived synthesis gas
23rd One-Day-Symposium, Electrochemistry, Paul Scherrer Institut, May 3, 2007.

I. Czekaj, F. Loviat, F. Raimondi, J. Wambach, S. Biollaz, A. Wokaun

Deactivation process of Ni/Al_2O_3 catalyst during methanation by biomass-derived synthesis gas
EUROPACAT VIII, From Theory to Industrial Practice, Catalyst Deactivation, Turku/Åbo, Finland, August 26-31, 2007.

P. Farquet, C. Padeste, H.H. Solak, S. Alkan Guersel, G.G. Scherer, A. Wokaun

EUV radiation grafting of nanostructured polymer brushes
Reactive Polymers in Inhomogeneous Systems, in Melts, and at Interfaces (REACT), Dresden, Germany, September 23-26, 2007.

L. Gubler, G.G. Scherer

Strategy for carrying out aging tests of proton exchange membranes
212th Meeting of the Electrochemical Society, Washington DC, USA, October 7-12, 2007.

F. Rosciano, F. La Mantia, N. Tran, P. Novák

An in situ study of the origin of the irreversible plateau observed at high potentials for the $Li_{1+x}(Ni_{1/3}Mn_{1/3}Co_{1/3})_{1-x}O_2$ system
11th Euroconference on Science and Technology of Ionics, Batz-sur-Mer, France, September 9-15, 2007.

G. Schuler, F.N. Büchi

A novel test rig for locally resolved gas analysis in PEFC
International Workshop on Degradation Issues in Fuel Cells, Hersonessos, Greece, September 19-21, 2007.

B.C. Seyfang, P. Boillat, M. Kuhnke, G.G. Scherer, A. Wokaun, T. Lippert

Micro-fabricated polymer electrolyte fuel cells – A novel concept with less particular parts
From Physical Understanding to Novel Architectures of Fuel Cells, Trieste, Italy, May 21-25, 2007.
58th Annual Meeting of the International Society of Electrochemistry, Banff, Canada, September 9-14, 2007.

F. Simmen, T. Lippert, P. Novák, A. Wokaun, B. Neuenschwander[1], M. Döbeli[2], M. Mallepell[2]

The influence of lithium excess in the target on the properties and compositions of the $Li_{1+x}Mn_2O_{4-\delta}$ thin films prepared by PLD
9th International Conference on Laser Ablation COLA 2007, Tenerife, Spain, September 24-28, 2007.
[1] Berner Fachhochschule Burgdorf
[2] PSI and ETH Zürich

W. Sugimoto[1], M. Hahn, R. Kötz, Y. Takasua[1]	*In-situ height change measurements during potential cycling of layered ruthenic acid* 58th Annual Meeting of the International Society of Electrochemistry, Banff, Canada, September 9-14, 2007. [1] Shinshu University, Japan
F. Wallasch, L. Gubler, M. Slaski, G.G. Scherer, A. Wokaun	*Neue strahlengepfropfte Membranen für Polymerelektrolyt Brennstoffzellen* GDCh-Wissenschaftsforum Chemie 2007, Ulm, Germany, September 16-19, 2007.
X. Wei, A. Reiner, E. Müller, G.G. Scherer, A. Wokaun	*Electrochemical surface reshaping of polycrystalline Pt: Morphology and crystallography* 23rd SAOG-GSSI Conference, Université de Fribourg - Institut de Physique Pérolles, Fribourg, January 26, 2007.
X. Wei, A. Reiner, E. Müller, A. Wokaun, G.G. Scherer, L. Zhang[1], K.-Y Shou[1], B.J. Nelson[1]	*Morphological evolution of polycrystalline Platinum during electrochemical roughening* 58th Annual Meeting of the International Society of Electrochemistry, Banff, Canada, September 9-14, 2007. [1] ETH Zürich.

CONFERENCES, WORKSHOPS & EXHIBITIONS

R. Kötz	*58th Annual Meeting of the International Society of Electrochemistry* Banff, Canada, September 9-14, 2007. Co-Organizer Symposium 2
R. Kötz	*ICAC2007, International Conference on Advanced Capacitors*, May 28-30, 2007. Member of the International Advisory Committee
P. Novák	*58th Annual Meeting of the International Society of Electrochemistry* Banff, Canada, September 9-14, 2007. Organizing Committee
G.G. Scherer, R. Kötz	*23. Tagessymposium – Electrocatalysis* Paul Scherrer Institut, May 03, 2007 Organizers
G.G. Scherer	*BFE Impulse-Day – Hydrogen and Fuel Cell* Paul Scherrer Institut, November 30, 2007. Co-Organizer

MEMBERSHIPS IN EXTERNAL COMMITTEES

R. Kötz	*Electrochimica Acta* Member of the Advisory Board
R. Kötz	*International Society of Electrochemistry* Member of the Publications Committee
P. Novák	*International Society of Electrochemistry* Member of Executive Committee (Treasurer) and Council
P. Novák	*International Society of Electrochemistry* Member of Scientific Meeting Committee
P. Novák	*The Electrochemical Society, Inc.* Member of the Technology Award Committee of the Battery Division

P. Novák	*Electrochimica Acta* Guest Editor
G.G. Scherer	*Beirat Forschungsallianz Brennstoffzelle Baden-Württemberg, Germany* Deputy Speaker
G.G. Scherer	*Maturitätsprüfungskommission der Kantonsschulen Baden, Wettingen und Wohlen* Member